DEPARTMENT OF ELECTRONICS UNIVERSITY OF SOUTHAMPTON

Final Report on Ministry of Technology Contract No. PD/40/049/AT

by

J.P. Dakin, W.A. Gambling, A.R. Henderson
P.J.R. Laybourn and D. Payne

FIBRE-OPTICAL COMMUNICATIONS

December 1970 (3)

C O N T E N T S

PREFACE

The work described in this final report has been carried out under the terms of Contract PD/40/049/AT from May 1968 to September 1970. It formed part of a programme to develop a restricted-bandwidth optical communications link using glass fibres, carried out jointly with S.R.D.E., Christchurch. The parts of the programme assigned to the Quantum Electronics Research Group in the Department of Electronics, University of Southampton, were as follows:

a) Measurement of optical absorption and scattering losses in high-purity bulk glass;

b) Development of equipment for pulling suitable cladded glass fibres from bulk glass;

c) Assessment of the quality of fibres so produced.

The necessary apparatus for the measurements in (a) has been designed and built, and measurements have been made and are still in progress. Fibre-drawing equipment has been designed and built, and fibres produced and assessed; meanwhile, modifications to the drawing apparatus are being made in the light of the quality of the initially-produced fibres. Some theoretical work on mode propagation in fibres was carried out in the early stages of the Contract, and is described in the first report on the Contract and elsewhere[1].

1. Laybourn, P.J.R., 'Group velocity of dielectric waveguide modes', Electronics Letters 4, 23, p.507, 1968.

1. MEASUREMENT OF ABSORPTION LOSS BY THERMAL METHODS

In order to isolate the absorption loss in a sample of glass from other losses, it is necessary to measure the actual temperature rise of the glass due to absorption, or alternatively some other effect within the glass that is temperature dependent, such as expansion or change in refractive index.

A simple mechanical measurement of the expansion may be dismissed, since the linear coefficient of expansion of glass is of the order of 5×10^{-6}, and the resulting temperature rise in glass in a beam of moderate power is only fractions of a degree centigrade. An optical method for estimating the expansion would be more feasible, but here again, at moderate powers, the expansion would be on the limits of such a detection system.

The thermal lens effect, observed when lossy materials are placed in a laser cavity operating in a fundamental mode, was investigated with a view to applying this technique to the measurement of glass's loss. With a beam of Gaussian intensity distribution passing through a material of finite absorption, differential absorption across the beam, due to the varying intensity, gives rise to a refractive index gradient which to a good approximation is parabolic, and the material behaves as a lens[1]. Measurement of the effective focal length of the lens, either directly or indirectly, allows the absorption of the material to be determined, and this technique has been used successfully in the

determination of absorption in liquid samples[2].

When glass is considered as the absorbing material, however, the effect is reduced by about two orders of magnitude due to the much smaller change in refractive index, and unless the incident power available is many watts, the lensing effect cannot be detected. This method has therefore been abandoned, at least until a high power CW laser becomes available. The technique of measuring directly the temperature rise in glass was chosen as being the most feasible.

1.1 Introduction

An apparatus has been set up to determine the absorption loss in glass by measuring directly the temperature increase in a sample of the glass on irradiation with a light beam of known power and spectral range. The apparatus has been designed to allow small, thin samples with an area of one cm^2 or less to be measured, and suitable samples can thus be easily cut from rod, or from thin-walled tubing used as the fibre cladding glass.

1.2 Theory of Method

For a given sample of glass having a finite absorption, the rate of temperature rise of the sample is proportional to the rate of absorption of energy from the light beam, thus

$$\frac{d\theta}{dt} = \frac{\Delta W}{H}$$

where ΔW is the rate of energy absorption and H is the thermal capacity of the sample.

Now $\Delta W = L.\ell.W$

where L = fractional loss per cm of glass

$= 2.3 \times 10^{-6} X$ where X is the loss in dB/km

ℓ = length (cm)

W = incident power (watts)

and $H = S.\rho.A.\ell$

where S = specific heat (Joules/gm.deg.C)

ρ = density (gm/cm^3)

A = area (cm^2)

Therefore $$\frac{d\theta}{dt} = \frac{2.3 \times 10^{-6} X.W.}{S.\rho.A}$$

and $$X = \frac{d\theta}{dt} \frac{S.\rho.A.}{2.3 \times 10^{-6}}.W. \qquad \ldots (1)$$

If no heat were lost from the sample, then $d\theta/dt$ would be constant.

However, in practice, the glass loses heat by convection, radiation, and by conduction along its supports.

If the rate of heat loss is assumed to be proportional to the temperature rise:

i.e. Heat loss = $K\theta$

then an equilibrium temperature, θ_{max}, will be reached where the heat lost is equal to the energy absorbed, and so:

$$\theta_{max} = \frac{\Delta W}{K}$$

and a plot of temperature increase against time will be exponential, of form:

$$\theta = \frac{\Delta W}{K}(1 - e^{-K/H\ t}) \qquad \ldots (2)$$

$$\frac{d\theta}{dt} = \frac{\Delta W}{H} e^{-K/H\ t)}$$

therefore initial slope $(\frac{d\theta}{dt})_{t=0} = \frac{\Delta W}{H}$

Thus the loss may be found by measuring the initial slope from an experimental curve, or indirectly from a number of points on the curve.

If, after the sample has been heated by absorption of the incident beam, it is allowed to cool, again a plot of temperature against time gives an exponential curve, of form:

$$\theta = \frac{\Delta W}{K} e^{-K/H\ t}$$

$$\frac{d\theta}{dt} = -\frac{K}{H}\frac{\Delta W}{K} e^{-K/H\ t} = -\frac{K}{H}\theta$$

Therefore

$$\mathrm{Log}_e \frac{K}{\Delta W}\theta = -\frac{K}{H} t$$

Thus a plot of $\mathrm{Log}_e\theta$ against t gives a straight line of slope $-\frac{K}{H}$

$$\text{i.e.} \quad \frac{\mathrm{Log}_e\theta}{t} = -\frac{K}{H} = m \qquad \ldots (3)$$

Therefore $K = -H\ m$

Now $\theta_{max} = \frac{\Delta W}{K} = \frac{-\Delta W}{Hm}$

therefore $\theta_{max} = \frac{-\ 2.3 \times 10^{-6}\ X.\ \ell.W.}{S.\rho.A.\ell.m}$

$$\text{therefore} \quad X = \frac{-\theta_{max} \cdot S.\rho.A.m.}{2.3 \times 10^{-6} W} \qquad \ldots (4)$$

Because of the difficulties of accurately measuring small temperature differences, it is advantageous to use equations (3) and (4) for the calculation of loss, rather than (1) and (2). θ_{max} can be averaged over a long time interval, and since K is a constant for a given sample of glass within the apparatus, the cooling curve may be obtained after irradiating the sample with the full light intensity available, without any narrowband filters in the beam, thus raising the temperature of the sample to a significantly higher value. The value of K thus obtained is applicable for all wavelengths and the only further measurements required at different wavelengths are θ_{max} and W.

1.3 Details of Apparatus

Since it is desirable to measure absorption loss over a wide range of wavelength, a high-power lamp was chosen, and the appropriate spectral range of interest is selected by inserting interference filters into the beam.

The lamp used is a 400watt compact source mercury iodide type, manufactured by Thorn Electrical Industries. This lamp maintains an arc of approximately 9mm x 5mm, with an output extending from 300 to 900nm, at high efficiency. The table shown overleaf indicates the total output power, per 30nm bandwidth, throughout the visible spectrum.

Wavelength Range (nm)	Output Power (watts)
340 - 370	3
370 - 400	2.5
400 - 430	7
430 - 460	7.5
460 - 490	7
490 - 520	7
520 - 550	13
550 - 580	11.5
580 - 610	25
610 - 640	16
640 - 670	12.5
670 - 700	16.5
700 - 730	7
730 - 760	6

The lamp is mounted in a force cooled lamp house, the arc being a few millimetres behind a removeable aperture. At present an 8mm diameter aperture is used. The lamp is run from the manufacturer's control unit, which incorporates an r.f. starting unit to initiate the discharge, and after starting, the lamp takes about one minute to warm up to full output power.

A large aperture lens system (about 3" diameter) collects the light and focuses the source onto the sample. The sample itself is located inside a box to eliminate outside disturbances, and the appropriate filters are mounted over the entrance window of the box. Since the light beam is not parallel, but converges onto the sample with a semi-angle of about 15^{o}, account must be taken of the effect

of this converging beam on the transmission of the interference filters. Barr and Stroud quote a shift of peak wavelength 1.5nm per 10^{o} of angle from the perpendicular for metal-dielectric filters, and 4nm per 10^{o} for all dielectric filters.

The experimental arrangement is shown in Fig.1. To measure the temperature increase of the glass, copper-constantan thermocouples are used, and the temperature difference between two similar samples measured on a Hewlett-Packard microvoltmeter. Both samples are mounted inside the same box, supported only by their thermocouple wires; one sample in the path of the beam, the other a few centimetres to one side of it. The box, constructed of brass, is lined with black flock paper, and since the beam rapidly diverges after passing through the sample, reflections from within the box are not a problem. The outside of the box is insulated with an inch thick covering of expanded polystyrene, and the whole unit mounted on an optical bench carrier, as are the lens mounts and the lamp-house.

The thermocouple leads are taken out from the top of the box through special mountings, which may be rotated to position the sample perpendicularly to the beam. In measuring the very small voltages obtained, care must be taken not to introduce further thermocouple junctions arising from connecting wires of dissimilar material. The copper and constantan thermocouple leads themselves are soldered to brass wires connected to the brass terminals of the voltmeter, the soldered joints being located very close to each

other and against a large copper block, electrically insulated from the block by a thin layer of mica. The copper block is thermally insulated by a covering of expanded polystyrene. The voltmeter itself must be operated from its internal batteries and isolated from the mains supply, and care is taken to earth the instrument only via the optical bench.

By taking these precautions it is possible to measure temperature differences of the order of 2.5×10^{-3} deg.C., with an accuracy better than $\pm 20\%$, though at present the drift in temperature difference between the two samples with no incident beam can be somewhat higher than this.

Another experimental arrangement that has been used incorporated a large spherical mirror, with which a significantly higher power density at the sample was obtained. This arrangement is shown in Fig.2. With this system however, there was obviously some difficulty in isolating the sample from the surroundings, and although the resulting temperature rise was considerable, it could not be measured with any reliability.

1.4 Measuring Glass Loss

The samples so far used in the apparatus have been either in the form of discs, about 2mm thick and cut from 1cm diameter rod, or of square section just less than 1cm square, cut from the wall of tubing. Two similar samples are used, and in the case of discs,

must be polished after cutting from the rod. The two samples are suspended from their thermocouple leads inside the box, and with the source on and with no filter, a glass slide is inserted in front of the box and used as a beam splitter to observe the alignment of the sample in the beam. Adjustments can be made by rotating the mounting on top of the box.

The source is then turned off and the temperature allowed to stabilise, as the beam may have impinged on the thermocouple junction during alignment. With the source on, and still without a filter, the glass is allowed to heat up in the beam of white light, reaching its equilibrium temperature after about 15 minutes. The sample is allowed to cool, and readings of temperature and time recorded. From these a value of the cooling constant, K, is obtained as previously described.

Selected filters are then introduced into the beam and the maximum temperature attained by the glass in each case recorded. The incident power is not measured at the time of irradiation, but must be done after removal of the sample box. The stability of the lamp output is within a few percent, and so introduces a very small error compared with the overall accuracy of the temperature measurement. Knowing the dimensions, density, and specific heat of the glass, the loss in dB/km may be calculated using equation (4).

The thermocouple leads have been supported by clamping between split brass cylinders, and clearly most of the heat loss is by conduction along these leads. The system is at present being modified to utilise thinner thermocouple wires, and the supports for these wires are being made from a thermally insulating material. In this way the heat loss will be significantly reduced, and a higher equilibrium temperature obtained which can be measured with greater accuracy.

1.5 Typical Results for Pyrex

With white light incident on a sample of pyrex, a maximum e.m.f. of 120μV was obtained, corresponding to a temperature increase of 3.0deg.C.

On cooling, readings of temperature and time were recorded, and the resulting graph of $\text{Log}_e\theta$ against time is shown in Fig.3. The slope of this graph is $m = -1.24 \times 10^{-2}$.

From equation (4)

$$X(\text{dB/km}) = \frac{-\theta_{max}\ S.\rho.A.m}{2.3 \times 10^{-6}\ W}$$

$S = 0.97$ Joule/gm.deg.C.

$\rho = 2.23 \text{gm/cm}^3$

$A = 1\text{cm}^2$

therefore $X = 1.16 \times 10^4 . \frac{\theta_{max}}{W}$

At 612nm

$W = 19\text{mW}$ (Bandwidth of filter $\sim$ 20nm)

and $\theta_{max} = 1.275 \times 10^{-1}$deg.C.

therefore $\underline{X = 7.8 \times 10^{4}\text{dB/km}}$

At 885nm

$W = 7\text{mW}$

and $\theta_{max} = 1.85 \times 10^{-1}$deg.C.

therefore $\underline{X = 3.1 \times 10^{5}\text{dB/km}}$

1.6 Conclusions

The method described has proved a feasible technique for measuring absorption loss of glass at any desired wavelength, and being independent of the length of the sample, has the advantage that very small amounts of glass can be used. As the apparatus stands at present, sensitivity is limited by the voltmeter used, which has a full scale deflection of 3μV on its lowest range, and by the heat loss from the sample as already mentioned, limiting the maximum temperature reached.

Losses of the order of 50,000dB/km can be measured with an overall accuracy of about 20%, but below this the error increases significantly, so that although losses of, say, 500dB/km or below can be detected, the error may be as high as 100%.

Some difficulty was experienced in aligning the samples in the beam , as it was not easy to see if the light was just hitting the thermocouple junction, and this gave rise to some falatious results.

However, with the experience gained in using this technique as described, modifications are now in hand to improve the overall accuracy.

References

1 J.P. Gordon, R.C.C. Leite, R.S. Moore, S.P.S.Porto and J.R. Whinnery, J. Appl. Phys. 36, p.3 (1965).

2. R.C.C. Leite, R.S. Moore and J.R. Whinnery, Appl. Phys. Letters, 5, p.141 (1964).

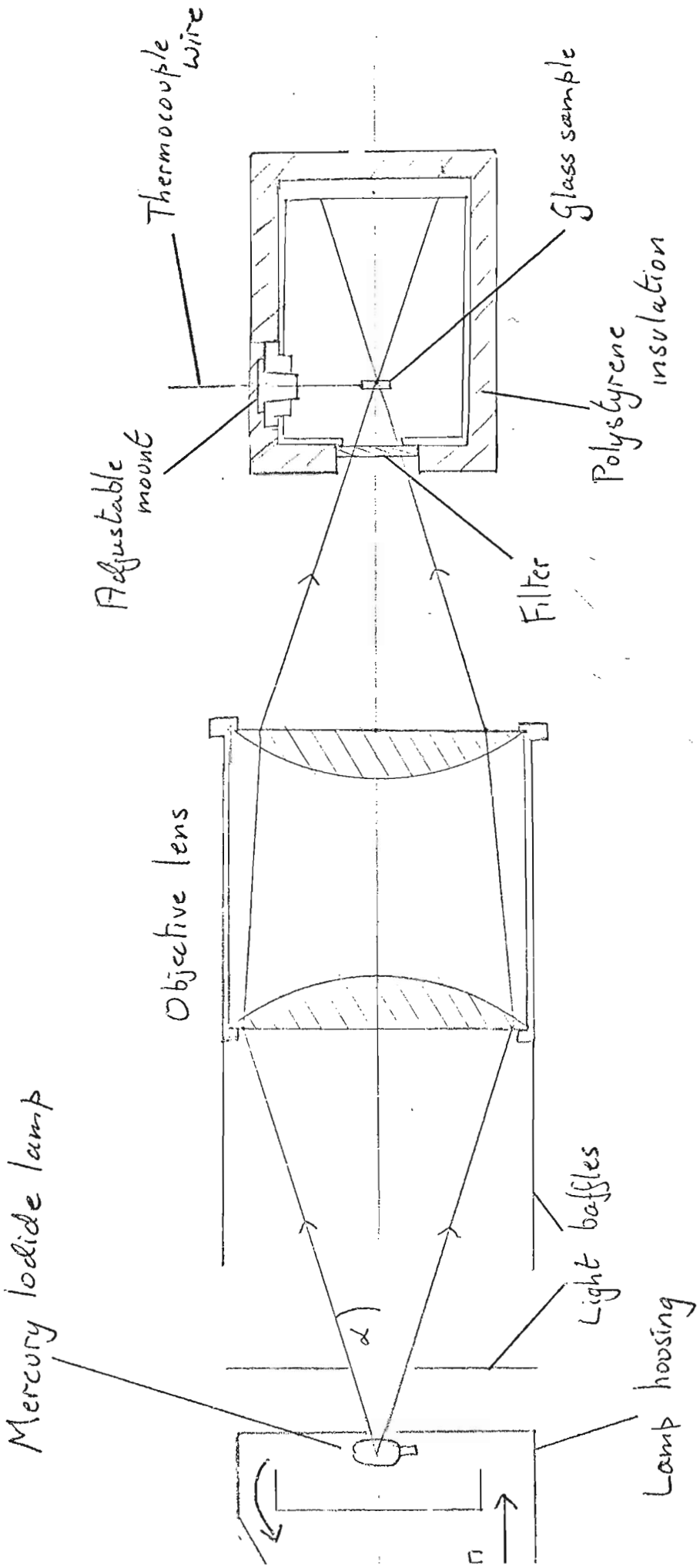

Fig. 1 Apparatus for Thermal Absorption Measurement

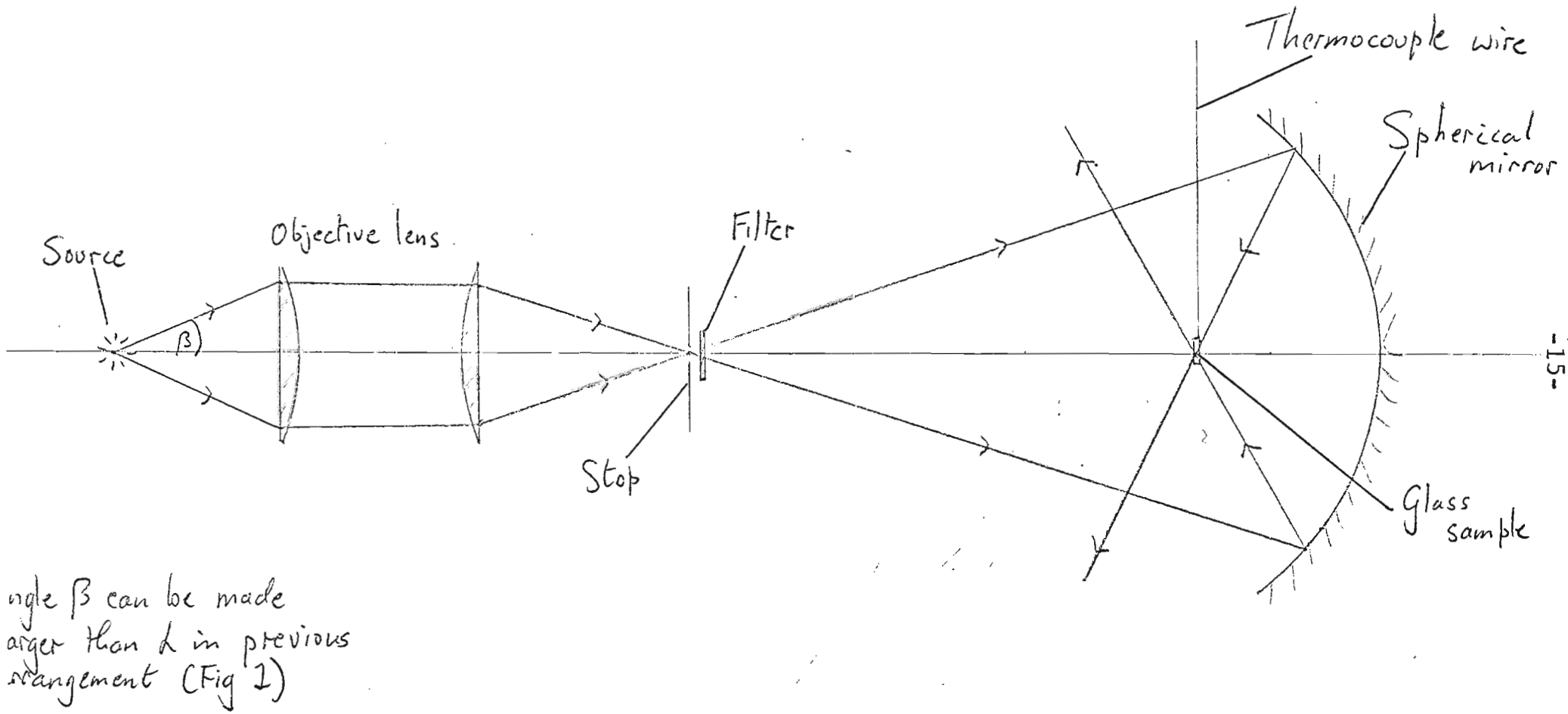

ngle β can be made
arger than α in previous
rrangement (Fig 1)

Fig. 2 Alternative Experimental Arrangement

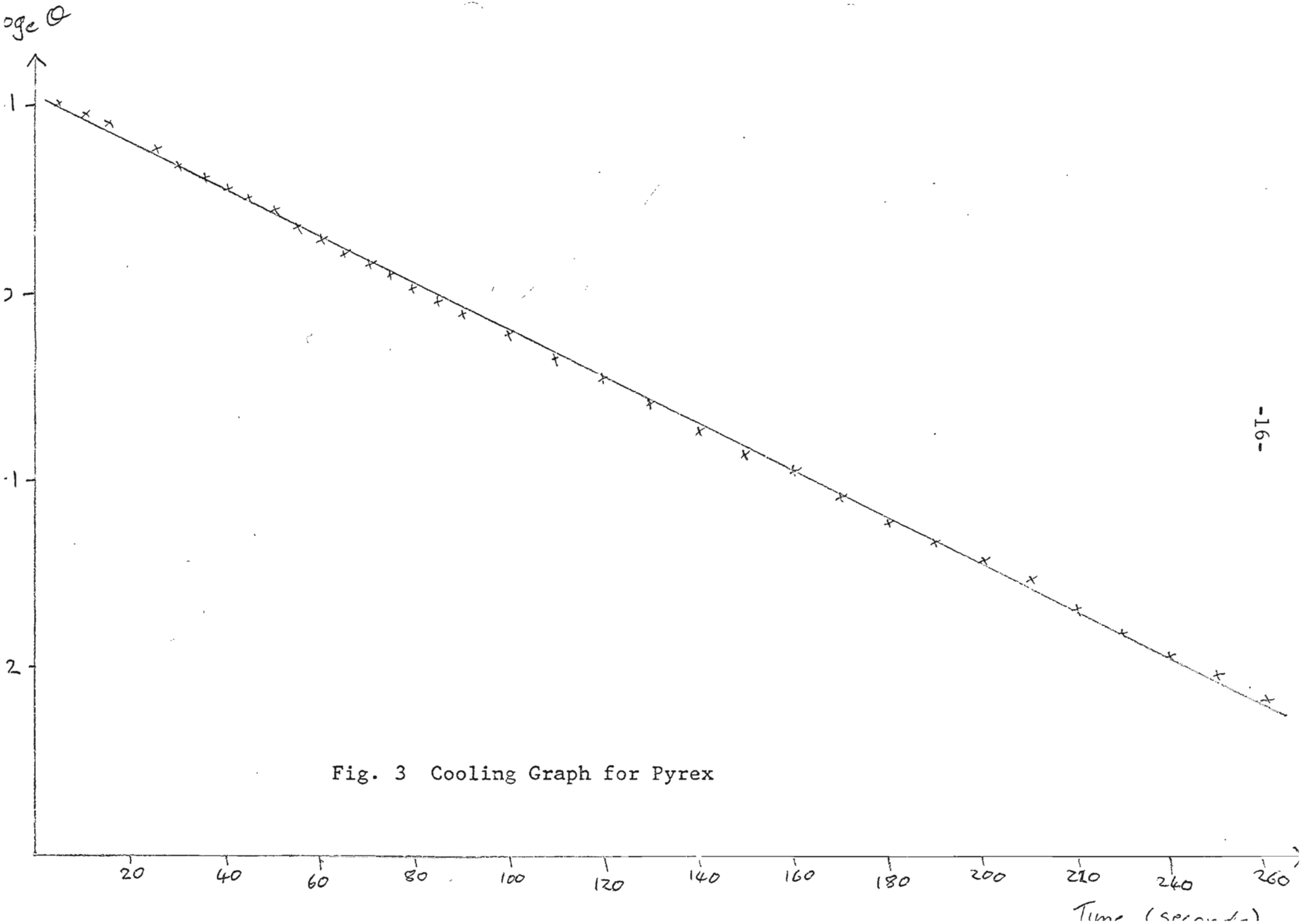

Fig. 3 Cooling Graph for Pyrex

2. MEASUREMENT OF BULK TOTAL ATTENUATION OF HIGH-QUALITY OPTICAL GLASS

2.1 Introduction

Previous reports have[1,2] outlined the methods to be used to measure the attenuation of samples of optical-quality glass, required as a starting material in the manufacture of multimode glass fibres for communication. It has been found convenient to draw fibre from glass rods of 1cm diameter, and consequently the apparatus has been designed to measure samples of such rods, up to 30cm long. Since fibre attenuation of the order of 20dB/km is aimed at, the starting material must have an attenutation of no more than this figure, and consequently the measuring apparatus has been designed with a resolution of 2dB/km as the target. This is equivalent to a loss of about 0.01% in 30cm. A two-beam spectrophotometer has been constructed, and measurements have been made on various high-quality glasses, of types suitable for the core of the fibre.

2.2 Discussion of available measuring techniques

The major obstacle to a direct photometric determination of the attenuation in the chosen samples is the uncertainty of the reflective end-loss. The reflection coefficient of light perpendicularly striking a glass surface of refractive index 1.6 is about 5%, and may be calculated accurately if the surface refractive index is known. Optical polishing may modify surface reflectance properties. In addition, slight imperfections remaining

after polishing will give rise to unpredictable scattering losses.

The two proposed measurement methods are designed to overcome the end-loss problem. In the double-sample method, long and short rod samples of the glass to be measured have their ends polished equally, perpendicular to the rod axis. The samples are placed one in each arm of a balanced twin-beam spectrophotometer, and the resulting optical imbalance is a measure of the bulk attenuation due to the differing lengths of the samples. The reflection and scattering losses at the first surfaces of each sample should be equal, while at the second surfaces the slightly greater bulk attenuation of order 0.1% in the long sample will only introduce a similar error, i.e. 0.1%, in the final result, much better than the required accuracy. The second method uses a single, long, sample whose ends are cut at Brewster's angle to the rod axis. With a plane-polarised light source in the twin-beam spectrophotometer, the reflection losses at each end of the sample may be greatly reduced, theoretically to zero.

It has been found that both methods present experimental difficulties. In the two-sample method, the end faces of the samples are perpendicular to the light beam axes, so that multiple reflections between front and back sample faces will be transmitted to the detector. The major double reflection will be about 2.5×10^{-3} of the main beam intensity. Ideally, the multiple reflections will follow the main beam axis, and will affect each arm equally. In

practice it has been the case that the end surfaces of the rod have not been exactly parallel, so that the double reflection from the long sample has not struck the detector surface at the same point as the main beam. A lack of parallelism of 1 milliradian would cause a shift of about 2mm at the detector. The main beam itself has been diverted slightly by the prismatic effect of the rod, and the tilt of the rod has to be adjusted to return the beam to its original position on the detector. The equality of end losses between samples is dependent on polishing techniques; polishing might best be carried out on a machine, to a fixed schedule. The surface finish may be investigated on an accurate ellipsometer[3].

The single Brewster-angle sample method is an attempt to eliminate the sources of error because of imperfect end faces. However, other inaccuracies are introduced, due to the problem of accurate alignment. The residual reflection loss at a Brewster-angle surface depends on the accuracy of setting the angle between incident beam and surface, on the angle between the plane of polarisation and the plane containing incident, transmitted and reflected beams (ideally zero) and on the amount of orthogonally-polarised light present in the beam. Some calculations have been presented in a previous report[2] on the magnitude of such errors. In addition, having set up the first surface of the rod in the correct plane relative to the input beam, it is unlikely that the second surface will be accurately aligned, although with an optically

homogeneous rod and perfectly parallel end surfaces it might be possible to ensure this. For each wavelength the whole system must be re-aligned, since due to dispersion Brewsters angle is wavelength-dependent. In the infra-red, with low illumination intensity, such a task would be formidable.

2.3 Experimental apparatus

After considerable experience with the spectrophotometer arranged to use Brewster-angle samples, it was decided to use the apparatus in the two-sample mode, since difficulties in alignment of the Brewster-angle rod and in obtaining samples finished to a satisfactory accuracy were great. The layout of the optical system is shown in Fig. 2.1. The components are clamped magnetically onto a plane steel table, allowing easy rearrangement when desired, and the table is enclosed by a laminar-flow clean-air cabinet, to obviate the problem of dust settling on optical surfaces.

The light source is a 12V, 100W tungsten-halogen projector lamp, which has a close-wound, flat spiral filament presenting a rectangular source 2mm x 3mm. It is stopped down by a 2mm diameter pinhole, and a 20cm focal length lens with a similar stop is arranged to produce a full-size image of the source pinhole, 40cm from the lens. In this manner the light beam travels entirely within a cylinder of 2mm diameter between the lens and the image; the samples will be placed within the image distance.

The light beam is split and redirected into two parallel paths by a beam-splitting cube and mirror. The two beams are extinguished alternately by a segmented chopper disc rotated by a synchronous motor which is supplied from a master oscillator, frequency divider and power amplifier. The samples are arranged one in each of the parallel beams; the holder for the long sample may be rolled out of the beam path and accurately repositioned, while the short sample is mounted in a removeable holder, also replacable with accuracy. The attitude of each rod may be adjusted using micrometer screws.

An additional mirror and beam-splitting cube recombine the two beam paths, through a wavelength-selective narrow-band interference filter and onto the detector surface. In earlier work the detector was a 56CVP photomultiplier, cooled by liquid nitrogen to reduce dark-current noise, but large-area silicon p-i-n photodiodes now available have proved superior. Consistent spatial sensitivity of the diode (fig. 2.2) has done away with the need for a scattering screen in front of the detector, and the signal-to-noise ratio of the system has improved considerably.

After preamplification, the electrical signal from the detector, basically a square waveform whose height represents the differential loss between the two arms of the spectrophotometer, is processed to remove the parts of the waveform where the changeovers occur, and the amplitude of the square wave is measured using a phase-sensitive detection system. The signal processing circuits are locked to

the master oscillator, and the whole of the electronic circuitry is shown in block form in fig. 2.3. The phase-sensitive detector is a commercial Brookdeal system, with some additional AIM filtering equipment. A detailed diagram of the signal blanking circuit is shown in fig. 2.4.

For ease of alignment, a small helium-neon laser has been incorporated into the system. It produces a single mode parallel-beam output of about 0.6mW, and has proved of great value when aligning the optical system. Its output enters the system through the back of the first beam-splitter, and is primarily aligned to be coaxial with the white light beams emerging from the beam-splitter. After its own alignment, the laser beam is used to align all other optical components. The beams travel parallel to the flat steel table, exactly 20cm above it. A removable target just in front of the detector is used from time to time to check alignment of the samples and the optical system.

2.4 Calculation of sensitivity

Source : tungsten-iodine lamp, at 3000°K (Colour temp 3121°K)
Assume it to be a grey body with emissivity E = .33; from Planck's black body radiation law:

$$\text{Power radiation } W_\lambda = \frac{E\, c_1}{\lambda^5 (e^{c_2/\lambda T} - 1)} \text{ watt/cm}^2/\mu\text{m bandwidth}$$

where $c_1 = 3.74 \times 10^4$

$c_2 = 1.439 \times 10^4$

Hence signal-to-noise ratio at the detector output

$$\frac{\overline{I_L}^2}{\overline{I_{SN}}^2} = 3.3 \times 10^{10} \alpha^2$$

for a minimum signal-to-noise ratio = 1, the differential loss detectable, $\alpha = 5.5 \times 10^{-6}$.

The apparatus should therefore have sufficient sensitivity for the glass loss measurements.

2.5 Measurement of glass samples

A number of types of optical glass were selected from the manufacturer's catalogue[4], as suitable for use in experimental fibre production. As the glasses chosen were to be used in the core of the fibres, only high-refractive index glasses ($n \simeq 1.6$) were considered. Four glass types, for which the manufacturers claimed low transmission losses, were obtained.

Type F7, a lead flint glass, was obtained in the form of 1cm diameter redrawn rods, with a fire-polished finish. The rods were not particularly straight, but this form of supply was relatively inexpensive and suited the fibre-drawing experiments. Long (30cm) and short (5cm) rods were cut, and their ends were polished by an optical firm. On examination after the polishing of their ends, the redrawn rod was seen to exhibit a strong diverging effect, and between crossed polarisers strain birefringence was visible (fig. 2.5a). The beam divergence was unacceptable, so the rods were

annealed for 2 hours at 420°C, and the strain was greatly reduced (fig. 2.5b)

Glass types F2 and F8 , also lead flint, and SK16, a dense barium crown glass, were obtained in the form of ground and cut rods of high optical quality. On polishing the ends of the rods no abberation could be seen. Annealing had already been carried out by the manufacturers.

Measurement of the differential loss was carried out on each pair of samples at wavelengths selected by narrow-band interference filters in the range 500-1000nm. At each wavelength, differential loss readings, zero readings and loss with a fused silica flat as a substandard were measured. The accuracy with which the loss of the thin silica flat was known was sufficient for this purpose. The reflective loss from the flat may be accurately calculated, and absorption and scattering loss in the 2mm path length are very small. The attenuations measured for the glass samples were expressed as decibels per kilometre, and plotted as a function of wavelength.

2.6 Discussion of results

Curves are presented in figs. 2.6 to 2.9 of the measured optical attenuation of the four glass types as a function of wavelength. It is at once apparent that some small values of attenuation, as low as 10dB/km, were measured. Having once aligned a set of samples,

the measurements were repeatable to 3dB/km, which bordered on the accuracy of the measuring system as a whole. The noise of the system, as seen on the digital output of the phase-sensitive detector, was at least 10% of the lowest observed attenuation. Thus if doubt is to be cast on some of these low measured attenuations, it would be on account of unequal end surface finish or misalignment of the rods, resulting in movement of the beam across the detector face. Great care was taken when aligning the rods, and further work is being carried out to measure the effect of known misalignment.

Whatever the accuracy of measurement of low values of attenuation, the curves obtained show some significant points. It is apparent that the lead glass samples exhibit particularly low loss in the 700-900nm region, and much higher loss in the visible region covered, 500-700nm. Of the three lead glass samples, the redrawn F7 is of slightly higher loss than the two optical glass samples of F2 and F8. A local loss minimum at about 580nm and a maximum at about 640nm are present in all three types.

The sample of SK16 glass shows a minimum attenuation at 700nm, of about 350dB/km, rising steadily at longer and shorter wavelengths. SK16 does not show much promise as a possible fibre core material.

2.7 Conclusions

A twin-beam spectrophotometer has been constructed, covering the wavelength range 500-1000nm. It is capable of measuring small

bulk glass attenuation to an apparent accuracy of 2dB/km. Preparation and alignment of the glass samples is critical however. Curves of attenuation vs. wavelength have been obtained for some lead glass samples which appear to exhibit very low loss at certain wavelengths; these results will be regarded with suspicion until further measurements have been carried out.

2.8 References

1. J.P. Dakin et al.: 'Fibre-Optical Communications - 1', 1968
2. J.P. Dakin et al.: 'Fibre-Optical Communications - 2', 1969
3. C.R. Wright and K.C. Kao :'Spectrophotometric Studies of Ultra Low Loss Glasses III: ellipsometric determination of surface reflectances', J. Sci. Instr., ser 2 2, p.579, 1969.
4. Optical Glass Catalog , Jena Glaswerk Schott and Gen., Mainz.

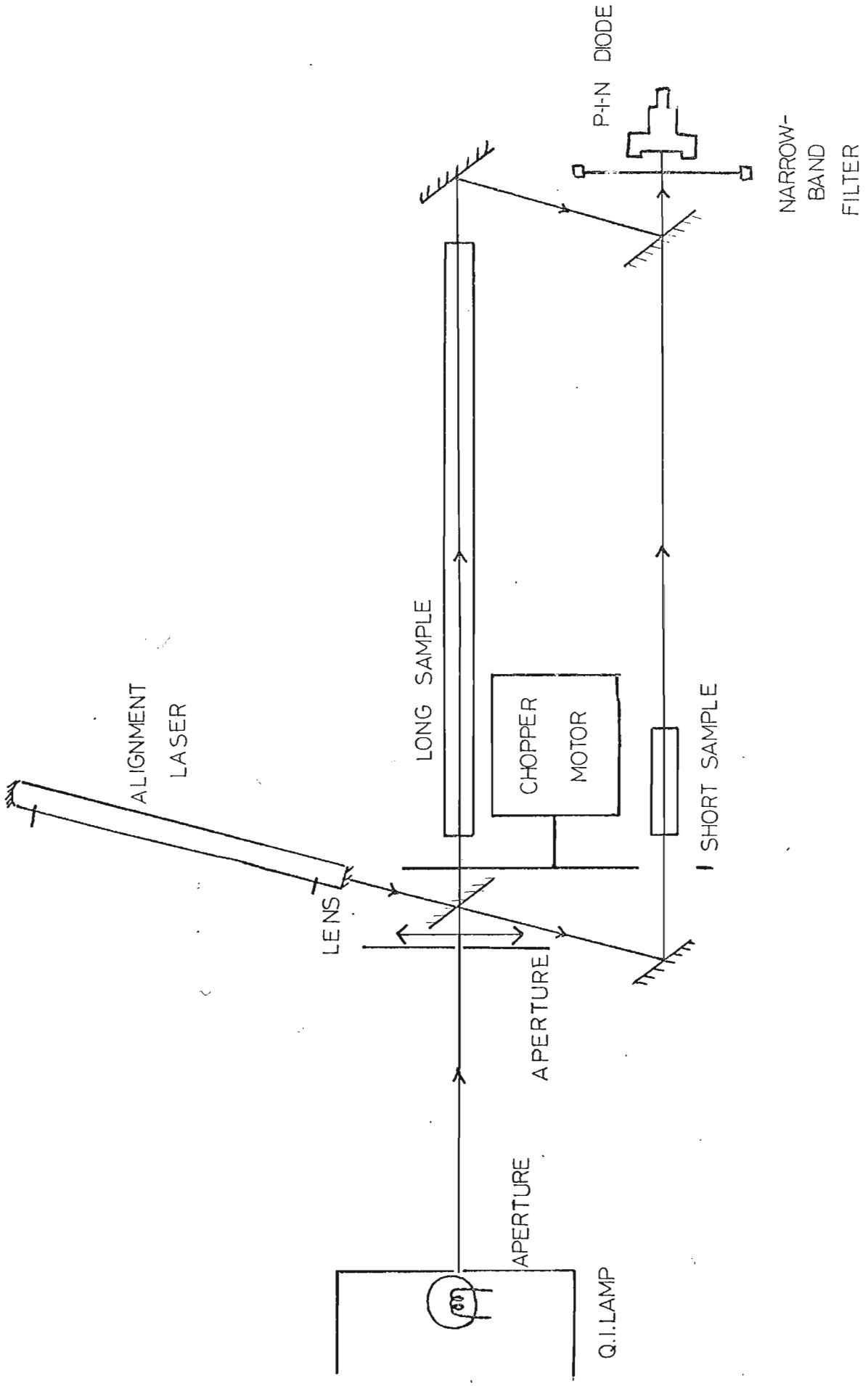

Fig. 2.1 Twin-beam spectro-photometer - optical system

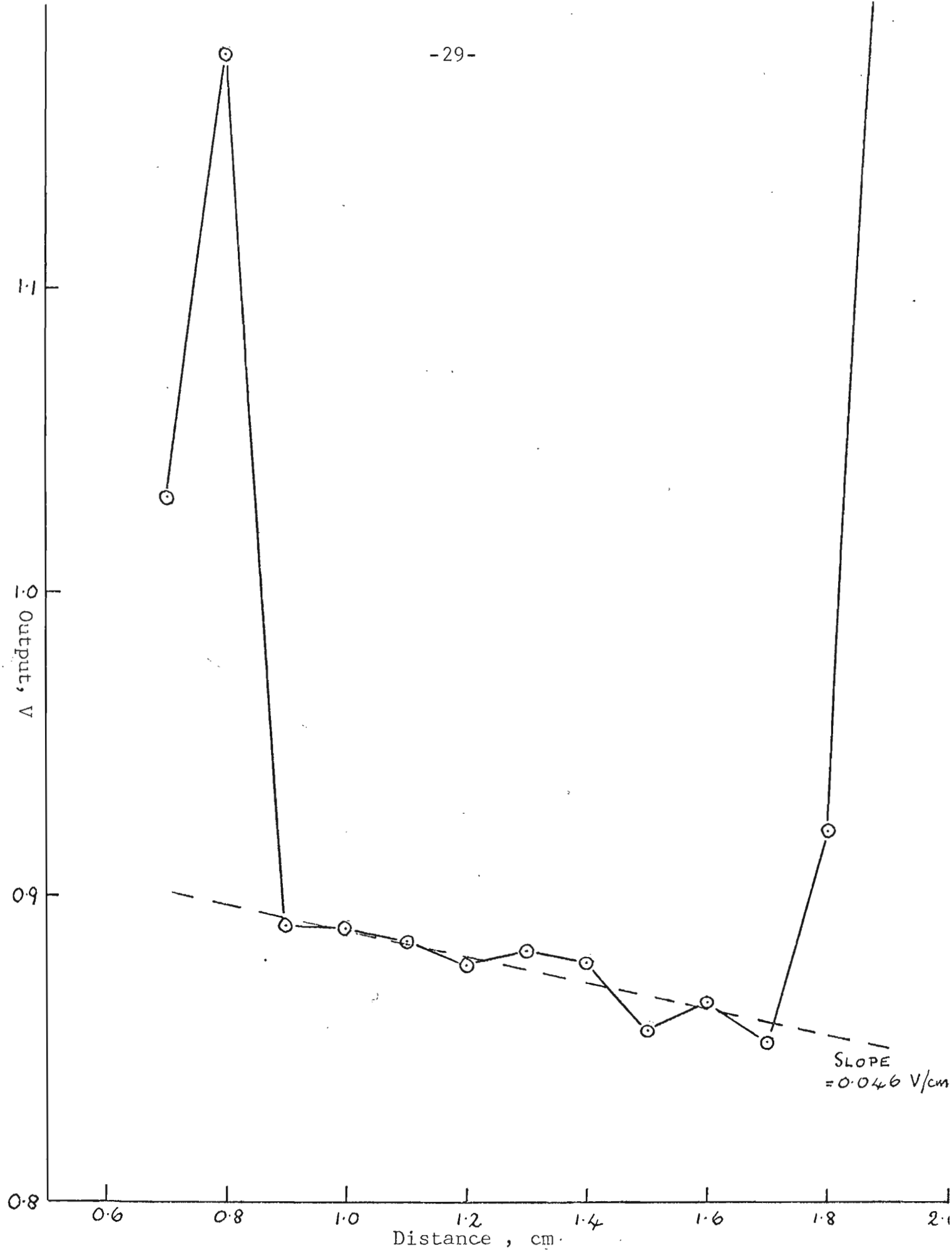

Fig.2.2 Variation of sensitivity of PIN 8-LC diodes with position across a diameter

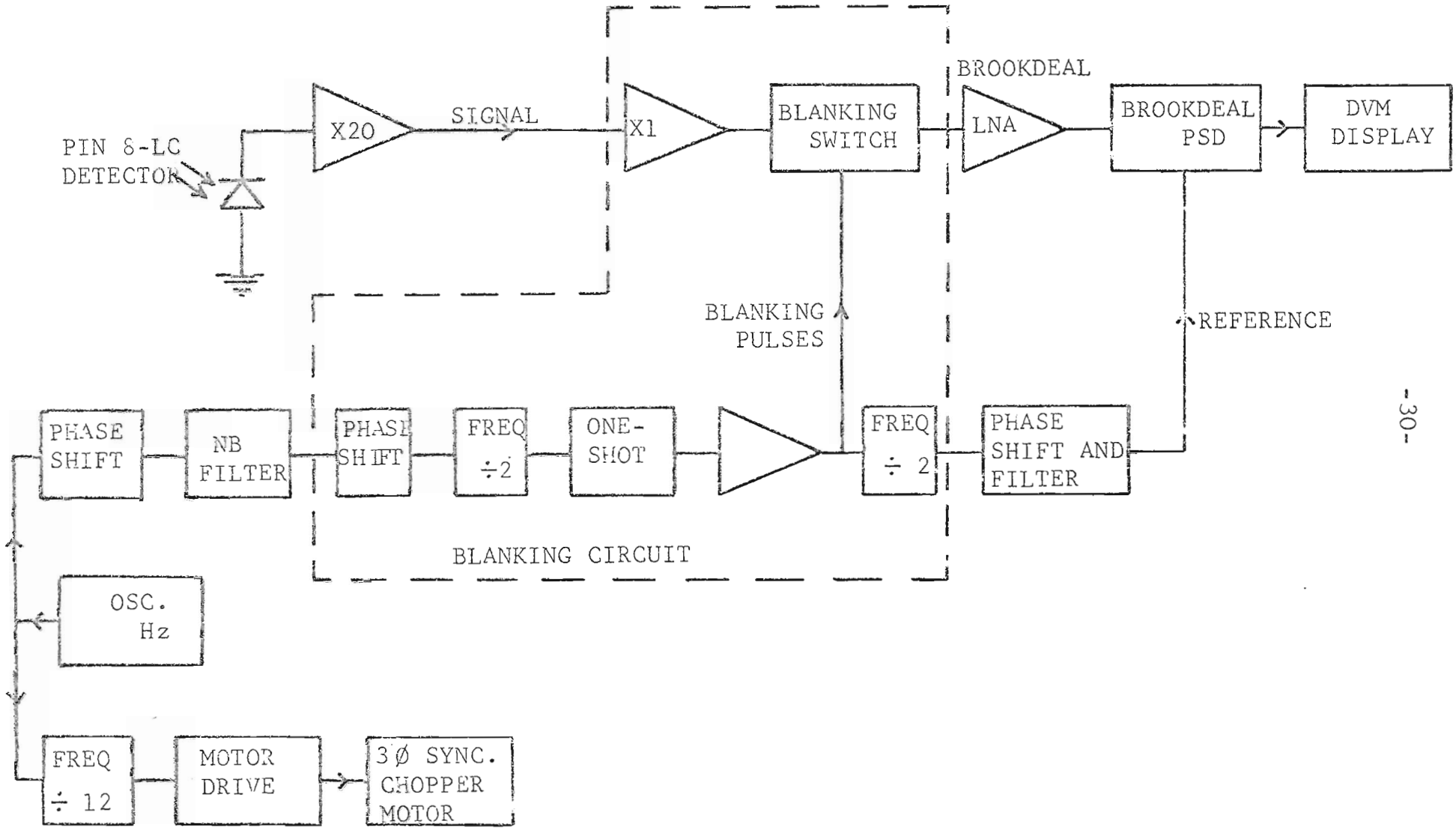

Fig. 2.3 Block diagram of synchronous drive and detection circuits

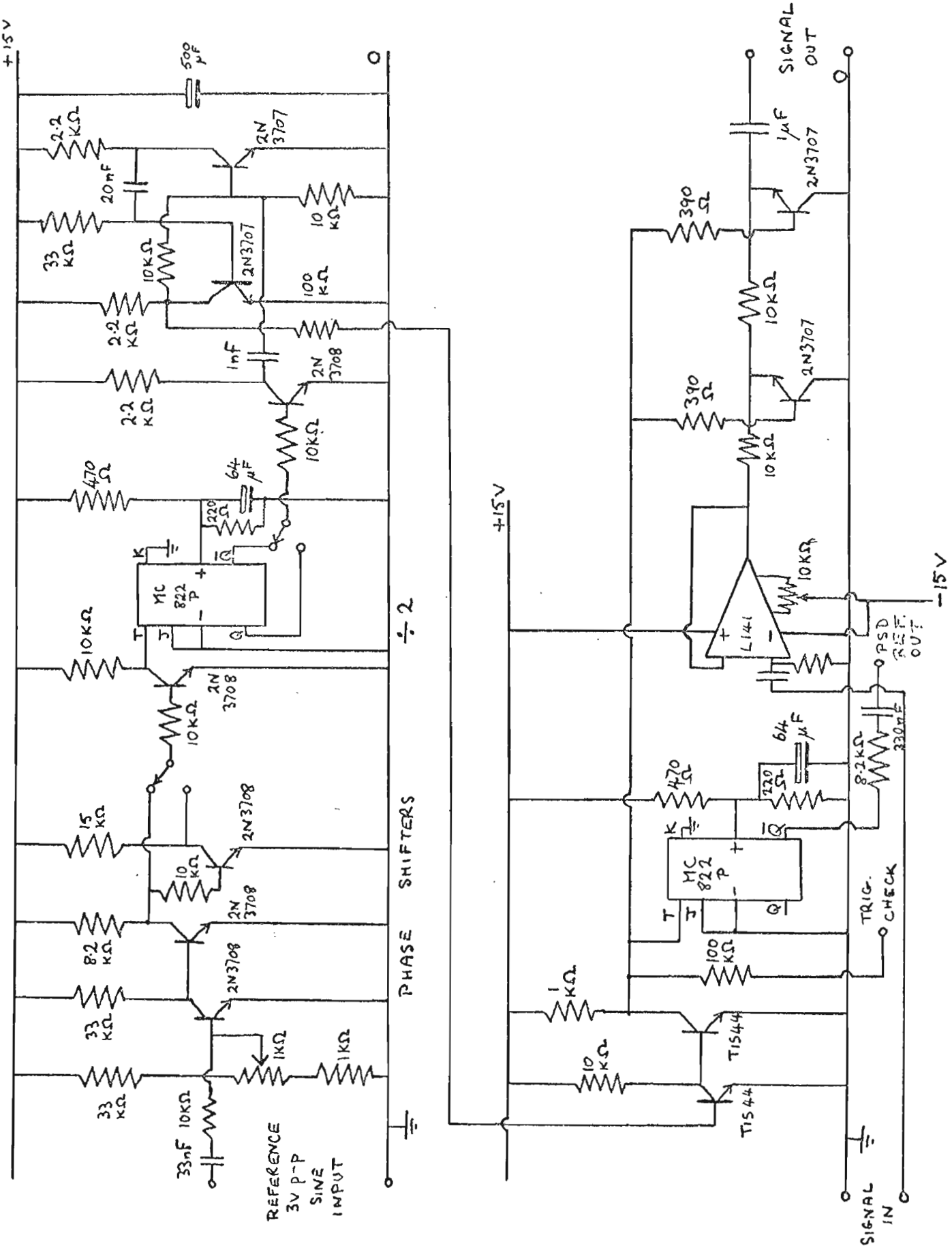

Fig. 2.4 Signal blanking circuit

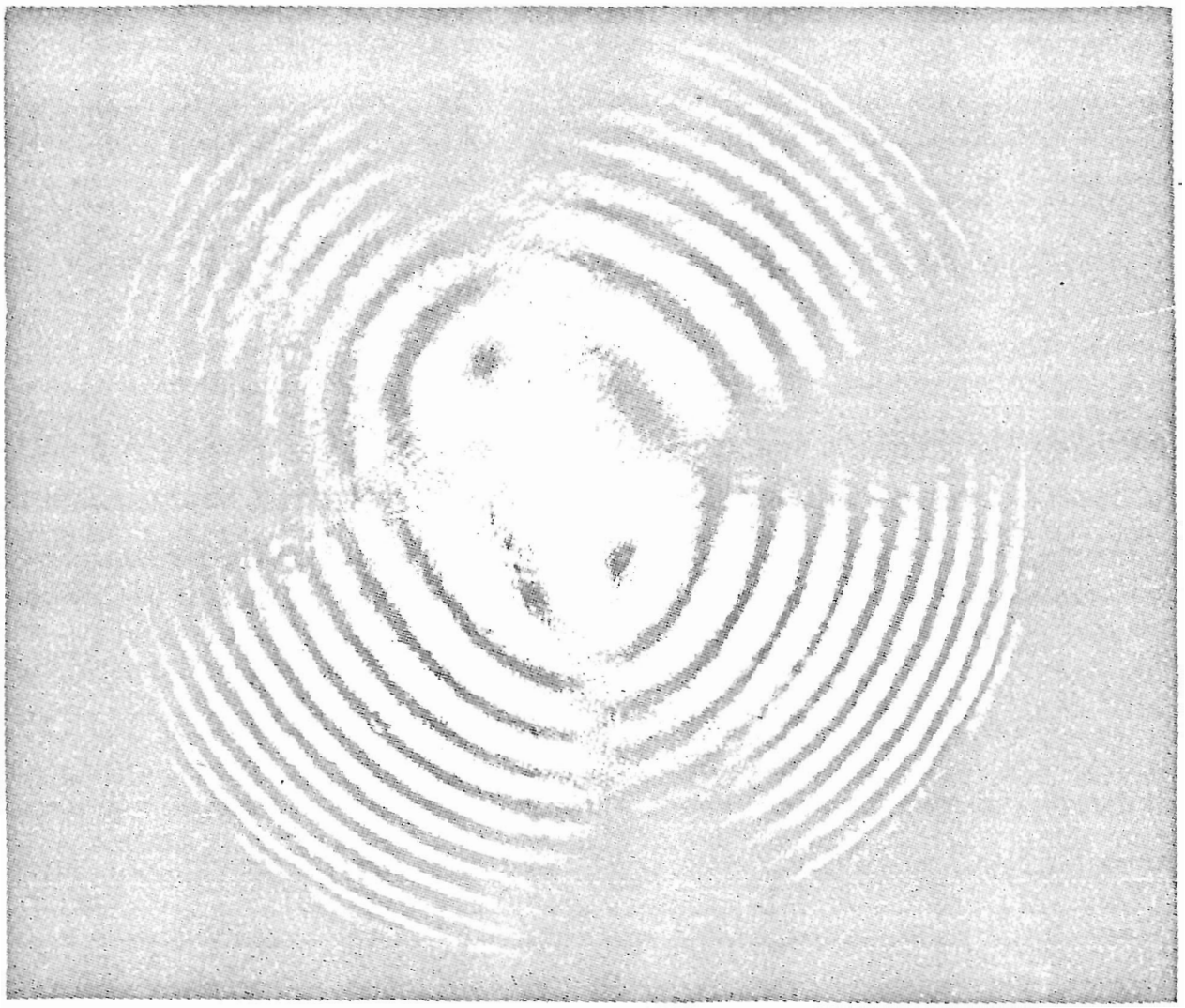

Fig.2.5a Strain birefringence of F7 rod, not annealed

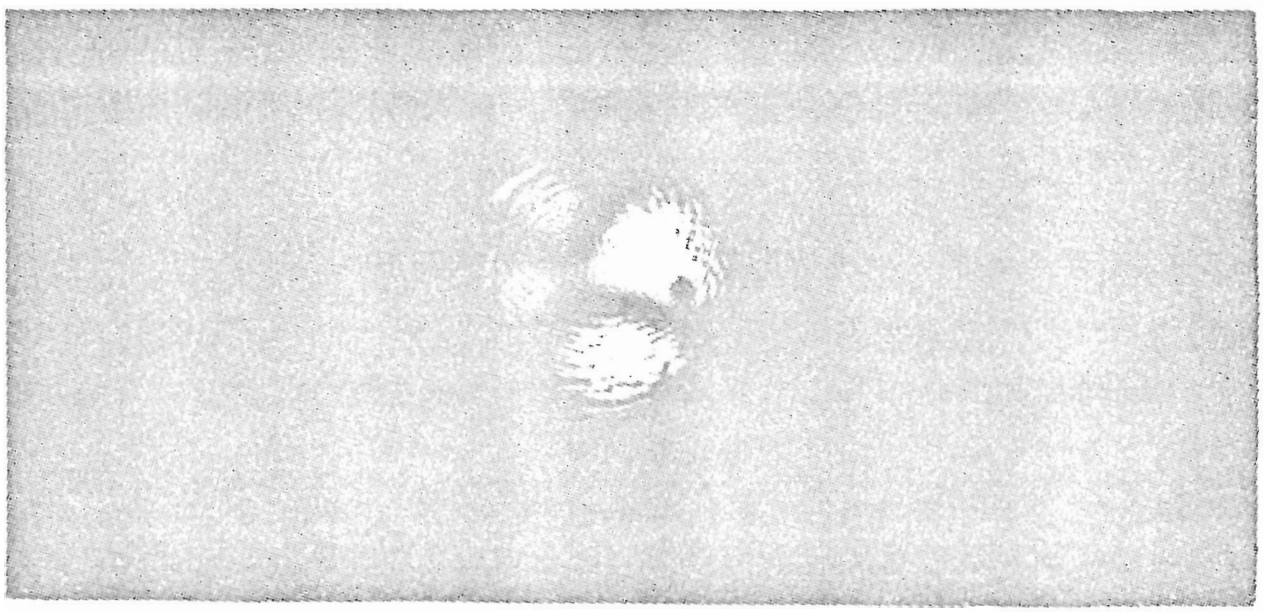

Fig. 2.5b Strain birefringence of F7 rod, annealed

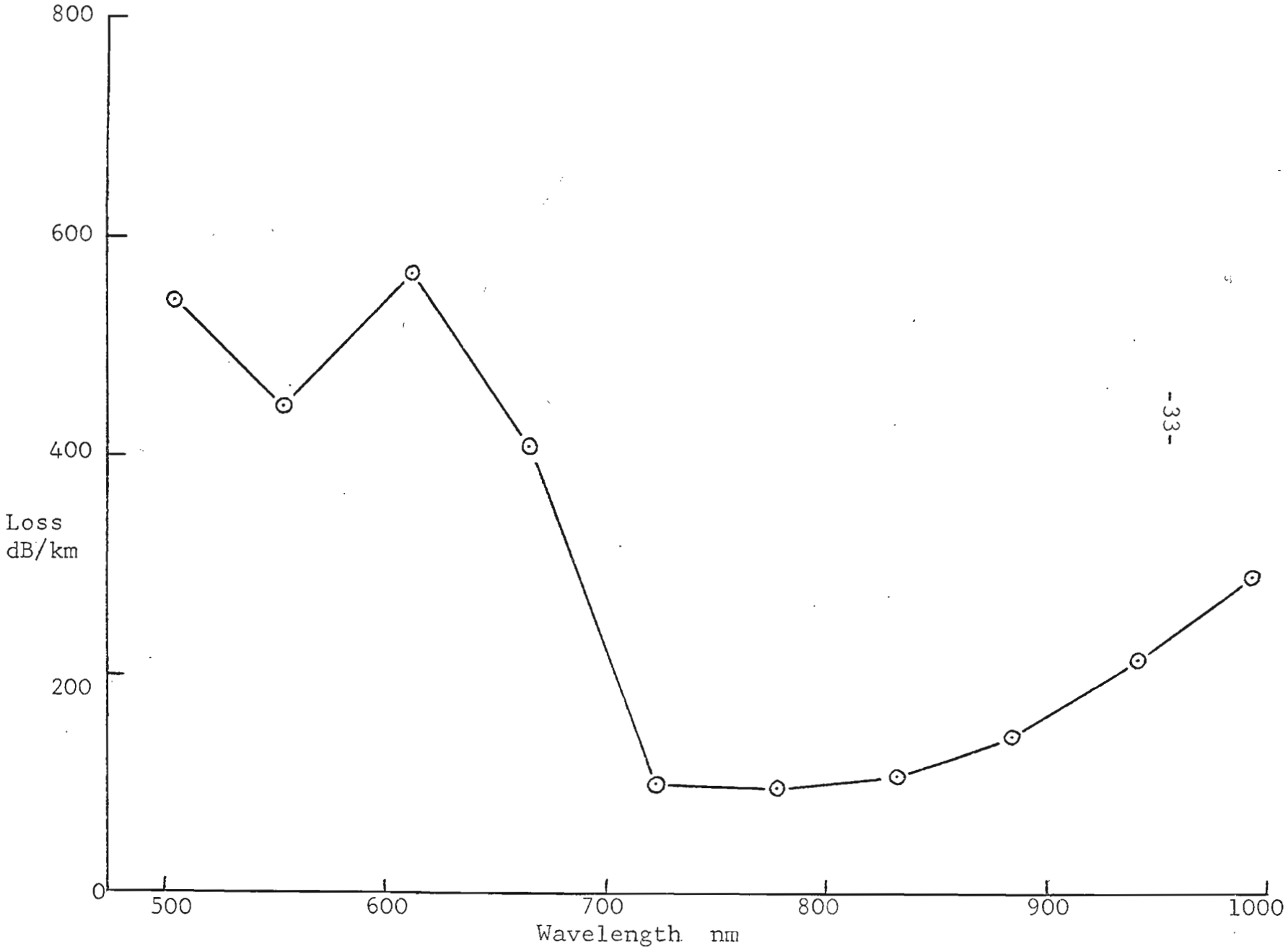

Fig. 2.6 Attenuation vs. wavelength, F7

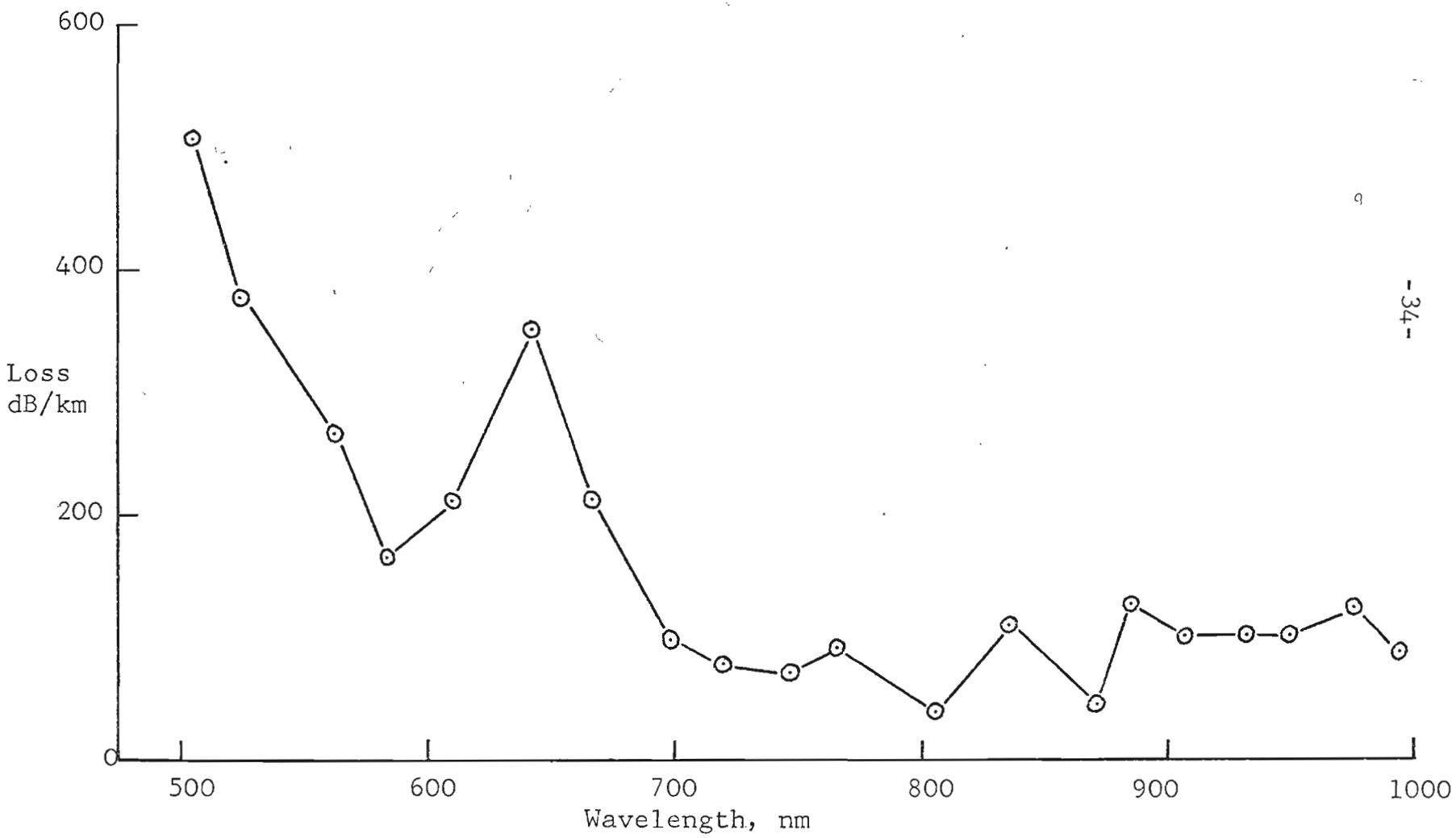

Fig. 2.7 Attenuation vs. wavelength, F2

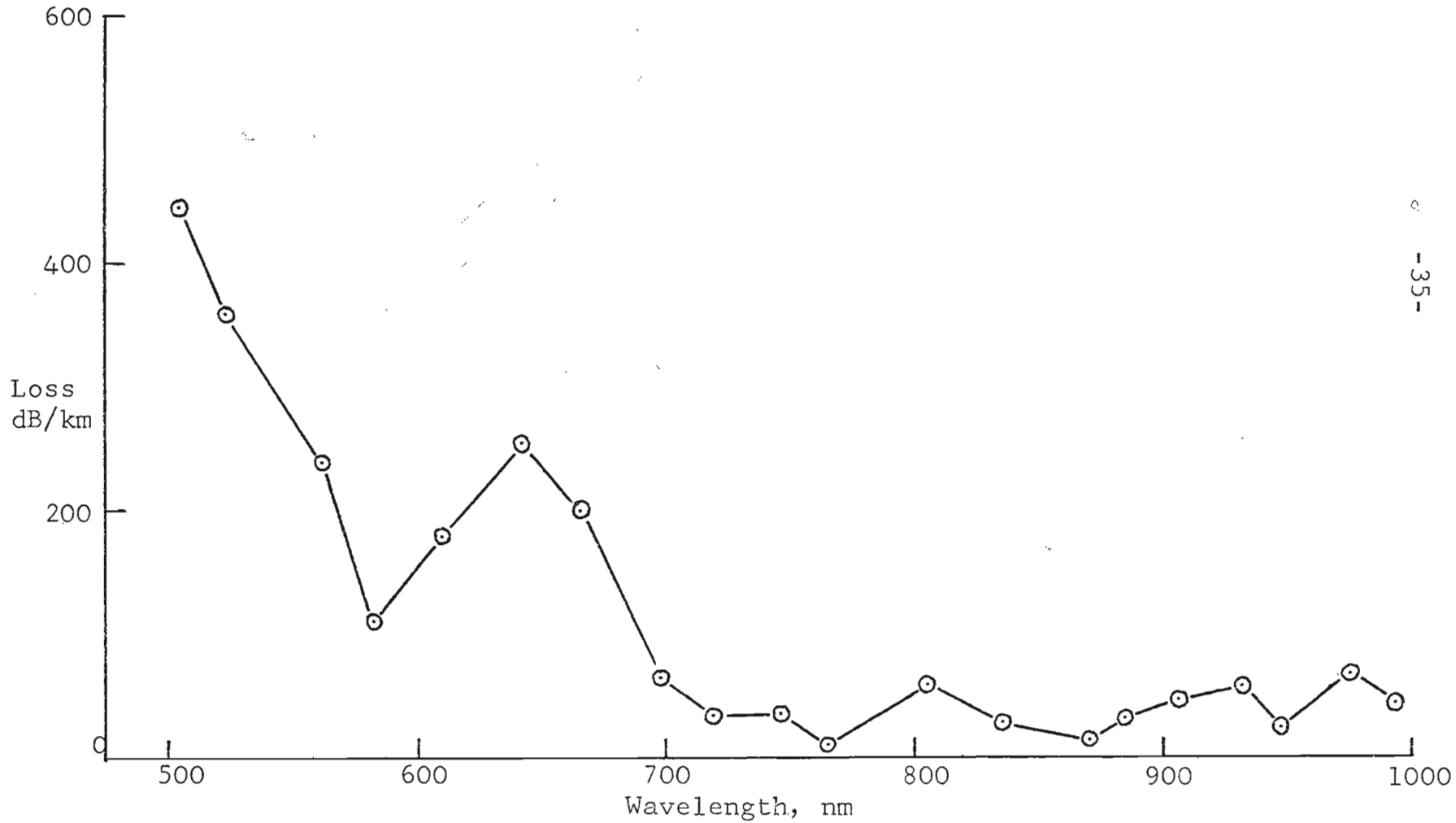

Fig. 2.8 Attenuation vs. wavelength, F8

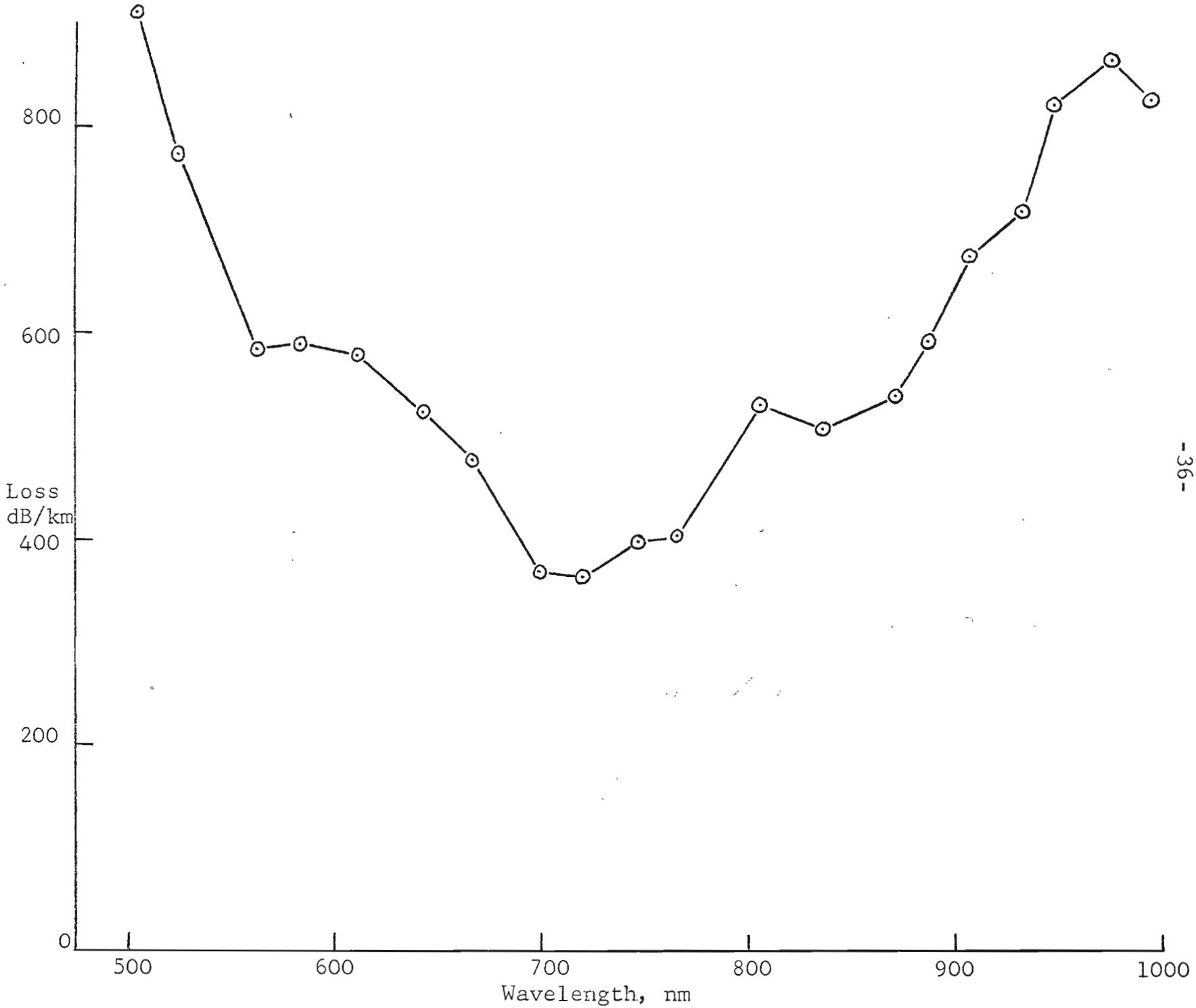

Fig. 2.9 Attenuation vs. wavelength, SK16

3. A PHOTOMETER TO MEASURE LIGHT SCATTERING IN OPTICAL GLASS AND GLASS FIBRES

3.1 Introduction

Interest in the development of cladded glass fibre, optical waveguides for long-distance, wide-bandwidth communication systems has prompted the study of losses in high-quality optical glasses. An economic figure for the overall loss permissible in such a system has been quoted as 20dB/km, equivalent to an attenuation of $4.6 \times 10^{-5} cm^{-1}$, and it is clear that the raw glass used in the manufacture of the glass fibre guide must have a bulk optical loss below this figure. Without considering the extra losses introduced in fibre drawing, the two sources of loss in the bulk glass may be divided into absorption loss due to ionic absorption bands, and scattering loss, possibly due to random density variations, concentration fluctuations characteristic of a frozen solution of inclusions of alien matter.

Previous measurements of scattering losses in optical glasses[1] have provided evidence for the supposition that the main scattering mechanism in such glasses is of a Rayleigh or Rayleigh-Gans type. This is in accordance with X-ray diffraction studies by Warren[2] which led to the conclusion that glasses had the microscopic structure of a liquid with small scattering centres caused by thermal density fluctuations, frozen into the glass on cooling from the liquid state. The spectral range of interest in a fibre-optical communication system, where the bulk losses are generally at a minimum, extends from 500nm to 1um. Since Rayleigh type scattering decreases rapidly with increasing wavelength, the scattering loss at 1um would be very low for good quality glass. Therefore an apparatus was required that could measure the angular scattering distribution within the above wavelength range down to a level equivalent to a scattering loss of 0.2dB/km at the long wavelength end of this range. Previous work on light-scattering in glasses, in common with scattering measurements on liquids, appear to have been confined to the visible region of the spectrum, while commercial light-scattering photometers are normally restricted to a few visible emission lines from standard arc sources. The apparatus to be described employed a high-pressure xenon arc, with an output approximating to the emission from a black body at 6000^{o}K[3] from which a particular narrow wavelength band in the required range can be selected using a multilayer dielectric interference filter. Measurements can also be made at a wavelength of 633nm using a 1mW He-Ne laser source.

It is intended to measure the fractional scattered power in a small solid angle at different angles and then to integrate over all angles (assuming a theoretical Rayleigh curve through the experimental points) to find the fractional scattering loss per unit length of sample. In order to neglect the error incurred due to the finite acceptance angle, an angular resolution of less than 9^{o} must be achieved[4].

The experimental technique involves projecting a quasi-parallel beam of light from the arc lamp through a sample of the optical glass under investigation, and measuring the intensity of the scattered radiation emerging at various angles from a specified volume inside the sample. The latter is in the form of a rod of square cross-section with highly-polished ends. The beam propagates in a direction parallel to the rod axis and the scattered radiation is viewed through one of the polished sides. The detector is pivoted so that it moves in an arc about the centre of the rod, and in a plane including the rod axis. The amount of light scattered at any given angle may be compared with the intensity of the transmitted beam, since the total optical loss through the sample will be small, and hence the fractional scattering loss per unit length which occurs at the selected angular direction can be obtained. It was decided not to rely on measurements from known scattering materials, such as benzene, to calibrate the transmitted beam, but to attenuate the beam by a known amount and to measure its intensity with the same detecting system as used for the scattering measurements.

3.2 Scattering Photometer.

3.2.1 Optical System

The arrangement of the experimental apparatus used to measure the angular variation of light scattering by optical glass samples is shown in figs.1 and 2. The glass sample is in the form of a cuboid, 2cm x 2cm x 10cm and is placed in a long rectangular trough. The inside of the trough is blackened, and provided with baffles, to reduce the intensity of stray light. Apertures in the baffles allow a light beam entering at one end of the trough to pass down it, close to one of the sides of the trough. The sample is placed against a rectangular slit 2cm high by 5mm wide in the side, through which a region in the centre of the sample is visible. Light scattered from the input beam emerges from the slit, and is received by a detector head rotating horizontally about the vertical axis of the slit, in a semi-circular trough. The rectangular and semi-circular troughs are filled with a refractive-index-matching liquid, the particular liquid used depending on the refractive index of the glass being measured. The ends of the rectangular trough are provided with glass windows; the window remote from the light source is not perpendicular to the beam, so that light reflected from its surfaces does not return to the sample but is diverted and absorbed by the baffles. By using an index-matching liquid, corrections to the results because of refraction are much reduced, and a larger range of scattering angles may be used. Scattering from the ends of the sample is also reduced. The angular range that can be covered is from 20° to 160° to the optical axis and is limited by mechanical factors.

A diagram of the detector head is shown in fig.3. Light scattered horizontally is reflected upwards by the prism, through a bank of filter holders and a collimating lens onto the end of a 4.5mm diameter glass fibre light guide. A rectangular aperture in front of the lens determines the acceptance angle of the scattered light. The position of the input end of the light guide is adjustable and is arranged so that an image of the circular end of the guide is focussed onto, and completely covers, the rectangular slit through which light is scattered Thus the image of the slit is focussed onto the end of the light guide and is smaller than the guide. A machined socket locates the guides in the detector head.

In order to obtain absolute scattering measurements the power in the input beam must be compared with the scattered power. Since, during measurement of scattered power, the light passes through a considerable length (about 30cm) of index matching liquid (which may absorb up to 70% of the light at the longest wavelength used) the attenuation of the liquid must be taken into account. The input beam is therefore passed through a trough of the same liquid, the length being the same as the path length in the scattering apparatus. Corrections for window and sample reflections must be made. Because of detector limitations the incident beam cannot be measured directly and known attenuators must be used.

The use of neutral density filters presented many problems as the input beam must be attenuated by as large a factor as 10^{10} in some cases

in order to operate the detector in its linear region. This involved the use of perhaps five filters, each with an attenuation of 100 times, which required a great deal of very accurate calibration to prevent large overall errors. Also the so-called 'neutral density' filters obtainable showed a large wavelength dependence of attenuation, having an attenuation of 100 times in the visible and only about 10 at 850nm. Thus with five filters in the detector head the sensitivity at 850nm is approximately 10^5 times that in the visible. The problem is made worse by the peak sensitivity of the S1 cathode lying near 850nm. When working in the visible region, the large increase in sensitivity in the near infra-red would necessitate the use of narrow band filters with very high infra-red rejection in order to ensure that the detector was actually measuring the required signal. Because of these difficulties, the use of neutral density attenuators was rejected.

Some attenuation was carried out by reducing the aperture size in the detector head with specially measured apertures, but the beam was mainly attenuated by shining it normally onto a white diffusing screen, and viewing the spot on the screen with the detector head from a distance of about 70cm. Thus it was not necessary to determine additionally the sensitivity of the detection system. The screen used could be coated with a fresh layer of smoked magnesium oxide or a thick coating of barium sulphate paint, or replaced by a disc of pressed barium sulphate powder. Over the wavelength range of interest, the last two types of diffusing screen have an absolute reflectance greater than 0.99^5 and

the angular reflectance of barium sulphate powder is nearly perfect. After some initial experiments with the other two types of diffuser, the pressed barium sulphate powder diffuser was used for incident beam attenuation.

3.2.2. Light Source

The light source is a PEK 75W high-pressure xenon arc lamp, mounted in a convection-cooled lamphouse as shown in fig. 4. The mounting allows the arc to be easily aligned with the optical system. Very little stray light emerges from the cooling openings. A magnified image of the 0.5mm diameter pinhole is formed by the lens, of focal length 3cm, at a distance of 33cm. This image is the same diameter (5mm) as the lens aperture and thus a parallel beam of 0.5cm diameter extending over 30cm is produced. Thus all the light passes through the glass sample and the maximum angular spread of the beam is 0.03 radian.

The lamp must be operated from a constant-current power supply to avoid output fluctuations. In addition the lamp requires an r.f. spark to ignite it, and an instantaneous starting voltage several times higher than the normal operating voltage must be applied. This requires additional circuitry, and precautions must be taken to prevent starting transients from damaging the power supply.

A simple starting system has been designed, and the complete circuit is shown in fig. 5. The power supply used is an Advance PM54 modular unit, and r.f. is generated by a Wotan 24000 ignitor.

To supply the initial starting voltage, the output from a 10A 110V isolating transformer is full-wave rectified and connected to the lamp in series with a large ballast resistor and choke. The lamp itself draws 6.3A at 12V. To start the lamp, switches S_1 and S_2 are set to the 'start' position, thus short-circuiting the output from the power supply, and applying the starting voltage directly across the lamp. On pressing the 'start' button, the arc is triggered, and the lamp immediately draws current through the ballast resistor from the d.c. supply, dropping the voltage down to 12V. The lamp is then running, and will continue operating without the stabilised power supply in circuit. To connect the power supply, the changeover switch S_2 is set to 'run'. On breaking the first contact, the power supply is connected in series with the circuit, controlling the current drawn from the rectifier. On making the second contact the unstabilised d.c. supply is shorted out, all the current being distributed in the ballast resistor. S_1 is then switched off, leaving the lamp running directly from the stabilised power supply. The power supply is, of course, generating current when shorted out, thus S_2 must be capable of carrying 13 amps.

3.2.3 Detection System

The scattered light collected by the detector head and focussed onto the light pipe is directed onto the cathode of a photomultiplier. A diagram of this arrangement and of the cooled housing is shown in

fig.6. To cover the wavelength range required, an EMI 9684 photomultiplier with an S1 type of photocathode is used, cooled in a liquid nitrogen enclosure to about $77^{o}K$ to reduce the dark current. The use of a sealed-in light pipe has obviated problems of the misting-up of input windows. Care must be taken to use only the most sensitive part of the photocathode[6]. In view of the low light intensities to be measured, and the small (order of 0.2%) quantum efficiency of the S1 photocathode, it was decided to use a photoelectron-counting technique in preference to the more usual phase-sensitive or synchronous detection. The signal/noise ratio of counting techniques at very low light levels has been found to be as good as, or superior to, the phase-sensitive detection method[7,8], while long integration times present no problems. The counting system shown in fig.7 is simple and relatively inexpensive and the numerous readings of the digital output are easy to record.

The photomultiplier dynode chain is fed from a stabilised EHT supply, and the dynodes give an electron multiplication of about 10^{6}. Thus a photoelectron gives rise to a charge pulse of 1.6×10^{-13}C at the anode, which has a load resistance of 4.7kΩ. A valve preamplifier (fig. 8) is used which has a maximum voltage gain of 15 and has a total input capacitance, including the photomultiplier, of 24pF so that an average photoelectron produces a 7mV pulse at the anode, and about 100mV at the preamplifier output.

The preamplifier is followed by further amplification and a pulse height discriminator circuit, fig. 9. In the first pulse height

discriminator used it was possible to count pulses of height between two selected voltage reference levels resulting in the removal of the pulses which were of very low or very high amplitude. The low amplitude pulses represent mainly amplifier noise, pick-up noise and thermal noise from the dynode chain, whereas the very high amplitude pulses can occur as a result of cosmic rays or bombardment of the cathode by positive ions in the tube[9]. It appeared experimentally that the high amplitude pulses were very infrequent and the added complication of the upper discriminator level and gating circuits (the provision of which slightly lowered the frequency response of the whole circuit) was thought to be unnecessary. The discriminator circuit has since been simplified to that shown in fig.9.

The dark pulse count of the photomultiplier when cooled is expected to be of the order of 100 pulses per second (from tube data). The discriminator gating level was adjusted, with a small illumination level, for optimum signal/noise ratio when the dark current actually measured was about 15 per second. A count is usually taken over a 10s period which is measured by a crystal-controlled oscillator. The amplifying, discriminating and counting circuits together are limited to about 2MHz maximum rate, and thus about 1% of pulses might be under-recorded, due to coincidence, at a count rate of about 20kHz.

3.3 Calculations on Scattering Photometer

3.3.1 Sensitivity and Angular Resolution of Scattering Apparatus

The output beam from the xenon arc is collimated and filtered to pass only a narrow wavelength band about 10nm wide. The brightest part of the arc was extremely small, and did not completely fill the aperture in front of the arc. On inspecting the magnified image of this aperture, it was seen that no more than a tenth of the source aperture was filled by the bright spot of the arc. Assuming this spot to be a black body radiator at $6000^{o}K$, the power in the beam after filtering was calculated to be $2 \times 10^{-5}W$. Of the scattered light, the detector accepts a solid angle of 1.5×10^{-3} steradian, scattered from an incident beam length of 0.5cm. A count of 10 photoelectrons per second corresponds to about $2 \times 10^{-16}W$ incident on the detector head, or $1.3 \times 10^{-13}W$ scattered per steradian. An isotropic Rayleigh scatterer would direct $3/16\pi$ per steradian of the total scattered power at 90^{o} to an unpolarised input beam, so that in the above example the total scattered power is about $2 \times 10^{-12}W$, equivalent to an attenuation by scattering of $2 \times 10^{-7}cm^{-1}$. This attenuation corresponds to a scattering loss of less than 0.1dB/km.

The net angle of acceptance of the detector head when measuring scattered light is 1^{o} in the horizontal plane and about 4^{o} in the vertical plane. Any divergence of the input light beam lowers the system resolution further. When a helium-neon laser is used the input collimation is very good and the resolution is given by the receiving

where $\delta\Omega_1$ = acceptance solid angle of scattered light calculated in the sample

a = aperture attenuation for incident beam measurement

ℓ = length of sample viewed = scattering slit width

Δ = diffusing screen attenuation factor = $\frac{\delta\Omega_2 . \mathcal{E} . \cos \phi}{\pi}$

$\delta\Omega_2$ = acceptance solid angle of detector head for incident beam measurement

$\mathcal{E}$ = reflectance of diffuser

ϕ = angle between viewing direction and normal to diffuser surface.

3.4 Experimental Method and Initial Checking of Equipment

3.4.1 Setting up and Checking of Detector System

(a) Discriminator Level Setting

The statistical variation of light counts and noise counts from the detector system necessitates care to obtain the best signal to noise ratio. This is not the ratio of signal count to noise count, as the signal is obtained by subtracting the noise count from the tota count and it is only the statistical variation of these quantities which gives rise to noise. The signal to noise ratio may be expressed as the ratio of the signal count obtained, to its standard deviation[9]. This deviation is a result of variations in both total count and noise count.

The low amplitude counts which represent largely noise signals can be removed by the pulse height discriminator as described previously. It was however necessary to select an optimum discriminator level, taking into account signal to noise ratio and also immunity to outside electrical interference which may be of an extremely random nature. Initial experiments suggested a slightly lower discriminator level than was finally used but then the system was somewhat sensitive to random interference. The interference was reduced considerably by suitable mains filtering but it was thought advisable to increase the discriminator level in order to increase noise immunity. This increase removed virtually all electrical interference whilst it only reduced the signal to noise ratio, in the absence of interference by about 20%.

(b) Effect of Cooling Photomultiplier Tube

The effect of cooling on the dark count is shown in fig.(10). The nitrogen tank was filled at time t=0 and the dark count was noted for a period of 3 hours. The temperature of the tube face was monitored throughout with a copper/constantan thermocouple The measured temperature of the tube went down to -200°C and the average noise count settled to about 14 cts/sec after passing through an erratic period between 20 and 30 minutes after cooling. This erratic nature was always observed a short while after cooling but the noise count settled down to its low value of 14 cts/sec after about 90 minutes of cooling. The tube was always cooled for at least 3 hours before taking measurements. A single charge of nitrogen in the cooling reservoir lasted for about 8 hours.

(c) Stability and Linearity of Detector

As the detector was used to compare incident and scattered intensities it must be both stable and linear over the range of intensities measured. The stability was investigated using a tungsten source powered from a stabilised supply. The tungsten lamp was placed close to a scattering screen and some of the scattered light was incident on the detector head, which contained several neutral density filters. The variation of the signal count with time is shown in fig.(11). This shows a total variation of only ±½% over a period of 3 hours which is well within requirements.

The linearity of the detector must be checked over a wide range of input signals as very low scattered light counts are usually obtained at wavelengths near 1um. These counts must be compared to the count obtained when making incident beam measurements. Even when using 1mm diameter apertures in the lamp housing and in the detector head, the latter is about a factor of 100 larger than the former. It was decided to check the linearity using geometrical attenuation by changing aperture sizes. A slit could be placed in the detector head to reduce the area of the aperture already present by a known factor (about 6 times). With this aperture present the detector head was used to monitor white light scattered from a diffuse screen at a distance of around 70cm from the screen. With two neutral density filters and two polaroids in the incident beam, the intensity of the beam was adjusted using the polaroids to give a signal count of around 40cts/sec (compared to the dark count of about 14cts/sec). The signal count was measured accurately with a long averaging period of about 5 minutes. The slit was then removed from the detector head and the new signal count was obtained. The reduction of signal count caused by the slit was measured accurately by repeating the above procedure several times in order to minimise the effects of drift in the equipment. The attenuation was found to agree with geometrical predictions to within ±1% The same procedure was then repeated but this time the input intensity with the slit present was adjusted to give a signal count equal to that with the slit out in the

previous case, and the slit was then removed and the new signal count noted. The new attenuation measured was again within 1% of that expected). By continuing in this way the detector was shown to be linear to within 1% from a signal count rate of around 40 cts/sec to one of 10,000 cts/s This linearity range is well within the limits required. The departure from linearity is shown in the graph in fig.(12). Having shown the detector to be linear over the above range, further points on the graph were obtained as follows. By taking a signal count near the top end of this range with the slit present in the detector head, the count obtained on removal of the slit was noted. The departure from linearity can be found by comparing the count measured, with the count expected if the detector were linear over this range also. In fig.(12) the readings with the slit present are denoted with a circle whereas those with the slit absent are denoted by a square. From the graph it is apparent that the detector departs significantly from linearity at counting rates greater than 17kHz. This is about the rate expected from the previous consideration of pulse coincidence in the counting circuits. In order to ensure good linearity, the measured light was attenuated to give a counting rate less than 10kHz for all measurements.

3.4.2 Other Equipment Checks

(a) Xenon arc stability of output power

The stability of the xenon arc lamp was investigated using a

Spectra Physics laser power meter in conjunction with an avometer. The output beam from the arc lamp was directed into the detector head of the power meter and the current output was monitored on the avometer for a period of seven hours. The graph of current against time is shown in fig. (13). The standard deviation of the measured current is 1.4%, showing the stability of the lamp to be at least as good as±2%.

(b) Methyl Salicylate absorption loss

The index-matching liquid finally selected was methyl salicylate. Although the absolute absorption loss of the methyl salicylate is not required in the calculation of Rayleigh's ratio, it is of use to know the magnitude of the loss in order to estimate the loss in sensitivity when using it as the index matching liquid. The loss was measured for a long trough containing methyl salicylate with a total path length of 32.4cm. This trough was inserted in the beam when making input light measurements. The filtered light from the xenon arc is allowed to impinge on the scattering screen and the spot is viewed with the detector head containing a small aperture. The light count is measured when the trough is not present. The trough is then placed in the incident beam and the new light count measured. The process is repeated using each of the narrow band filters to find the loss at each wavelength. The loss must be corrected for reflection losses at the windows at each end of the trough, which are calculated from the measured refractive indices. (The absorption loss of the glass slides used for the windows was negligible at all wavelengths used.)

The maximum absorption loss occured at 993nm where the transmission was only 10%. The transmission was far greater for the other wavelengths used, being close to 100% at all visible wavelengths.

(c) Scattering screen cosine law check

The calculation of Rayleigh's ratio assumes a perfect diffusing screen, which when illuminated normally gives a scattered radial intensity proportional to cos θ where θ is the angle to the normal at which the light is received. The relationship was checked by illuminating the screen normally and moving the detector head around in an arc centred on the point where the incident beam strikes the screen. A polar graph was plotted of light count against cos θ (fig.14). The theoretical cosine variation is represented by the semicircle shown. It can be seen from the graph that the experimental points depart from the theoretical curves by only about 3% at most showing good agreement within experimental error.

3.4.3Measurement of Scattered and Straight Through Light

(a) Alignment Procedure

The optical arrangement for scattering measurements is shown in figs. (1) and (2). The detector head must be adjusted to receive all the light scattered from the glass in the required receiving angle. This is ensured by inserting into the detector head a second light guide similar to that fixed to the detector system, and shining light from a tungsten source into the other end. The image of the end of the light guide is then projected onto the area near the slit in the

horizontal trough. The image can be focussed, and its position adjusted to cover the whole of the slit area, by using the adjustment screws on the detector head. When the image covers all the slit, all light passing out of the slit and through the receiving aperture will be focussed onto the end of the detector light guide when it is inserted.

A similar setting-up procedure is used for the incident light intensity measurement. Here the image of the light guide is projected onto the scattering screen and is focussed and adjusted to completely cover the bright spot from the incident beam.

(b) Reduction of the effects of drift

When measuring Rayleigh's ratio in the above manner the apparatus is used to alternately measure incident and scattered light, up to 3 measurements of each being taken to minimise drift of equipment between incident and scattered measurements.

When polar scattering diagrams are required it is not necessary to measure the incident beam intensity. In this case the effect of drift is minimised by measuring intensities at each angle required and then repeating these measurements several times. By taking sufficient sets of measurements, the relative intensities received at each angle can be found accurately even when the light source intensity is drifting significantly.

A further example of the way in which drift effects can be reduced occurs when the variation of scattered intensity with wavelength is required. With the methyl salicylate trough in both beams the only

significant factors giving rise to variation with wavelength are the actual variation of Rayleigh's ratio with wavelength and the relative intensity of the light source at each wavelength. The second factor is removed when the ratio of scattered to incident light is taken. In order to reduce drift effects when finding the wavelength variation in this way, the scattered light is first measured at each wavelength and then the process is repeated several times. The same procedure is carried out when measuring the straight through intensity. Thus the variation of scattered light intensity with wavelength can be found free from the effects of drift.

3.5 Results

Initial experiments have been carried out on two samples of optical glass supplied by Schott and Co., a lead flint glass, type F7, and a dense barium crown glass, type SSK2. The polar scattering diagrams for $U_h(\theta)$ and $U_v(\theta)$ were obtained at 633nm using the He-Ne laser source, and are shown for the respective glasses in figs. (16) and (17). Superimposed on the experimental points are theoretical curves of $U_v(\theta)$ and $U_h(\theta)$ calculated from the depolarisation

$$\rho(90) = \frac{U_h(90)}{U_v(90)}$$

measured perpendicularly to the input beam. The 'peaks' at about 37° and 143° are attributable to light scattered from the entry and exit faces of the sample being reflected into the detector from the polished back face of the sample. This is confirmed by the fact that the 'peak' angle agrees with geometrical predictions and varies as the sample is moved in the longitudinal direction. In order to eliminate these reflections in later measurements, the backs of the cuboids are to be cut at a suitable angle, leaving rods of approximately triangular section. Throughout the angular range over which the photometer can be used the scattering in our samples of F7 and SSK2 glass are within 3% of the ideal Rayleigh curves except where these 'peaks' occur. Curves of similar shape have also been obtained at other wavelengths. It is therefore not unreasonable to compute the total scattering loss by integrating, on the basis of the experimental results, over a solid angle of 4π assuming a Rayleigh scattering law.

Thus the scattered light has been measured at specified angles over the whole wavelength range and the computed variation of scattered power per unit length with wavelength is shown in figs (18) and (19). It can be seen that for both glass samples the scattered power varies as $\lambda^{-4.5}$. The wavelength of particular interest for fibre optical communication applications is that corresponding to the output of a gallium arsenide semiconductor laser operated at room temperature, namely 900nm. At this wavelength the bulk scattering loss of the F7 sample is 4.3dB/km, and that of the SSK2 sample is 5.0dB/km. These figures are considerably less than the total allowable loss in an optical communication system. At shorter wavelengths the loss by scattering increases to about 20dB/km at 630nm for the F7 sample.

Results have also been obtained for a fused silica sample (Corning 7940) supplied by Dr. H. N. Daglish. These results agree closely (within 2%) with results Dr Daglish obtained for the same sample at 900nm Dr Daglish's results were obtained by extrapolation of results obtained at shorter wavelengths using a mercury arc line source. The scattering diagram and scattering attenuation vs wavelength plots are shown in figs. (21),(22).

The calibration of the instrument has been checked by measurements of two samples of commercial high-purity benzene and also on one re-distilled sample. The scattering attenuation coefficient α for a sample of benzene is shown as a function of wavelength in fig.(20) and varies at $\lambda^{-4.0}$ which corresponds to ideal Rayleigh-type scattering as might be expected. R(90) has

has been found at 546nm and compared with some previous calculated and experimental values[10]. For the two commercial samples $R(90) \times 10^5$ was found to be 1.67 and 1.81cm^{-1} respectively. For the redistilled benzene $R(90) \times 10^5$ was 1.65cm^{-1}. Values calculated[10] for pure benzene by two different methods are 1.55 and 1.64cm^{-1}, while selected previous experimental values[10] are 1.54, 1.58 and 1.60cm^{-1}. In view of the measured wavelength dependence and the difficulty in obtaining dustfree benzene the agreement is satisfactory.

3.6 Measurement of Fibre Scattering

(a) Using existing apparatus

Using the scattering photometer in unmodified form it was possible to measure angular scattering functions of fibres over a limited angular range. This was achieved by mounting the fibre behind and close to the existing window in the horizontal trough and measuring as before. The liquid in the tank should match the refractive index of the cladding in order to obtain the scattering distribution from the core-cladding interface. The problem of finding a suitable non-toxic matching liquid is simplified here as the refractive indices of cladding materials used so far are considerably lower than those of the core glasses, (e.g. pyrex cladding tube n_o = 1 475, MEI cladding tube n_D = 1.487) enabling the use of harmless liquids such as liquid paraffin (n=1.47-1.48).

A scattering diagram obtained in this manner is shown in fig. (23). The fibre used had an F7 core and pyrex cladding and illumination was from an unpolarised 633nm He-Ne laser source. The length of fibre between source and photometer was two metres and the fibre was illuminated along its axis by the unfocussed laser beam. Light propagated in the cladding was removed by a lossy medium on the outside of the fibre. From the diagram it may be seen that the majority of scattering may occur at angles less than 25^o and greater than 155^o. As the photometer was not designed to measure low angle scattering it was clearly unsuitable for fibre scattering measurements and therefore considerable modification to the existing apparatus was necessary.

(b) Modification to apparatus

The principle modification necessary is the provision for measurement at low scattering angles. Several factors limit the angular range of the apparatus. They are :- (i) Physical restriction on the movement of the detector head; (ii) Thickness of the window which restricts the scattering length; (iii) Poor index matching at the glass liquid boundary gives rise to total internal reflection at angles close to axis; (iv) Poor separation of incident beam and scattered beam. With fibres the last factor is not a serious problem as the incident beam is contained by the fibre.

The modified apparatus enables a full 180^{o} movement of the detector head, unlike the original which could only rotate from 20^{o} to 160^{o}. The window of the new apparatus was made photographically on glass plate and so it is physically very thin enabling measurement at low angles. The index matching system is the same as before with index matching liquid in the semicircular trough. The method of supporting the fibre is to lightly clamp it to the photographic plate forming the window. The glass plate is fastened to a metal plate with a large window and the metal plate is held in position by button magnets set in the central support pillar. The modified apparatus is shown in figs. (24), (25).

Apart from the above modifications the apparatus has now been mechanised by the addition of a D.C. stepping motor which drives the detector head in 1.8^{o} steps to the desired angle. The provision

of this eliminates the need to switch off the photomultiplier supply and switch on the lights for each manual angle adjustment. This should therefore improve the short term stability of the measurements. The driving circuits for the motor are shown in figs. (26) and (27). The number of steps the motor takes is recorded on a resettable electro-magnetic counter enabling remote indication of the position of the detector head, knowing the starting position.

The addition of the stepping motor also makes possible the future automation of the apparatus. Using an electronic counter with output to a tape punch the equipment could be set up to automatically record signal counts, and then the detector head would move to the next position and new counts would be recorded.

The modified apparatus in its semi-automatic form is ready to be tested with fibres. The light propagated will be from a laser or from the xenon arc lamp used previously and it is hoped that useful information on scattering centres will be obtained from scattering diagrams and wavelength dependence of scattering. If the very low angle scattering can be measured effectively it should also be possible to make quantitative total scattering loss measurements although it is thought by the author that this is best done using an integrating sphere technique.

3.7 CONCLUSIONS

A light-scattering photometer has been constructed to measure the scattering loss of optical glass, in the visible and near-infra-red region of the spectrum. The instrument has a high sensitivity and the measured signal counts at different wavelengths are in good agreement with those predicted. The accuracy of the values obtained for Rayleigh's ratio in benzene is satisfactory. The main advantage of the instrument is its ability to measure small scattering losses, down to $5 \times 10^{-7} cm^{-1}$ (0.2dB/km), out to lum wavelength, without the need for a calibration standard. Measurements on samples of F7 and SSK2 glass indicate Rayleigh-type scattering at a level corresponding to 4.3 and 5.0dB/km respectively, at 900nm.

It was found possible to measure fibre scattering in the existing apparatus but only over a limited angular range. A modified apparatus has been constructed for fibre measurements and is expected to be in operation in the near future.

APPENDIX

1. Theory for Small Anisotropic Scattering Centres

Rayleigh's ratio $R(\Theta)$ is the fractional scattered power per unit solid angle per unit sample length viewed at an angle Θ to the input beam axis. Analysing the light scattered at angle Θ, from an unpolarised input beam, into horizontally and vertically polarised intensity components $H_u(\Theta)$ and $V_u(\Theta)$, the depolarisation $\rho(\Theta)$ is defined[6] as $\frac{H_u(\Theta)}{V_u(\Theta)}$.

The attenuation coefficient α due to scattering may be determined by integration of the polar scattering diagram. From a medium whose irregularities are small compared with the wavelength of light, the shape of the scattering diagram may be computed theoretically[11]. Polarising the input beam either vertically or horizontally results in detected scattered intensity components $U_v(\Theta)$ and $U_h(\Theta)$, where U denotes that no analyser was used at the detector head. It is easily shown that

$$U_h(\Theta) = U_h(90) + \left[U_v(90) - U_h(90)\right]\cos^2\Theta$$

and

$$U_v(\Theta) = U_v(90).$$

The depolarisation $\rho(90)$ may be expressed as

$$\frac{U_h(90)}{U_v(90)},$$

and hence α may be expressed[6] as a function of the Rayleigh ratio and the depolarisation perpendicular to the input beam:

$$\alpha = R(90) \frac{8\pi}{3} \frac{2 + \rho(90)}{1 + \rho(90)}$$

The theoretical scattering diagrams for horizontally and vertically polarised incident beams are shown for different depolaristions in fig. (15). The diagrams are normalised to a value of 1 for the vertically polarised case. These diagrams are valid for non-isotropic particles which are small compared with the wavelength.

2. Reflection Loss Correction Factor, $T(\theta')$

(a) Scattered measurements

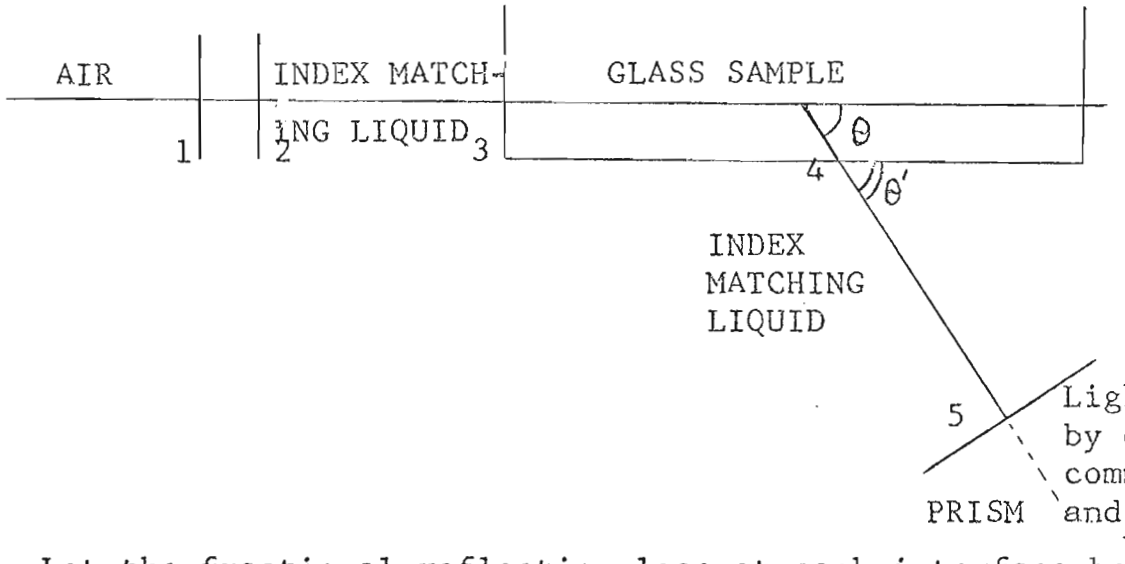

Let the fractional reflection loss at each interface be denoted by r.

The reflection losses at each interface are :-

1) From air to glass slide $= r_{ag}$

2) From glass slide to index matching liquid $= r_{g\ell}$

3) From index matching liquid to sample $= r_{\ell s}$

4) From sample to index matching liquid $= r_{\ell s}(\theta')$

5) From index matching liquid to prism $= r_{\ell p}$

Overall reflection loss is given by :

$$1 - (1-r_{ag})(1-r_{g\ell})(1-r_{\ell s})(1-r_{\ell s}(\theta'))(1-r_{\ell p})$$

(b) Incident Light Measurement

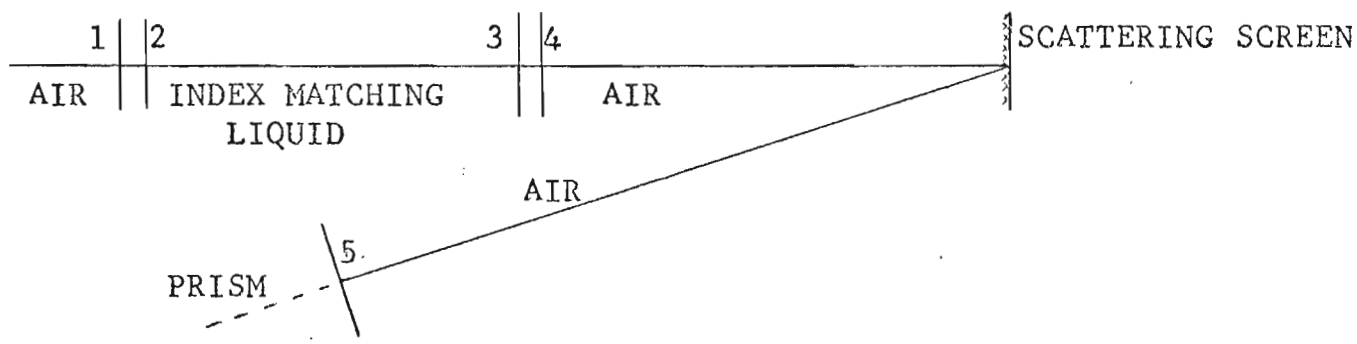

Reflection losses at each interface are :-

1) From air to glass slide $= r_{ag}$

2) From glass slide to index matching liquid $= r_{g\ell}$

3) From index matching liquid to glass slide $= r_{g\ell}$

4) From glass slide to air $= r_{ag}$

5) From air to prism $= r_{ap}$

Overall reflection loss (not including screen)

$$= 1 - (1-r_{ag})^2(1-r_{g\ell})^2(1-r_{ap})$$

From parts (a) and (b) above the factor $T(\theta')$ is given by

$$\frac{(1-r_{ag})(1-r_{g\ell})(1-r_{\ell s})(1-r_{\ell s}(\theta'))(1-r_{ip})}{(1-r_{ag})^2\,(1-r_{g\ell})^2\,(1-r_{ap})}$$

$$T(\theta') = \frac{(1-r_{\ell s})(1-r_{ip})(1-r_{\ell s}(\theta'))}{(1-r_{ag})(1-r_{g\ell})(1-r_{ap})}$$

3. Calculation of Detector Head Acceptance Angle $\delta\Omega$ and Scattered angle, Θ in terms of the scattering angle Θ_L measured in the index matching liquid

(a) Acceptance Angles Expressed in the Index Matching Liquid

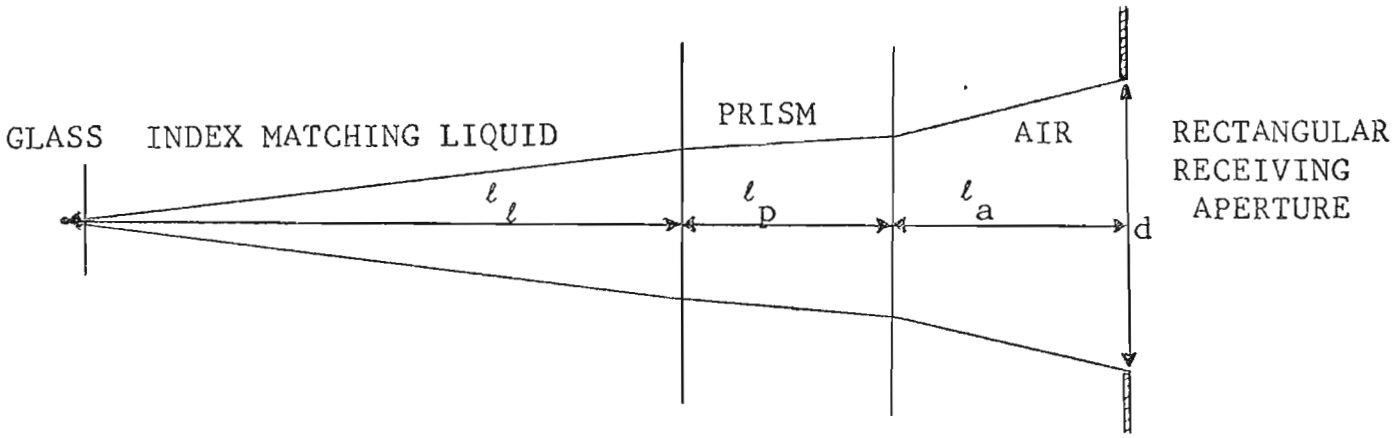

$\Delta\phi$ is the receiving angle expressed in the liquid in the plane considered above.

$\Delta\phi$, if small, is given by $\dfrac{\text{length of the aperture, d}}{\text{'Apparent depth' of aperture expressed in terms of the liquid}}$

$$= \frac{d}{\ell_\ell + \ell_p \frac{n_L}{n_p} + \ell_a \frac{n_L}{1}}$$

In the vertical plane $\Delta\phi = \Delta\phi_v$

$$= \frac{L}{\ell_\ell + \ell_p \frac{n_L}{n_p} + \ell_a n_L} \qquad \text{(i)}$$

where L is the length of the receiving aperture.

In the horizontal plane $\Delta\phi = \Delta\phi_H$

$$= \frac{W}{\ell_\ell + \ell_p \frac{n_L}{n_p} + \ell_a n_L} \qquad \text{(ii)}$$

(b) Conversion of Scattering Angles and Acceptance Angles from the Liquid to the Glass Sample

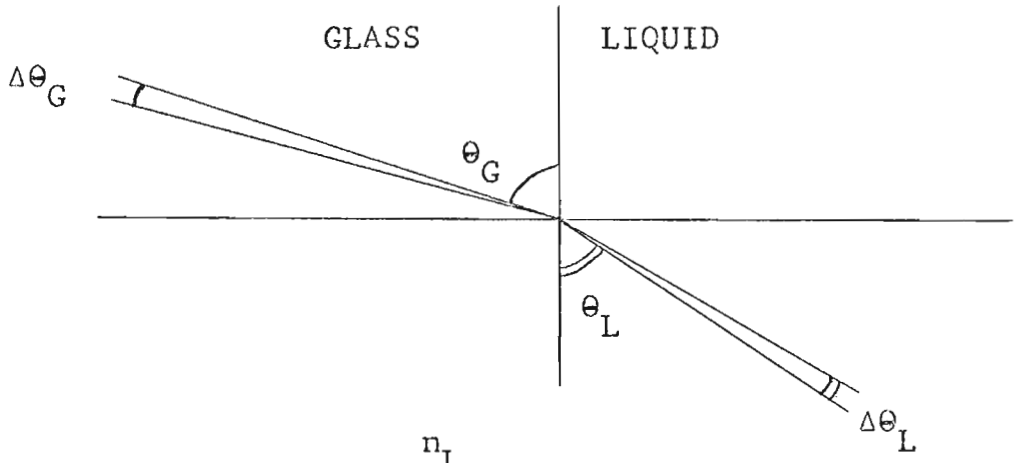

$$\cos\theta_G = \frac{n_L}{n_G}\cos\theta_L \quad \text{Snell's Law}$$

$$\theta_G = \cos^{-1}\left[\frac{n_L}{n_G}\cos\theta_L\right]$$

Differentiating :-

$$\sin\theta_G d\theta_G = \frac{n_L}{n_G}\sin\theta_L\, d\theta_L$$

$$d\theta_G = \frac{n_L}{n_G}\frac{\sin\theta_L}{\sin\theta_G}\, d\theta_L$$

For small $\Delta\theta_G$ and $\Delta\theta_L$:-

$$\Delta\theta_G = \frac{n_L \sin\theta_L}{n_G \sin\theta_G} \qquad \text{(iii)}$$

$$\Delta\theta_G = \frac{n_L \sin\theta_L\ \Delta\theta_L}{n_G \sin\left[\cos^{-1}\frac{n_L}{n_G}\cos\theta_L\right]} \qquad \text{(iv)}$$

Therefore a small angle $\Delta\theta_G$ in the glass can be found from the corresponding small angle $\Delta\theta_L$ in the liquid.

(c) Horizontal Scattering Angle and Acceptance Solid Angle in the Glass Sample

From part (b) the scattering angle Θ in the glass is given by

$$\Theta = \cos^{-1}\left[\frac{n_L}{n_G}\cos\Theta_L\right]$$

where Θ_L is the scattering angle measured in the index matching liquid

When expressed in the glass the vertical receiving angle, $(\Delta\Theta)_v$, is given by

$$(\Delta\Theta)_v = \frac{n_L}{n_G}\Delta\phi_V \qquad \text{from (iv) above with } \Theta_L = 90^\circ,\ \Delta\Theta_L = \Delta\phi_V$$

$$= \frac{n_L}{n_G}\left[\frac{L\, n_L}{\ell_\ell + \ell_p \frac{n_L}{n_p} + \ell_a n_L}\right]$$

$$(\Delta\Theta)_h = \frac{n_L \sin\Theta_L \,\Delta\phi_H}{n_G \sin\left[\cos^{-1}\frac{n_L}{n_G}\cos\Theta_L\right]}$$

$$\frac{n_L}{n_G}\left[\frac{\sin\Theta_L}{\sin\cos^{-1}\frac{n_L}{n_G}\cos\Theta_L}\right]\left[\frac{W}{\ell_\ell + \ell_p\frac{n_L}{n_p} + \ell_a n_L}\right]$$

Receiving solid angle $\delta\Omega_1 = (\Delta\Theta)_v.(\Delta\Theta)_h$ as rectangular aperture

$$\delta\Omega_1 = \left[\frac{\sin\Theta_L}{\sin\cos^{-1}\frac{n_L}{n_G}\cos\Theta_L}\right]\left[\frac{A}{\ell_\ell\frac{n_G}{n_L} + \ell_p\frac{n_G}{n_p} + \ell_a n_G}^2\right]$$

$A = W.L$ = area of receiving aperture.

The first term is a correction factor which must be applied to results to obtain scattering diagrams.

4. Calculation of $\delta\Omega_2$

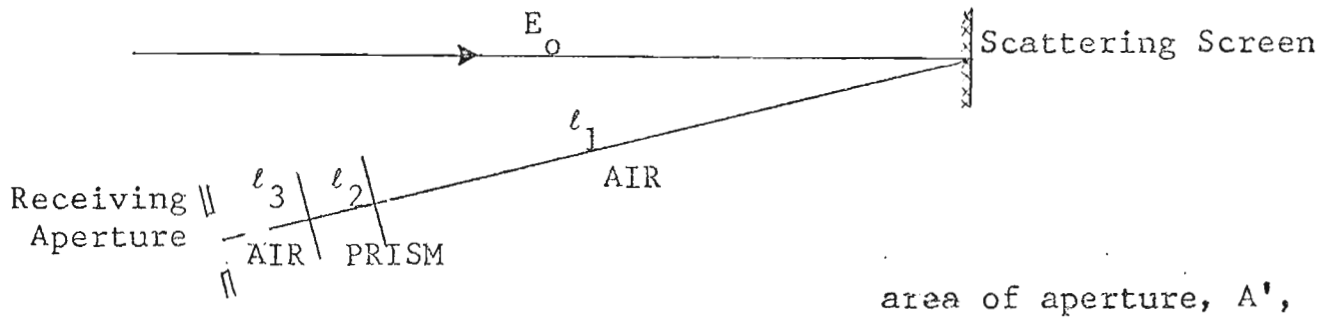

Received solid angle, $\delta\Omega_2$, is given by : $\dfrac{\text{area of aperture, A', in detector head}}{\left[\text{'App.depth' of receiving aperture from screen as expressed in air}\right]^2}$

$$= \frac{A'}{\left(\ell_1 + \ell_3 + \frac{\ell_2}{n_p}\right)^2}$$

where n_p is refractive index of the prism.

A' = area of receiving aperture when making incident beam measurement

REFERENCES

1. (a) R.D. Maurer, J. Chem. Phys., 25, no.6, (1956) p.1206

   (b) Parthasarathy, Sirkar and Niyogi, Proc. Natl, Inst. Sci. India 7 (1941) p.247

2. B.E. Warren, J. Appl. Phys., 8 (1937) p.645

3. R. Kingslake, Appl. Optics and Optical Eng., Vol.1, Academic Press (1965), p.82

4. P. Wolston, Brit.J.Appl. Phys., 16 (1965), p.1187

5. F. Grum and G.W. Luckey, Appl. Optics 7 (1968),p.2289

6. W.A. Gambling and H. Edels, Brit.J. Appl. Phys. 8 (1957), p.481

7. J.K.Nakamura and S.E.Schwarz, Appl.Optics 7 (1968), p.1073

8. R.R. Alfano and N. Ockman, J. Opt. Soc. Am., 58 (1968), p.90

9. G.A. Morton, Appl Optics 7 (1968), p.1

10. G. Deželić, J. Chem.Phys. 45 (1966) p.185

11. W.H. Martin, Trans. Roy.Soc.Canada, 17, III (1923), p.151

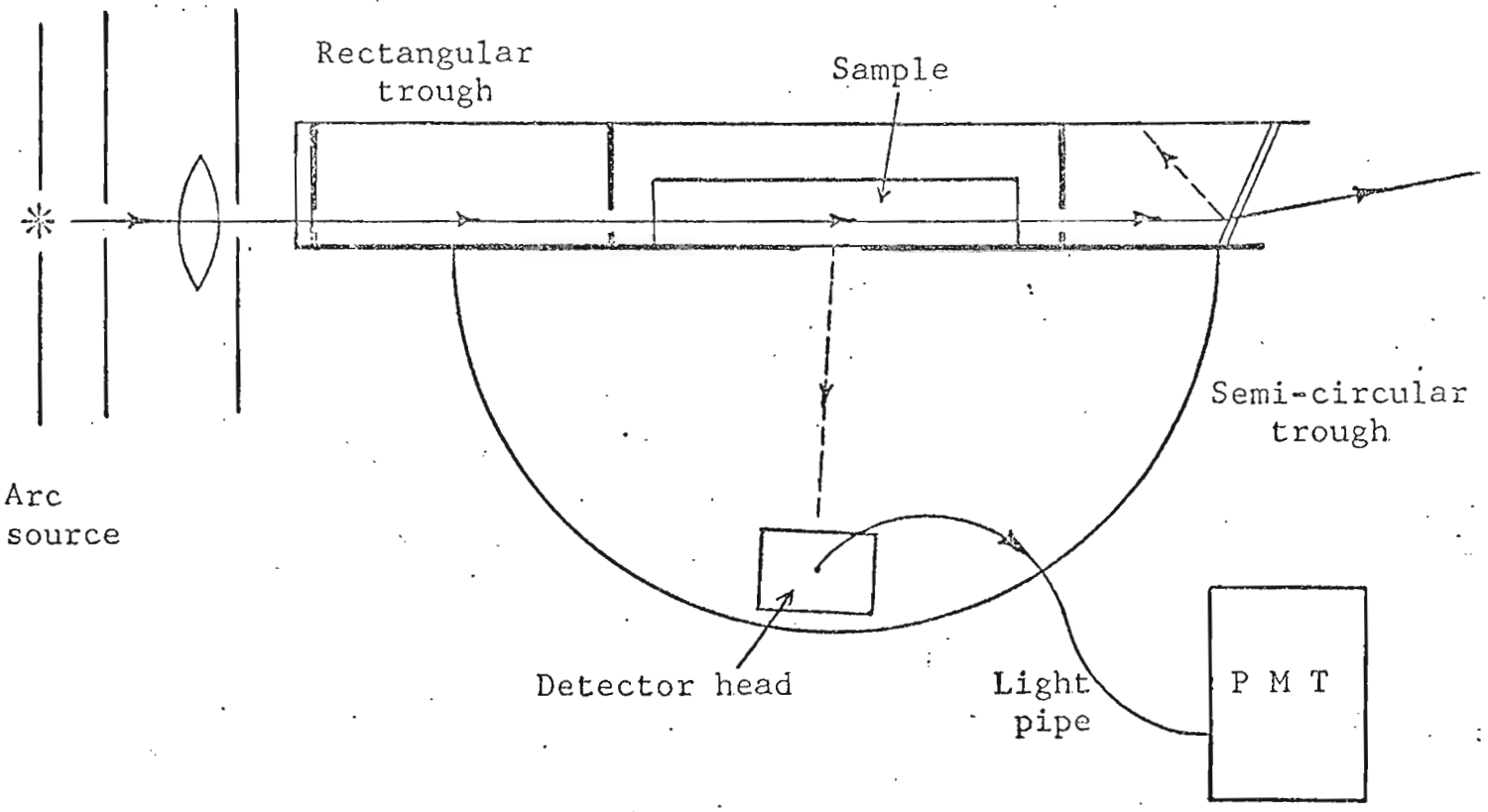

Fig. 1 Optical arrangement of scattering photometer (plan view)

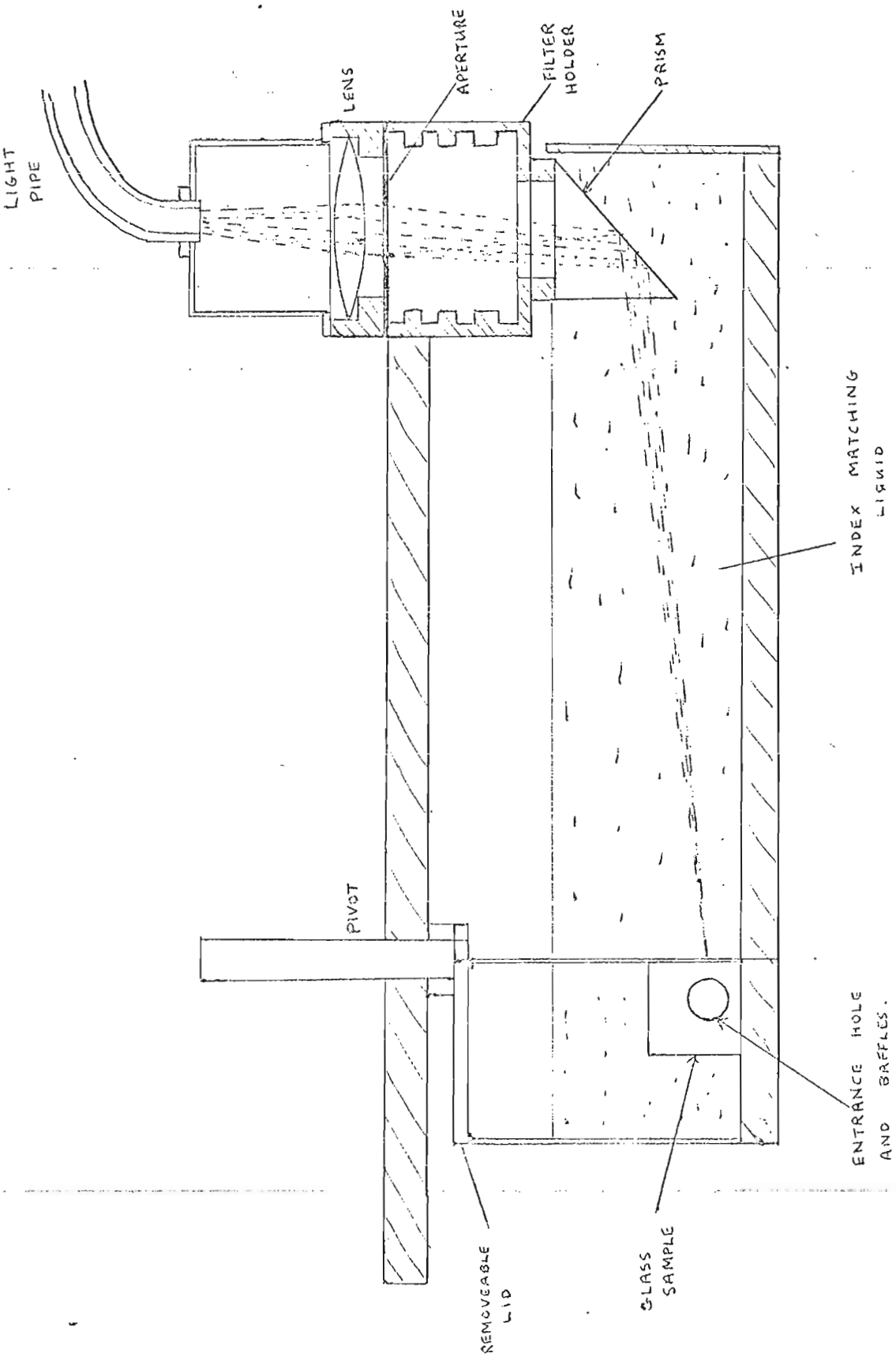

Fig. 2

Optical arrangement of scattering photometer (side view)

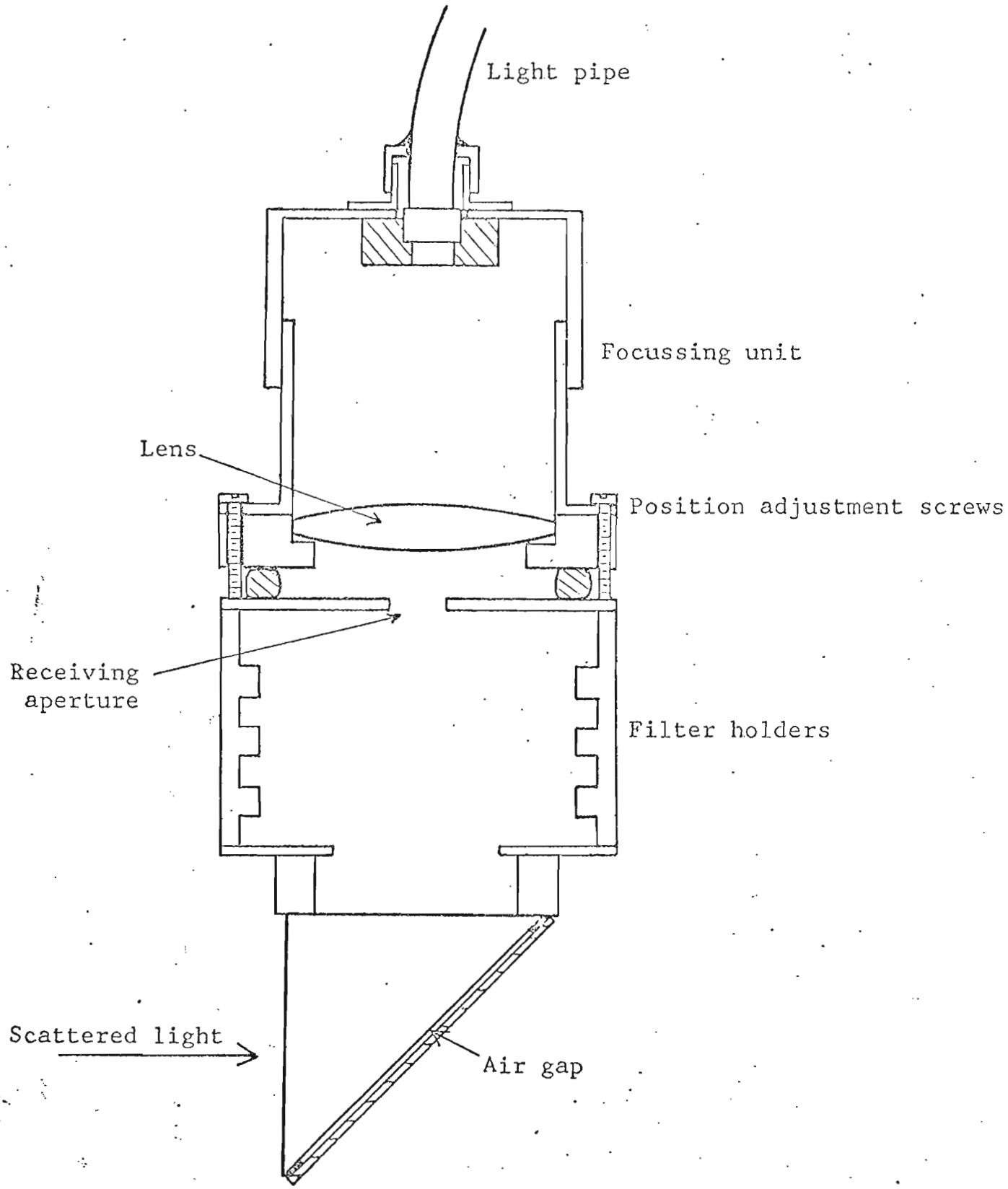

FIG. 3
Detector head assembly

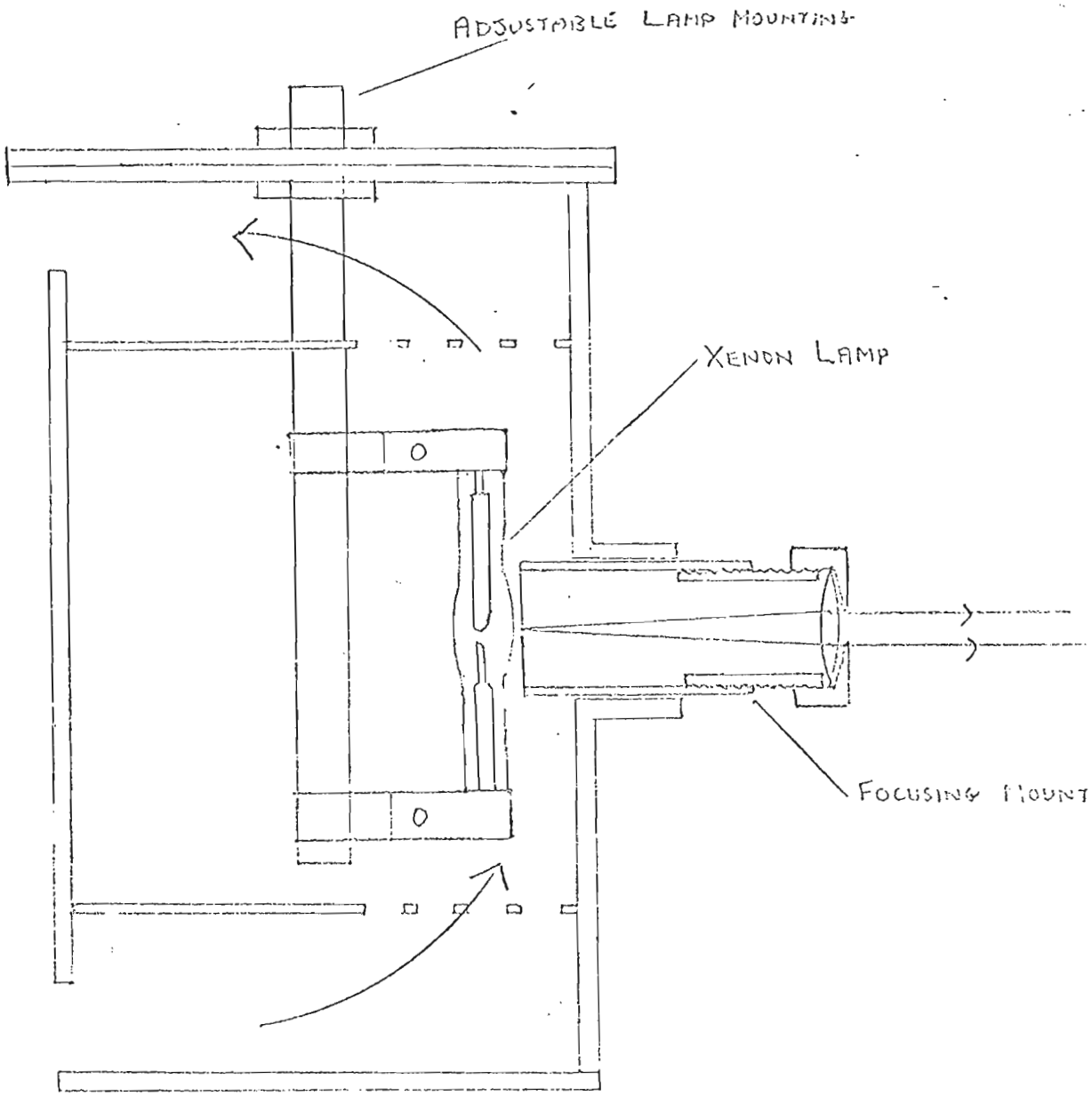

FIG. 4

Lamp housing

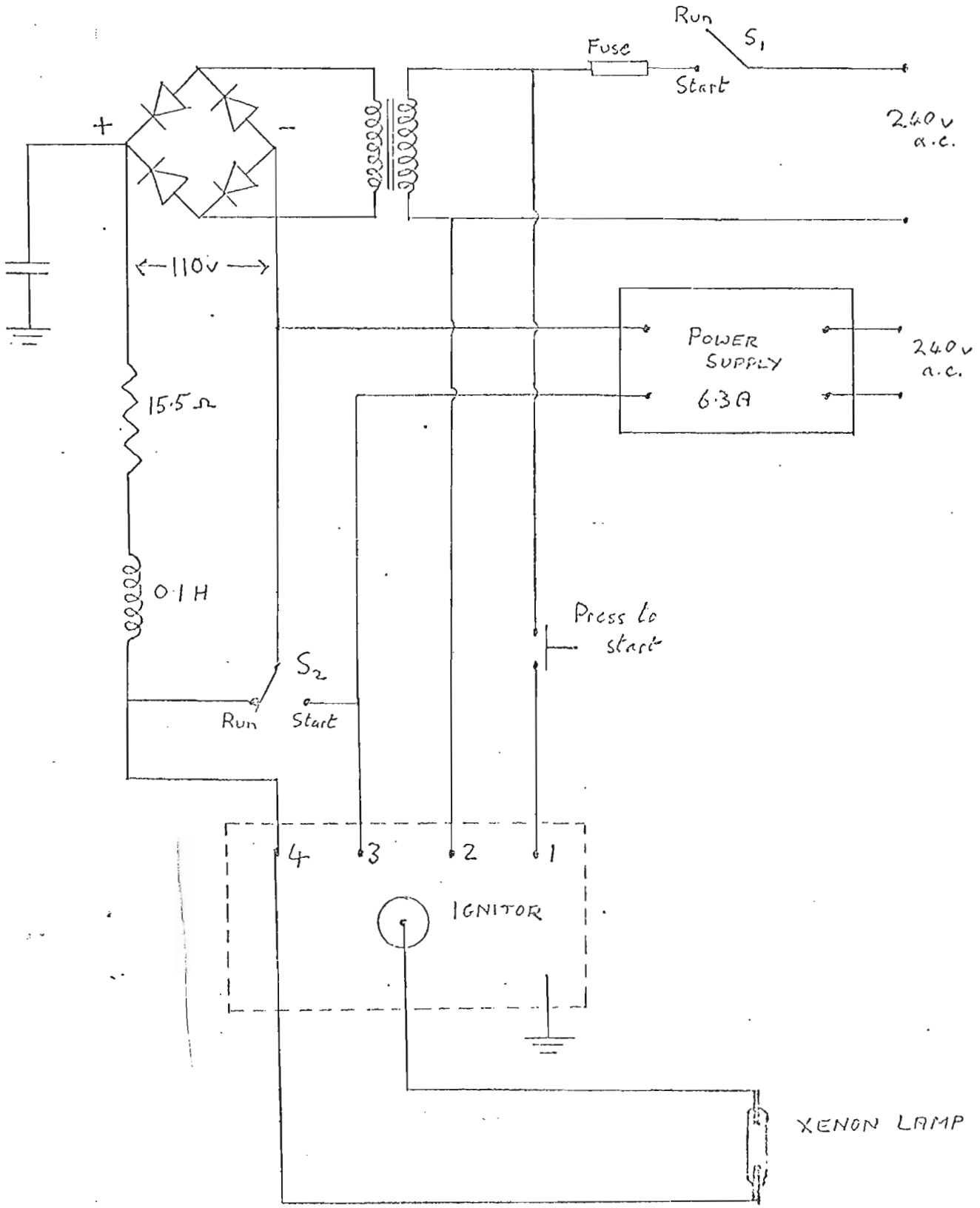

FIG. 5. Xenon lamp starting circuit

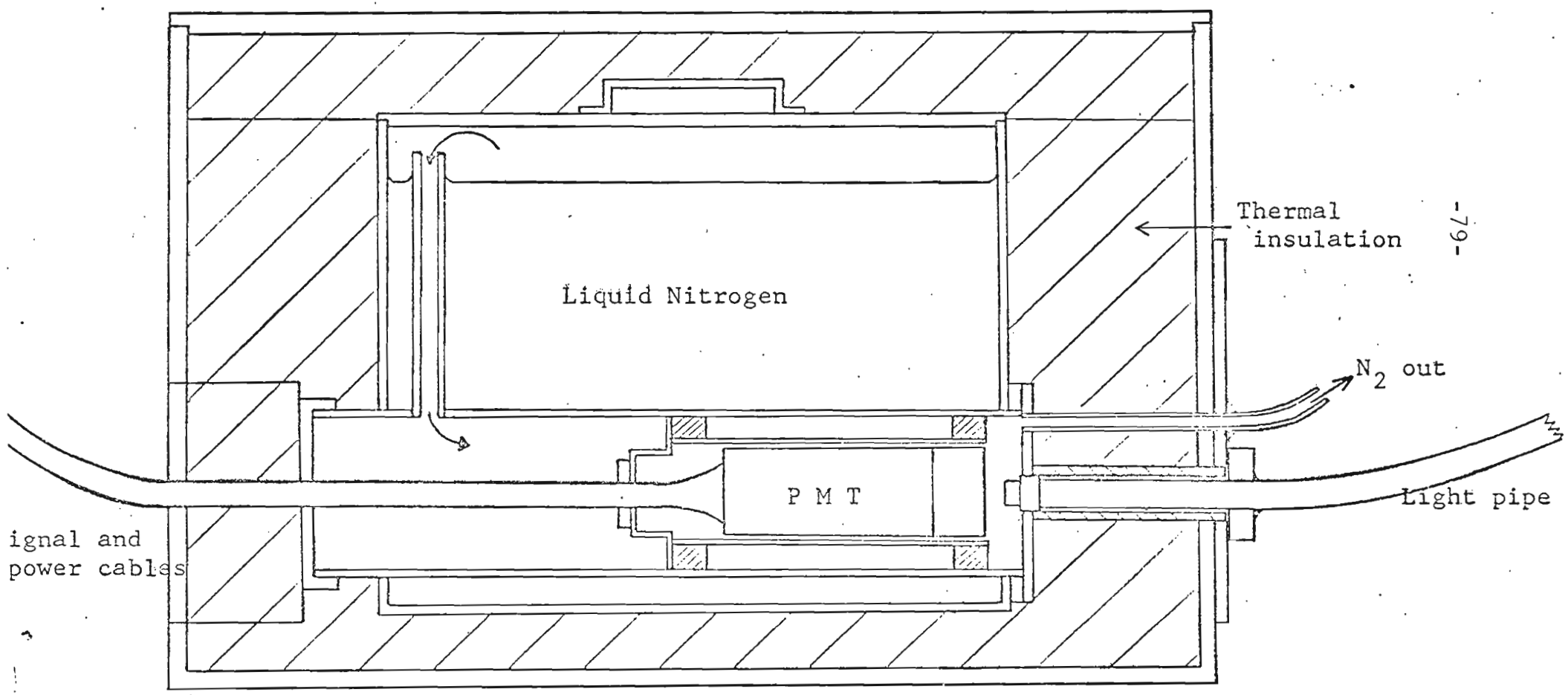

Fig. 6
Photomultiplier cooled housing

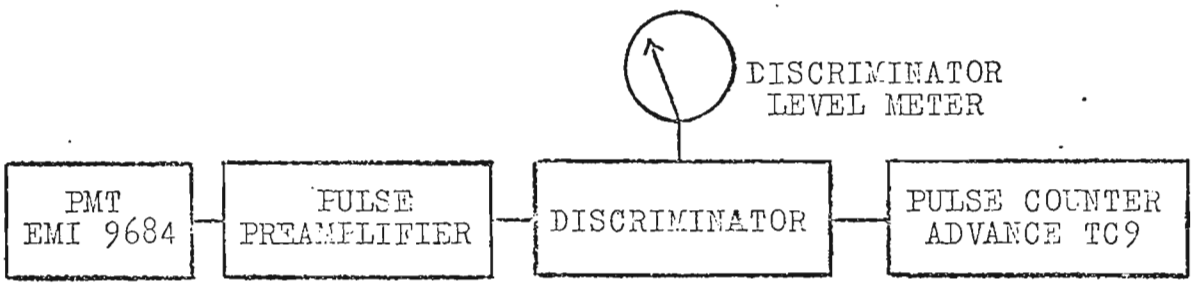

Fig. 7. Counting system, block diagram.

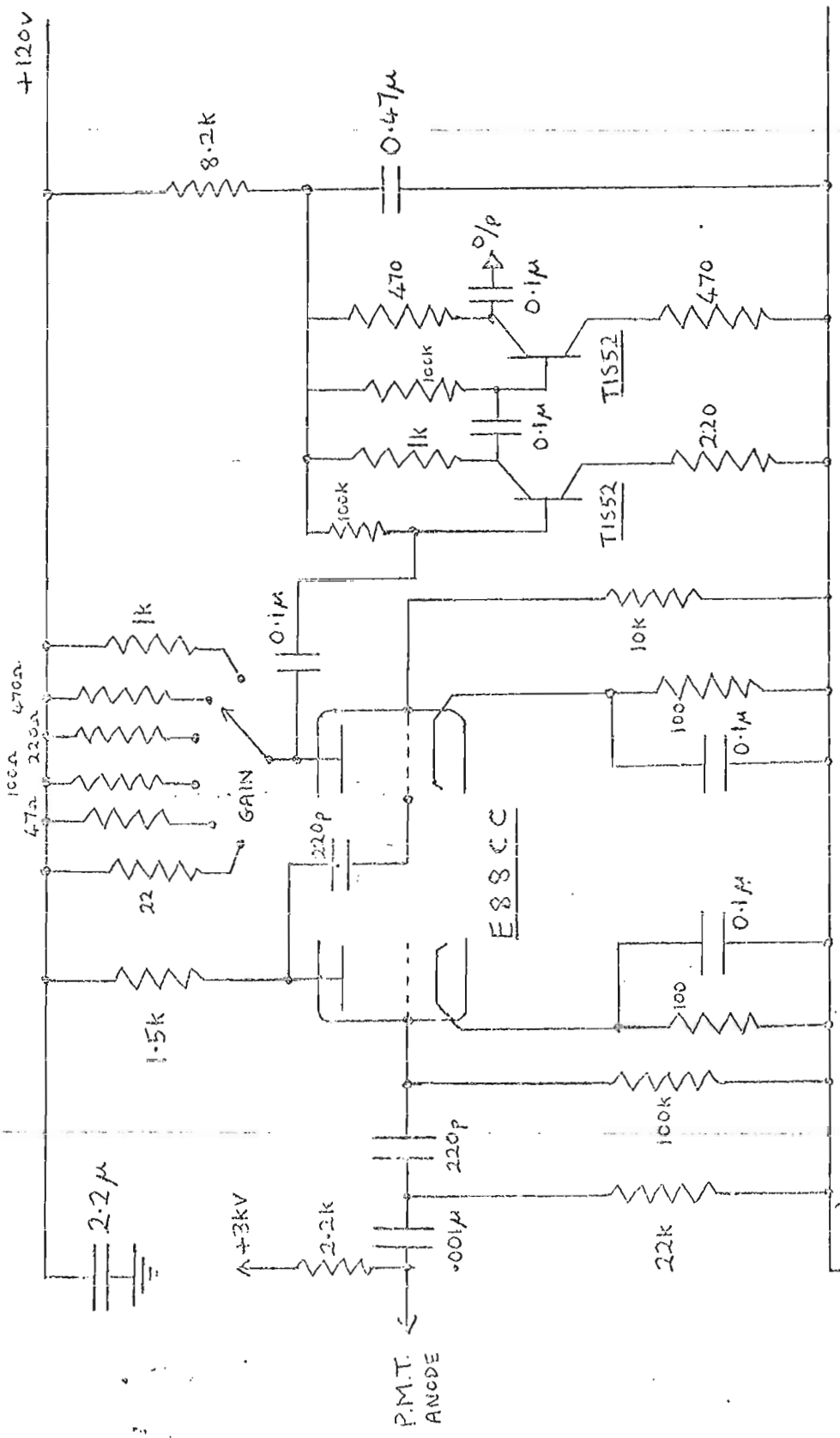

Fig.8 PULSE PREAMPLIFIER

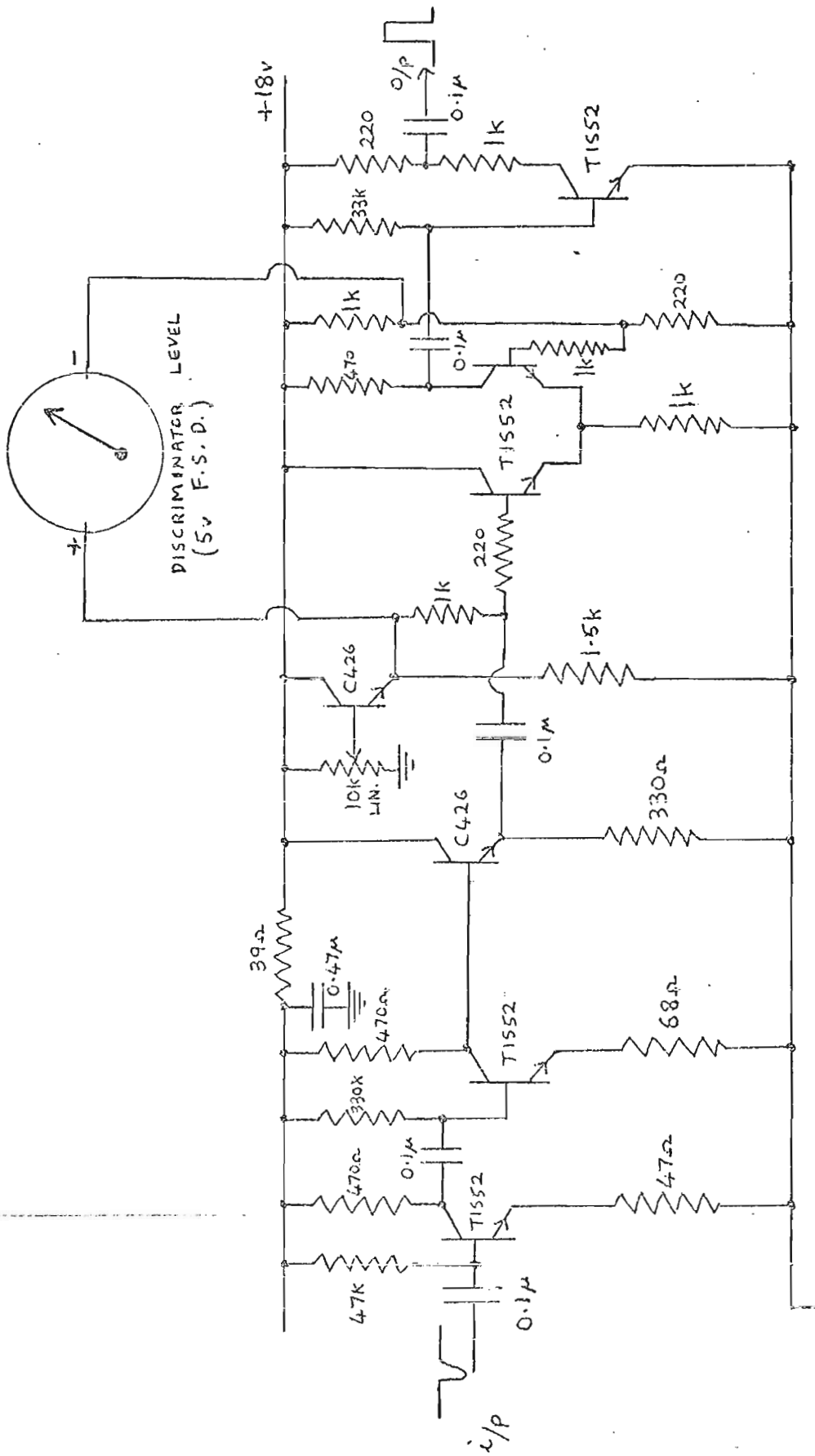

Fig. 9 PULSE HEIGHT DISCRIMINATOR

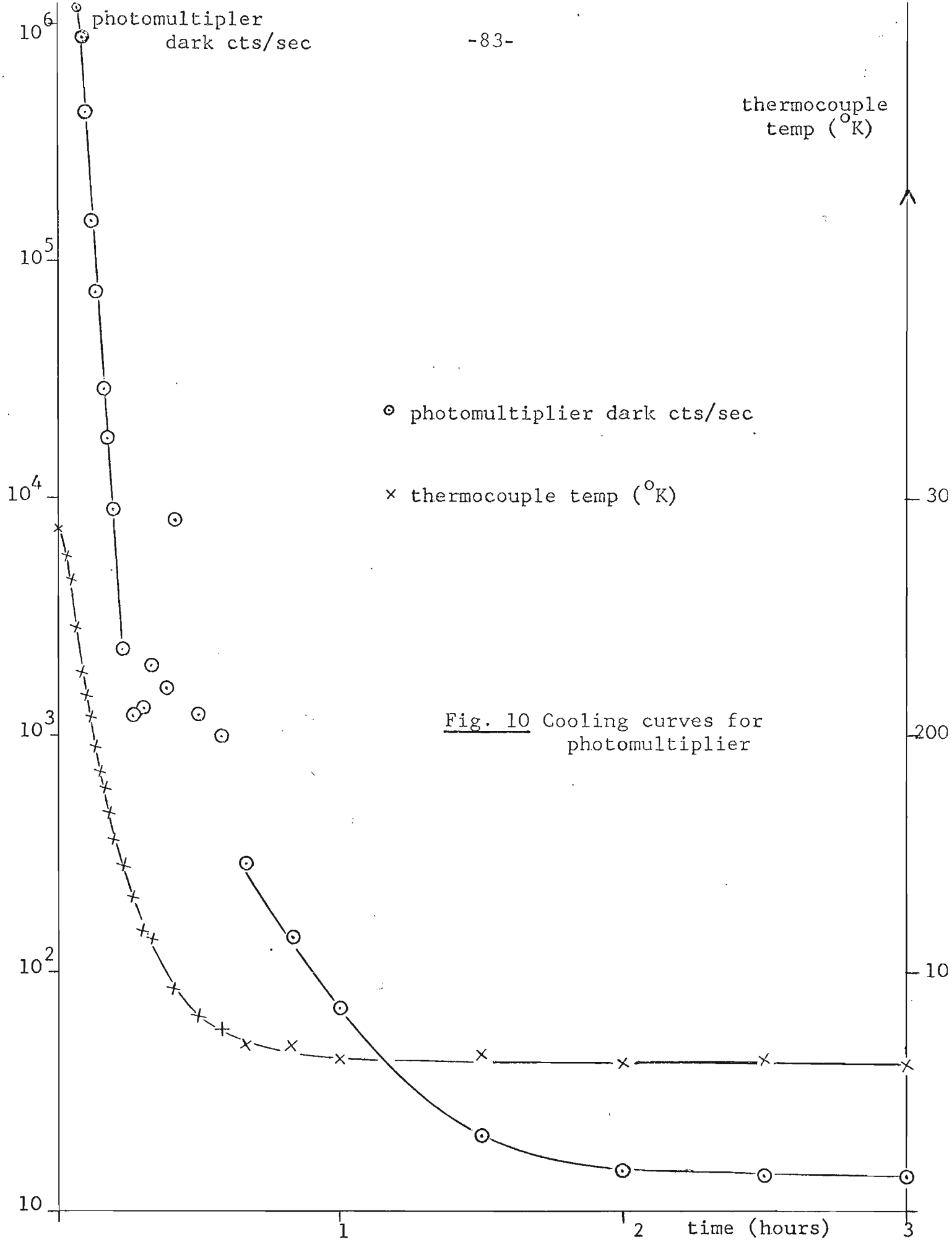

Fig. 10 Cooling curves for photomultiplier

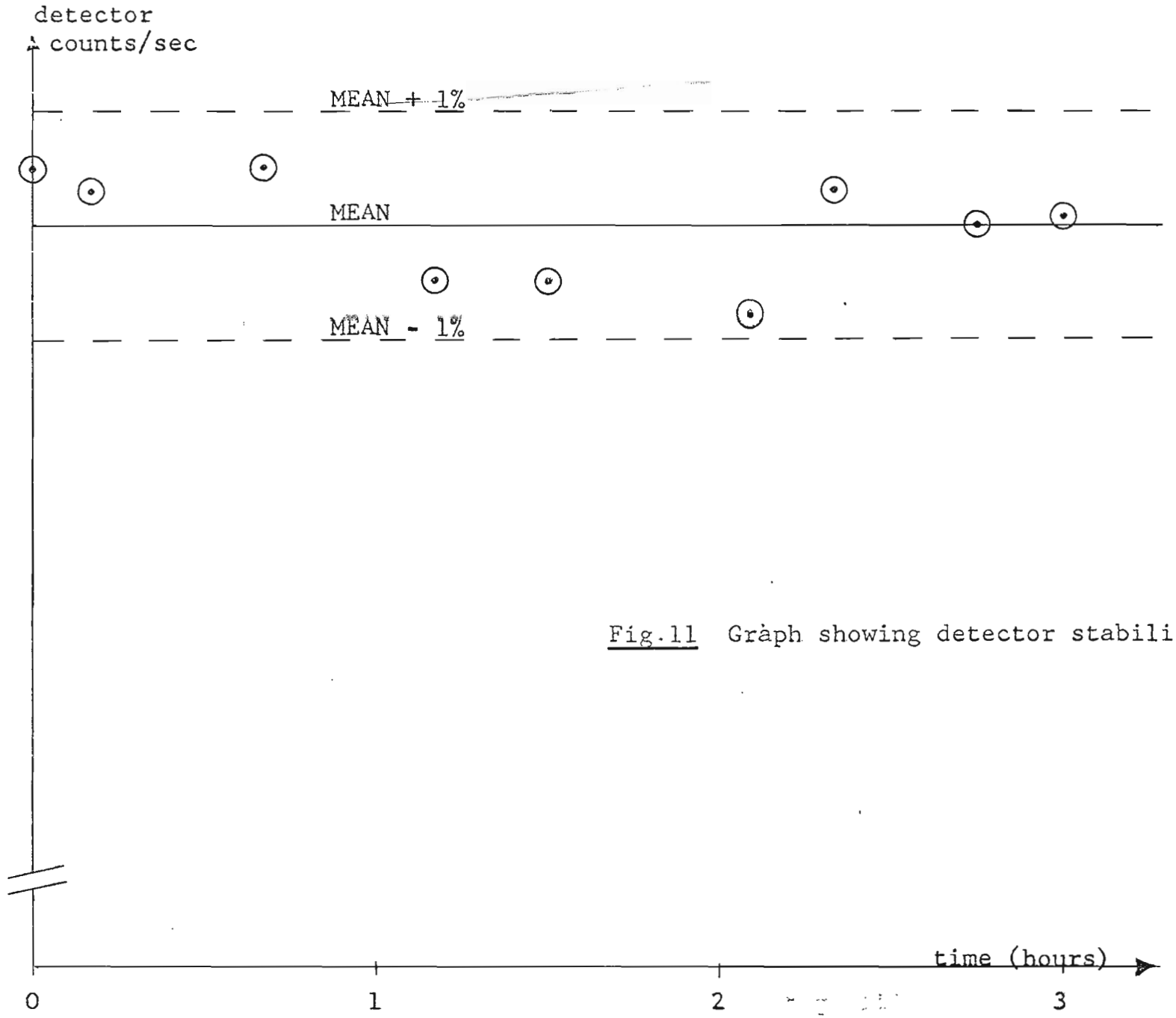

Fig.11 Gràph showing detector stability

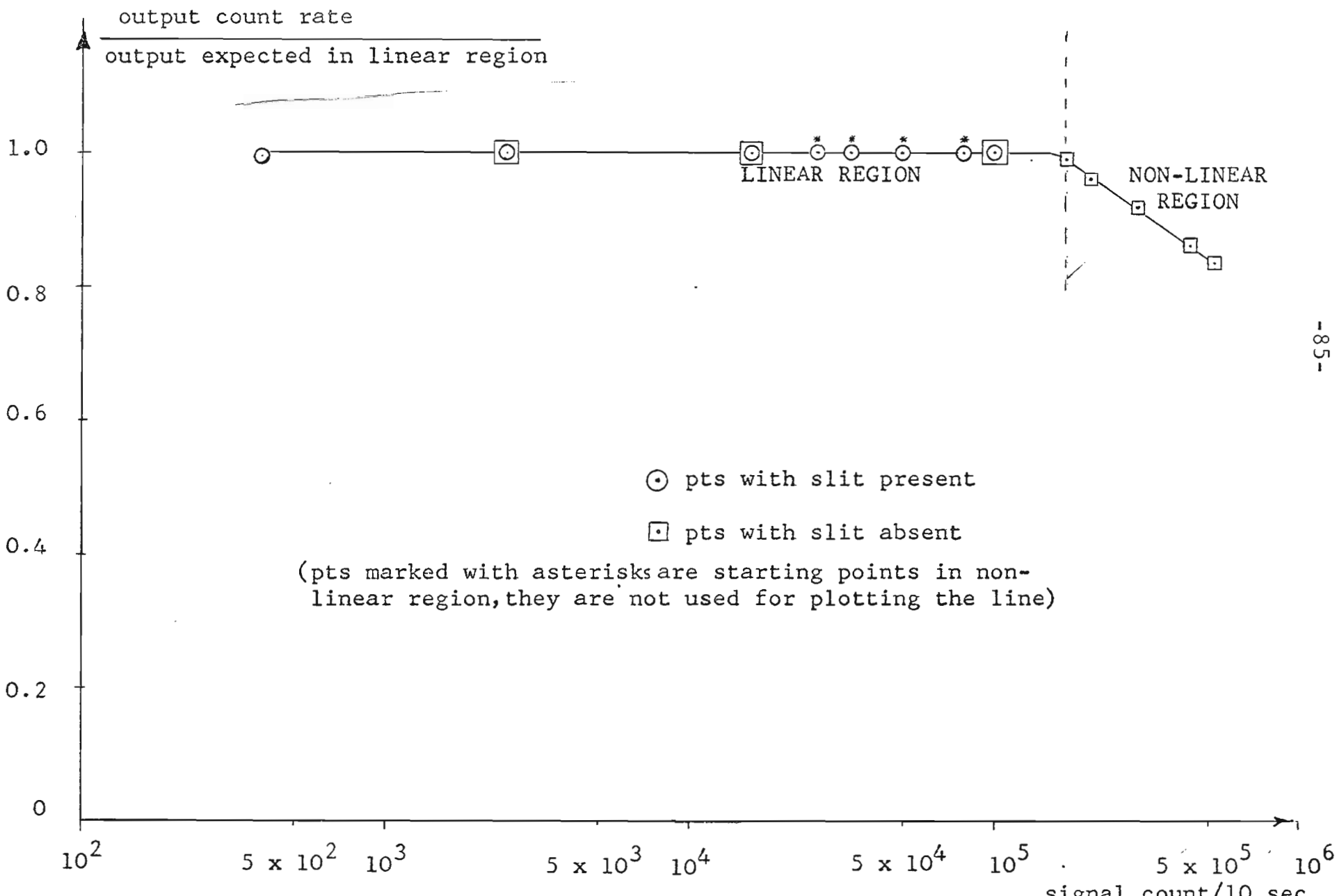

Fig.12 Graph showing linearity of detector

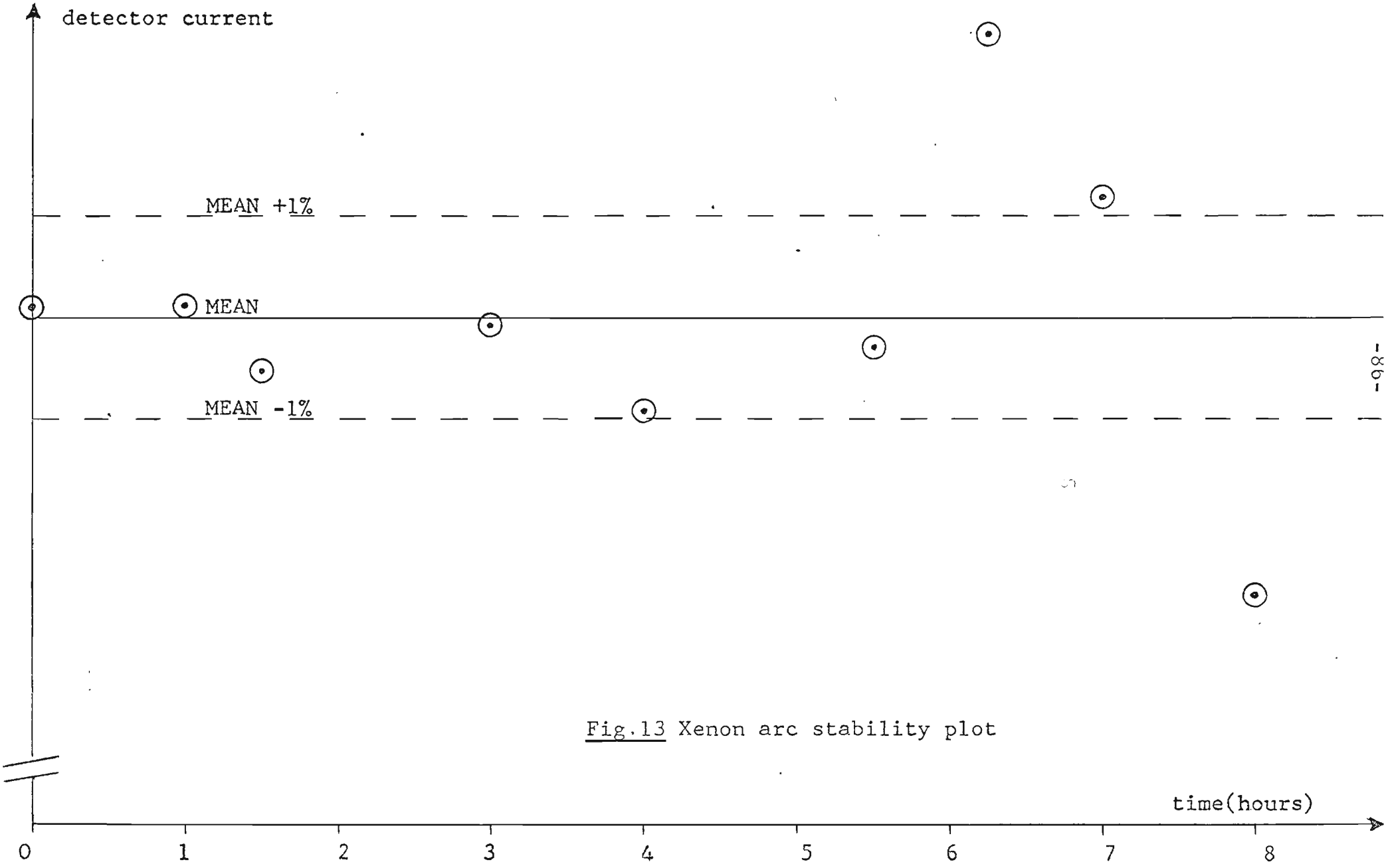

Fig.13 Xenon arc stability plot

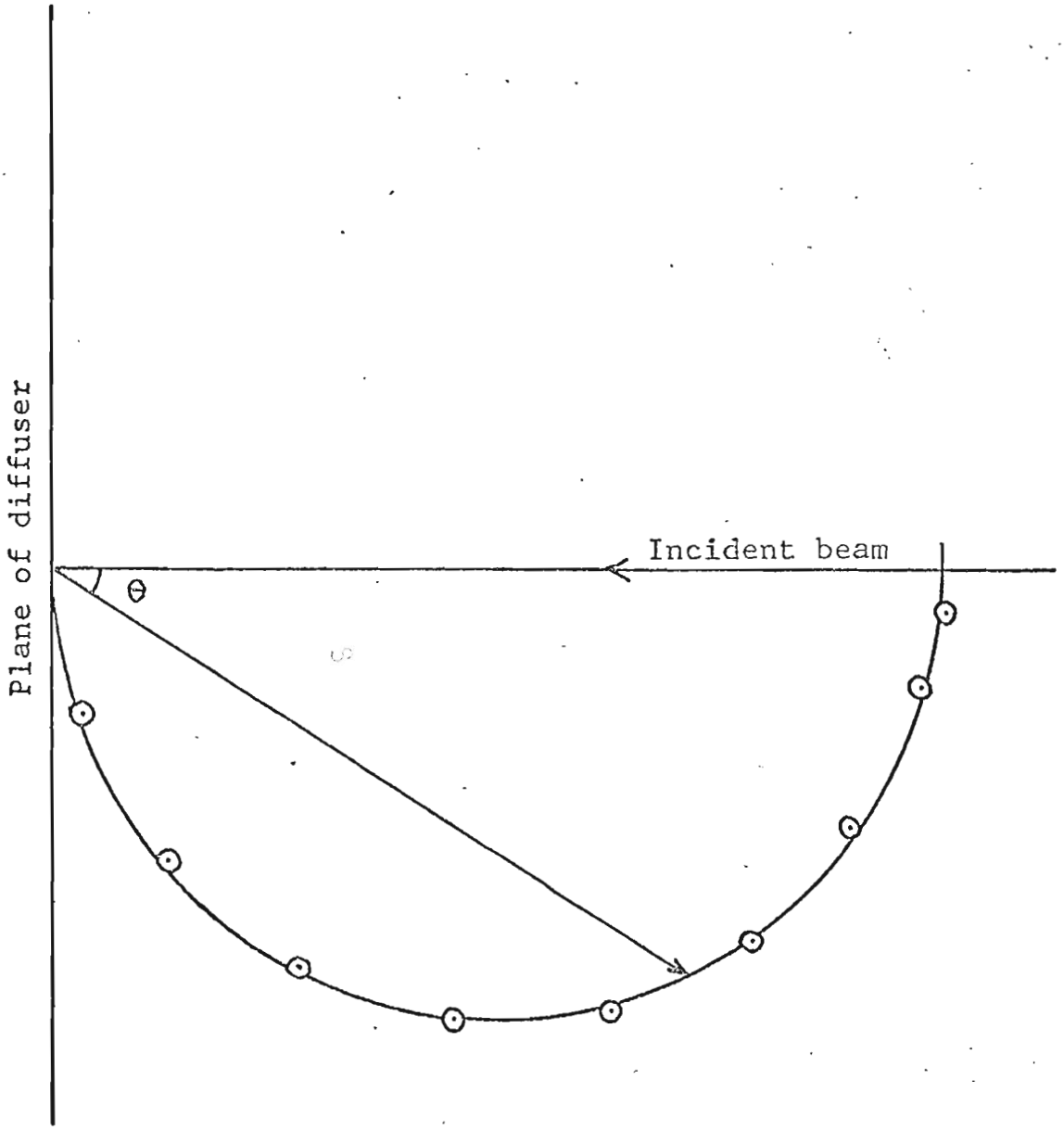

Fig. 14

Variation of scattered intensity with θ for pressed barium sulphate diffuser illuminated normally.

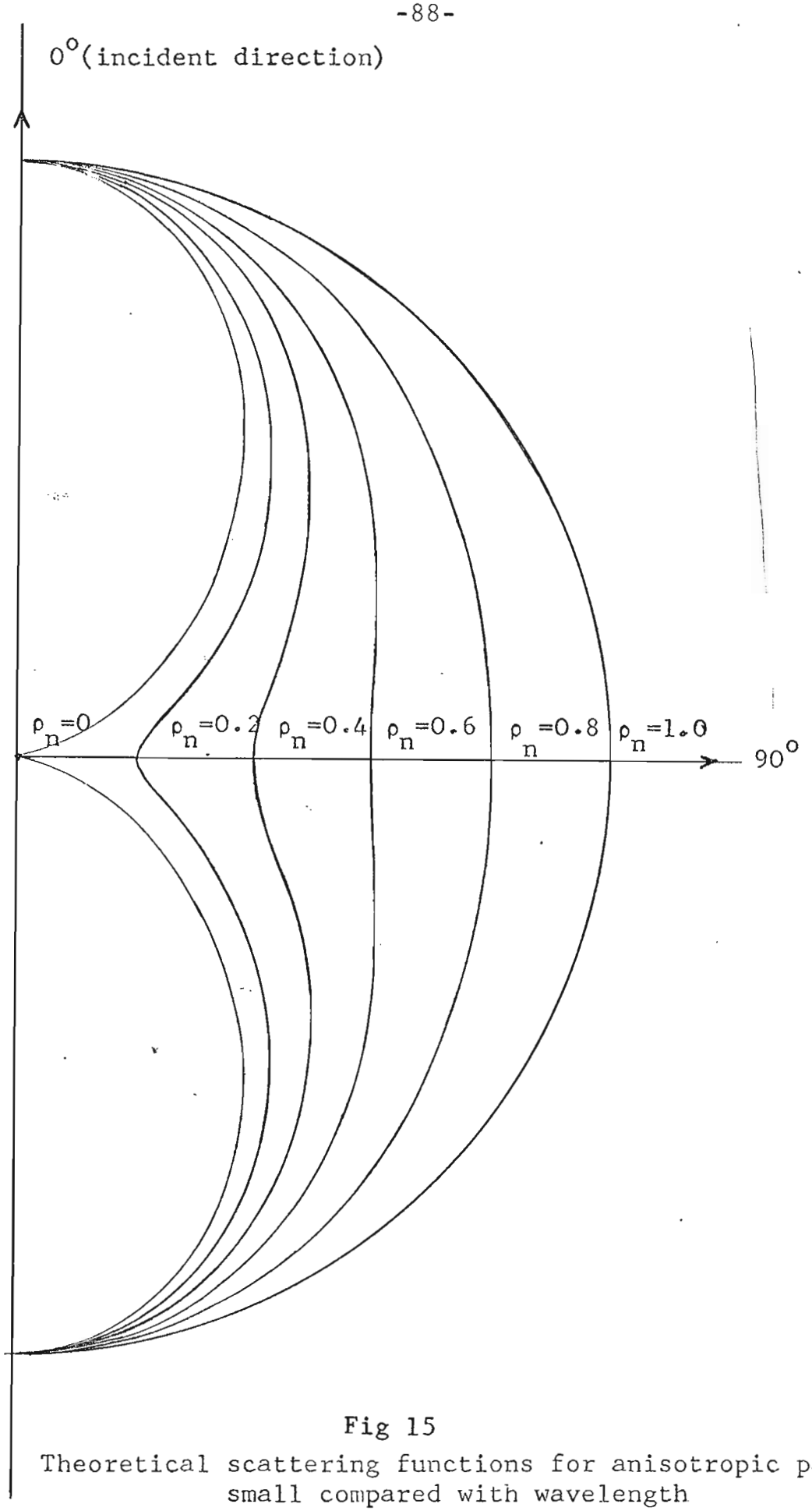

Fig 15

Theoretical scattering functions for anisotropic particles, small compared with wavelength

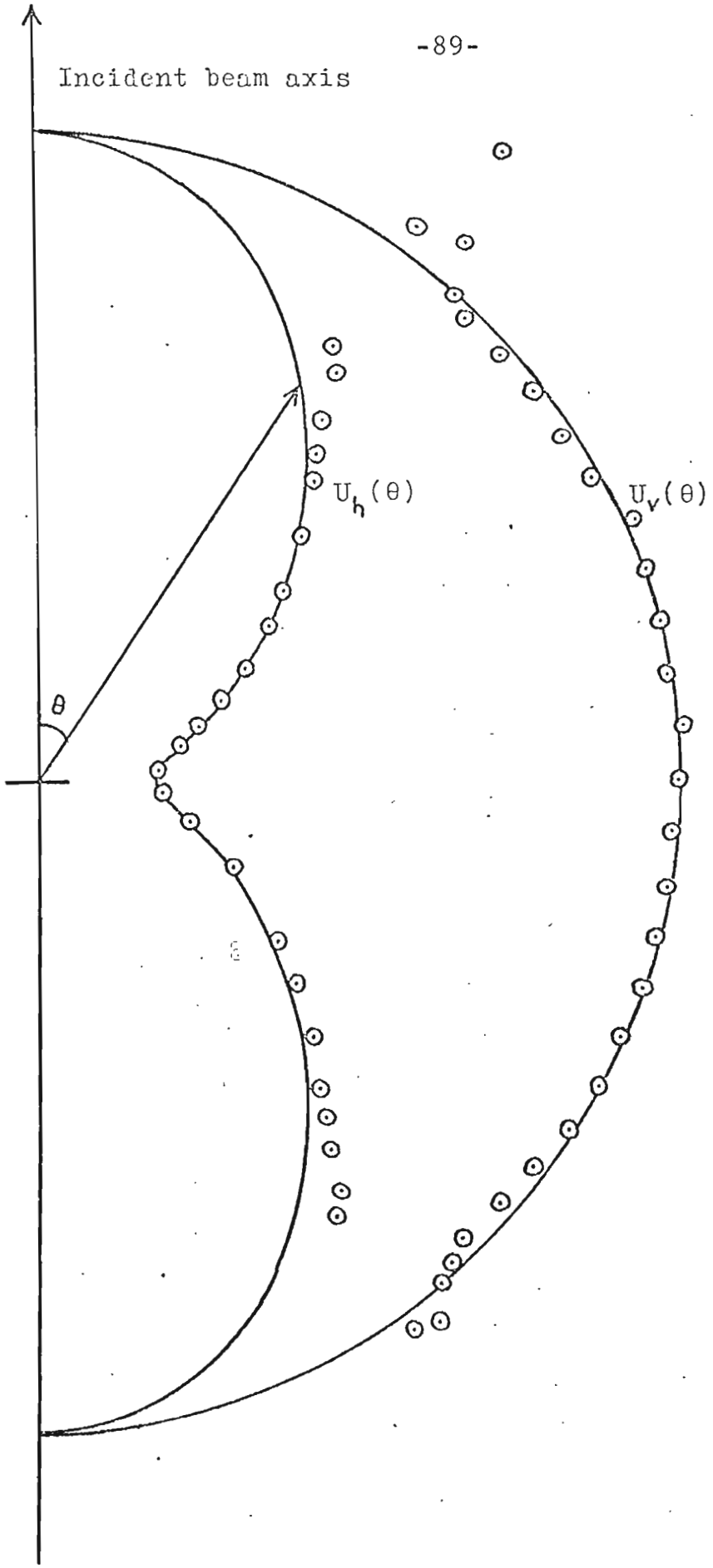

Fig.16. Polar scattering diagram for F7 glass at 633nm (experimental values of $U_v(\theta)$ and $U_h(\theta)$ superimposed on theoretical curves.)

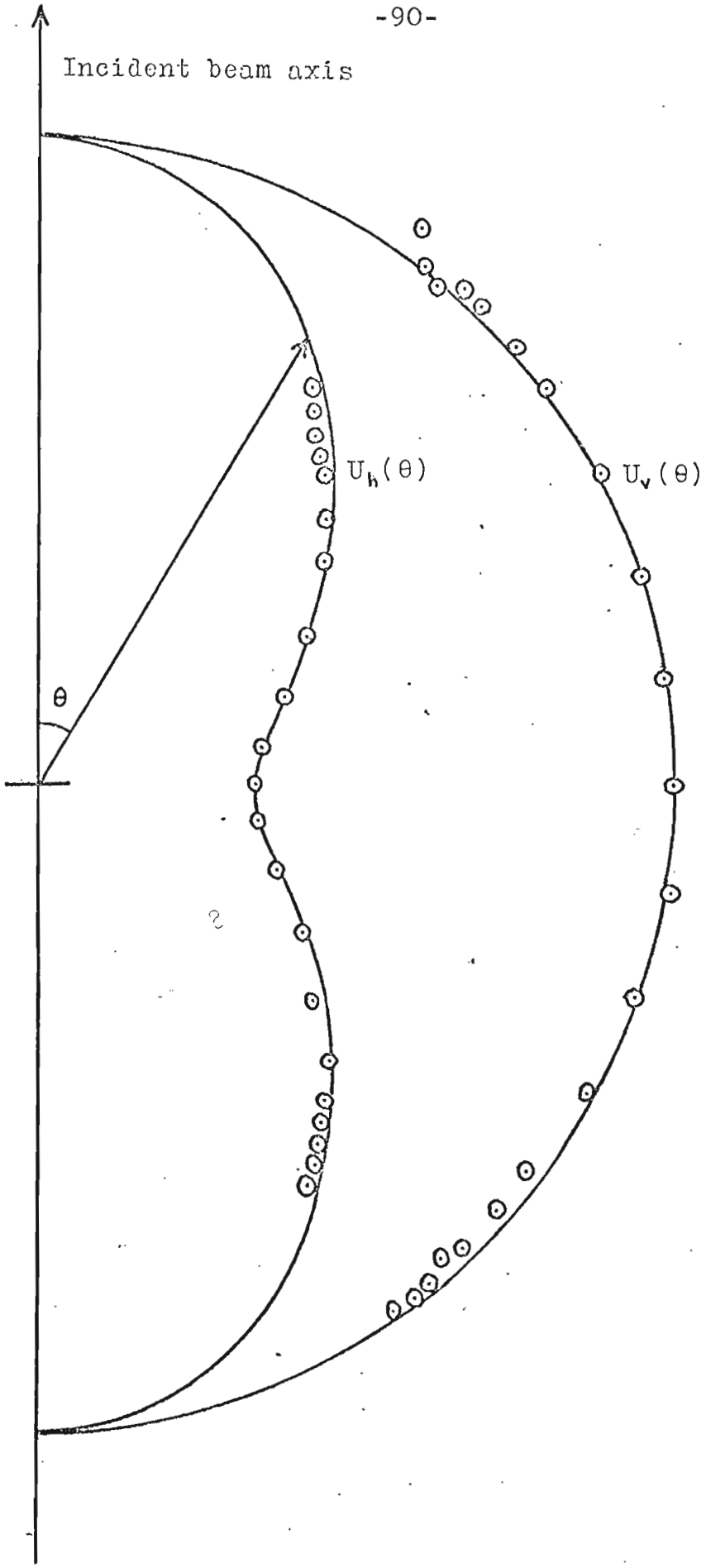

Fig.17. Polar scattering diagram for SSK2 glass at 633nm (experimental values of $U_v(\theta)$ and $U_h(\theta)$ superimposed on theoretical curves.)

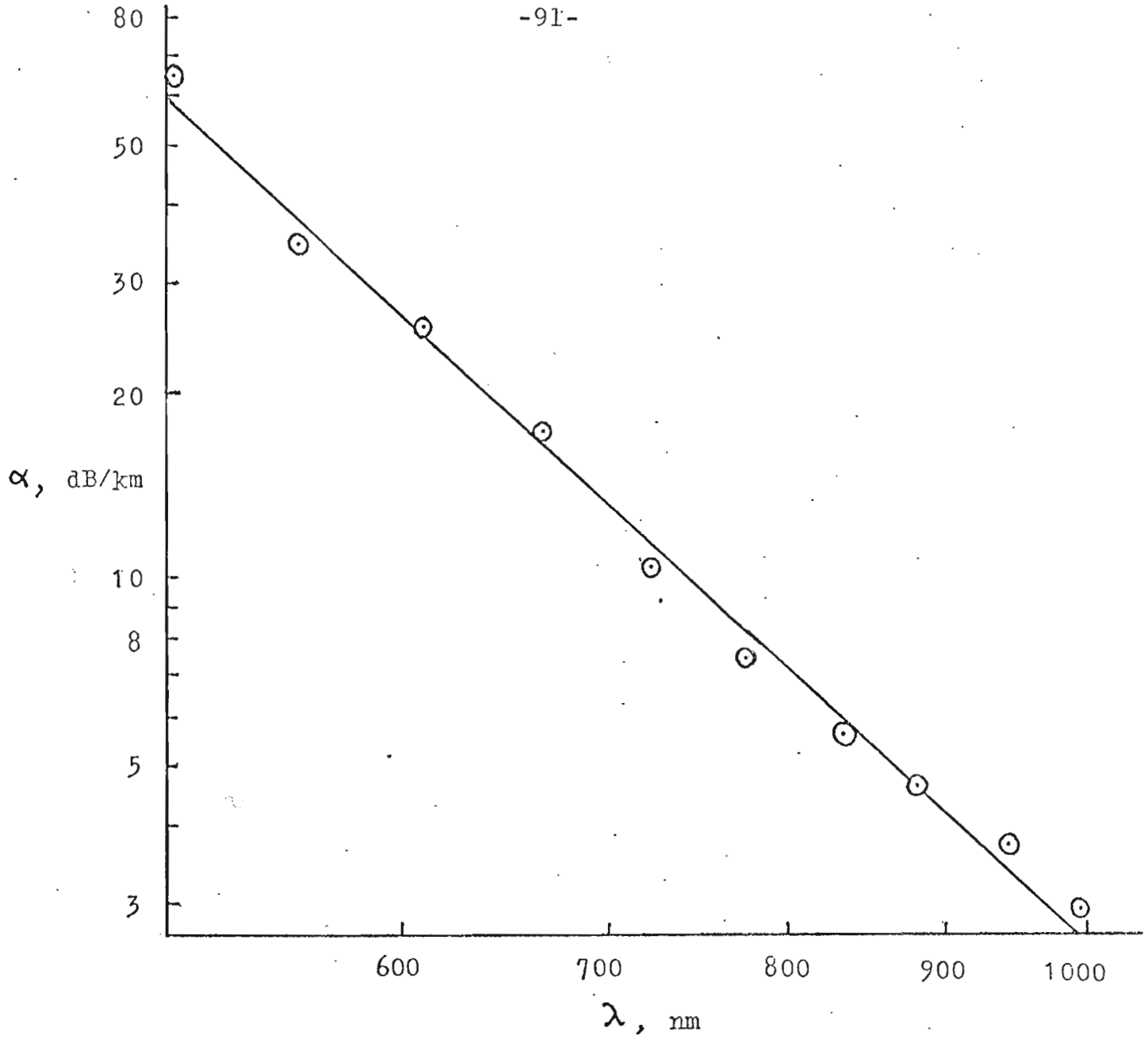

Fig.18. Type F7 glass: scattering loss per unit length, α, vs. wavelength, λ.

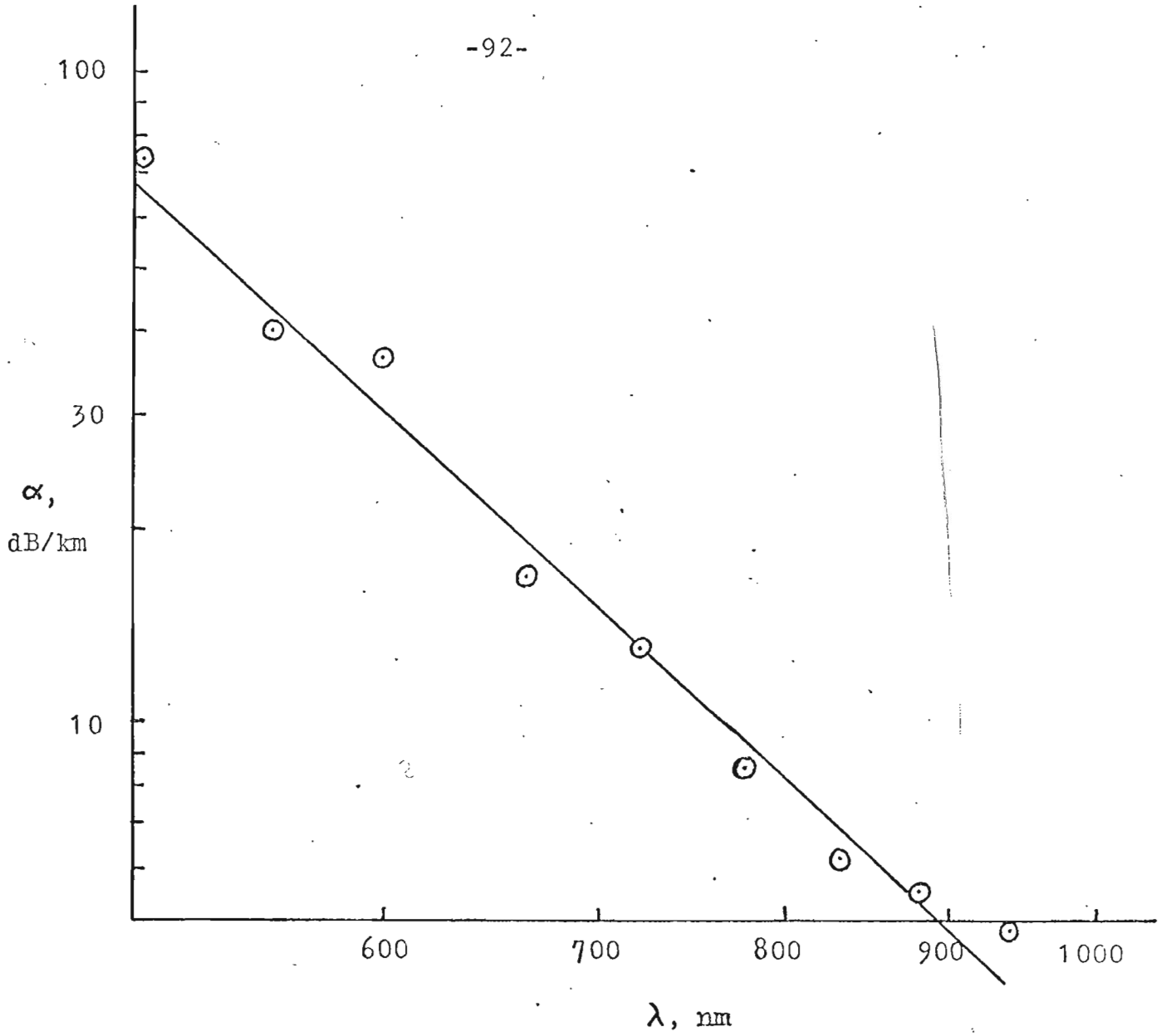

Fig. 19. Type SSK2 glass: scattering loss per unit length, α, vs. wavelength, λ.

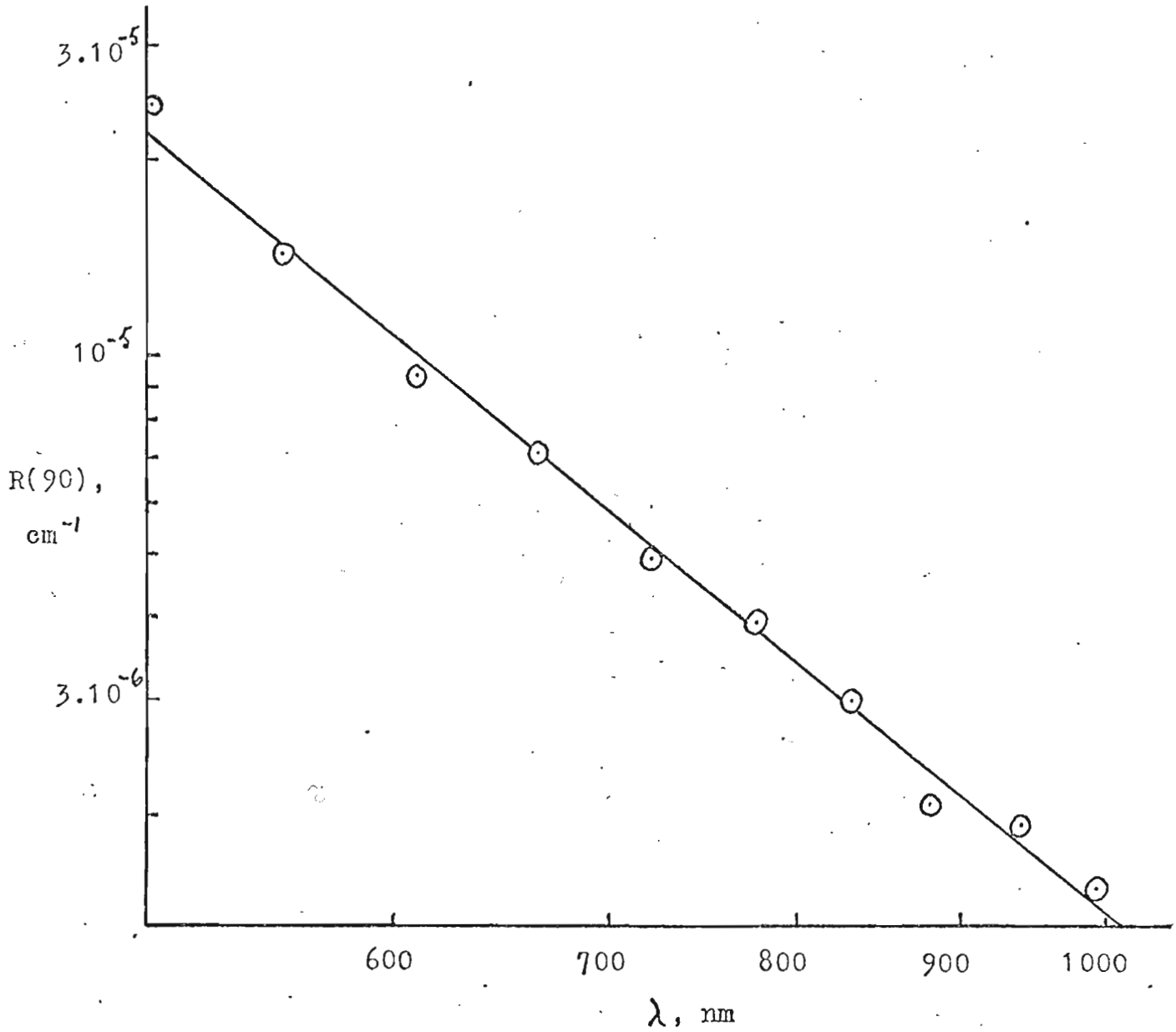

Fig. 20. Dependence of Rayleigh's ratio, R(90), on wavelength, λ, for benzene.

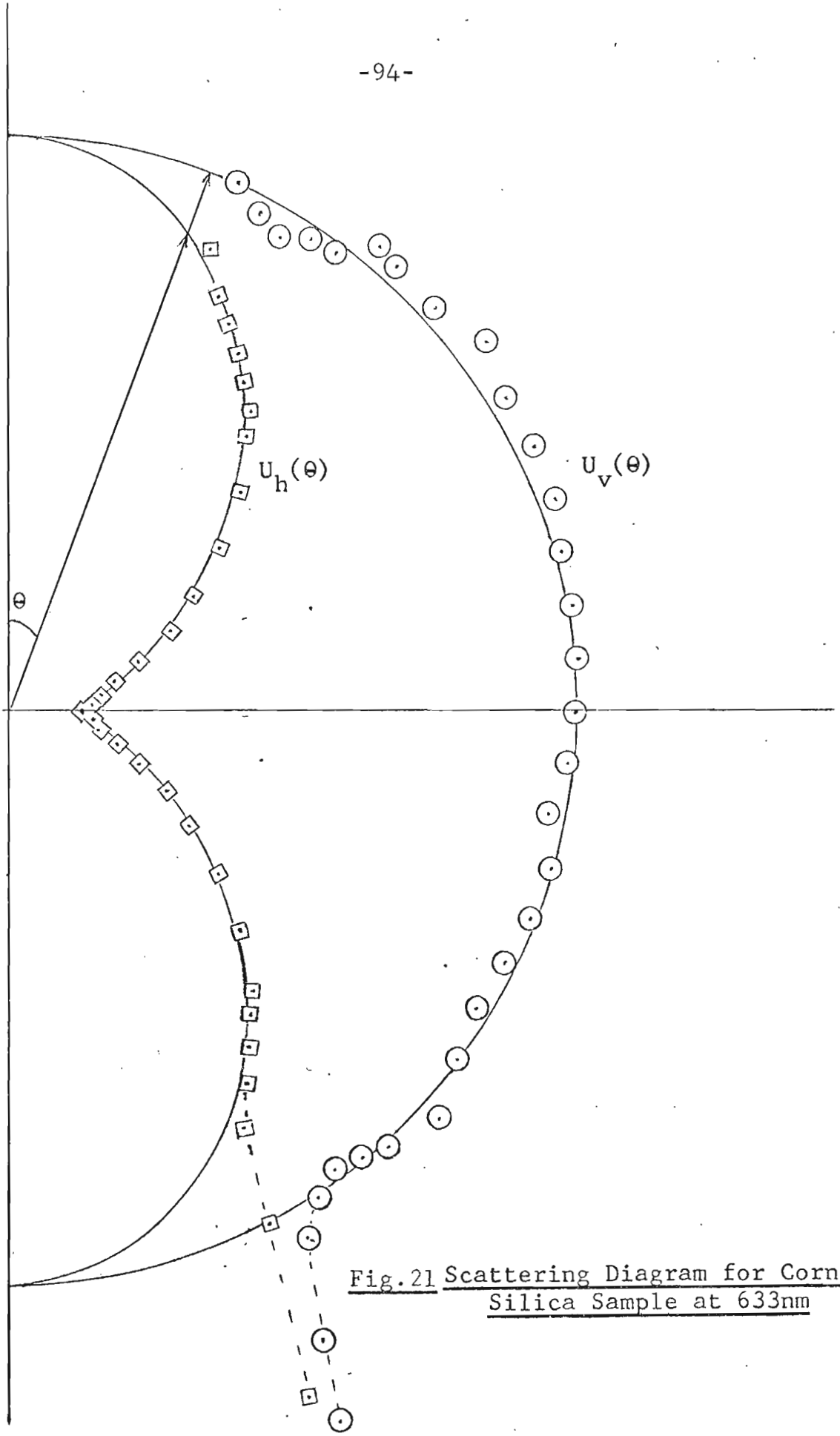

Fig.21 Scattering Diagram for Corning Fused Silica Sample at 633nm

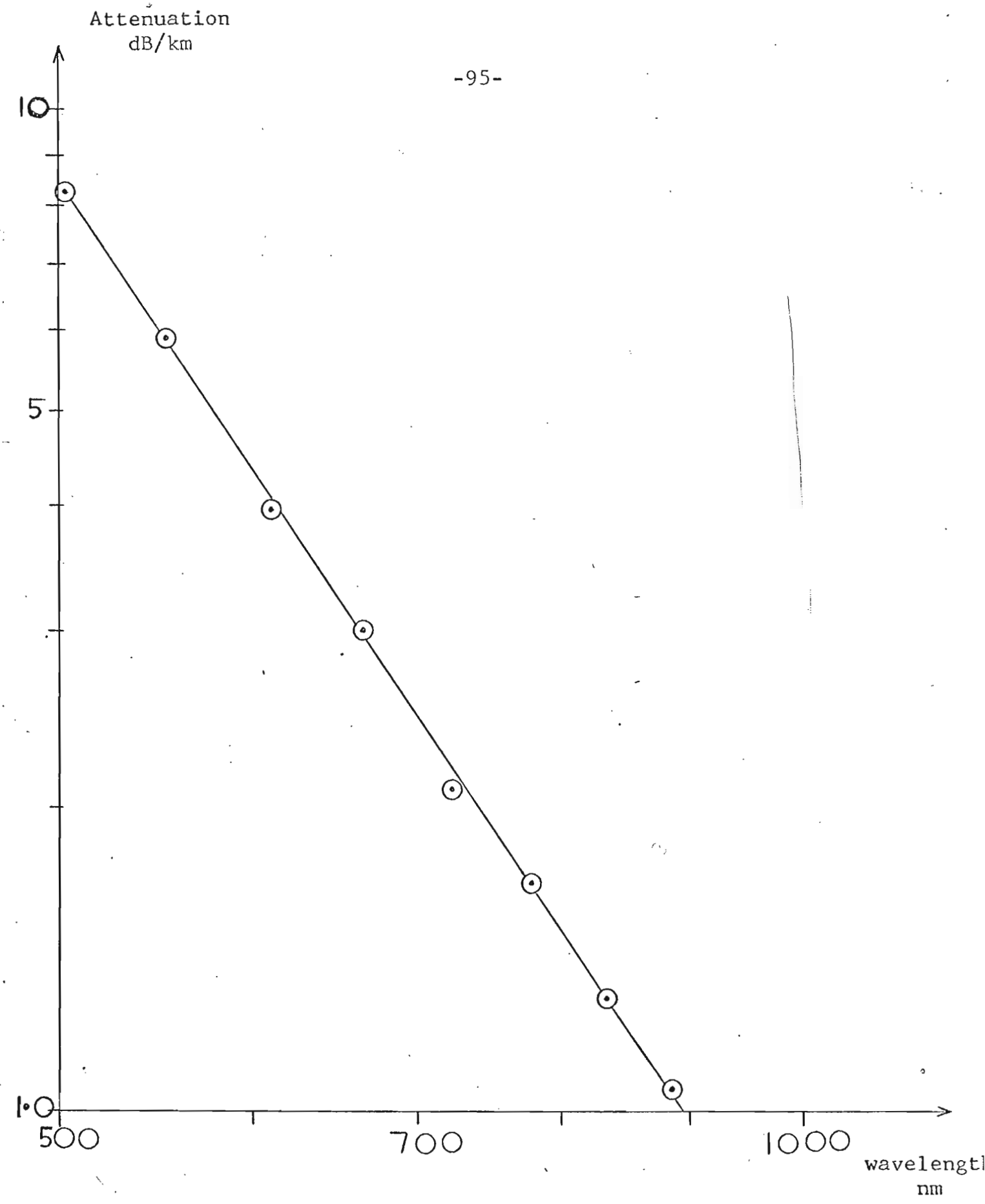

Fig.22

Corning Silica Sample : attenuation due to scattering vs. wavelength

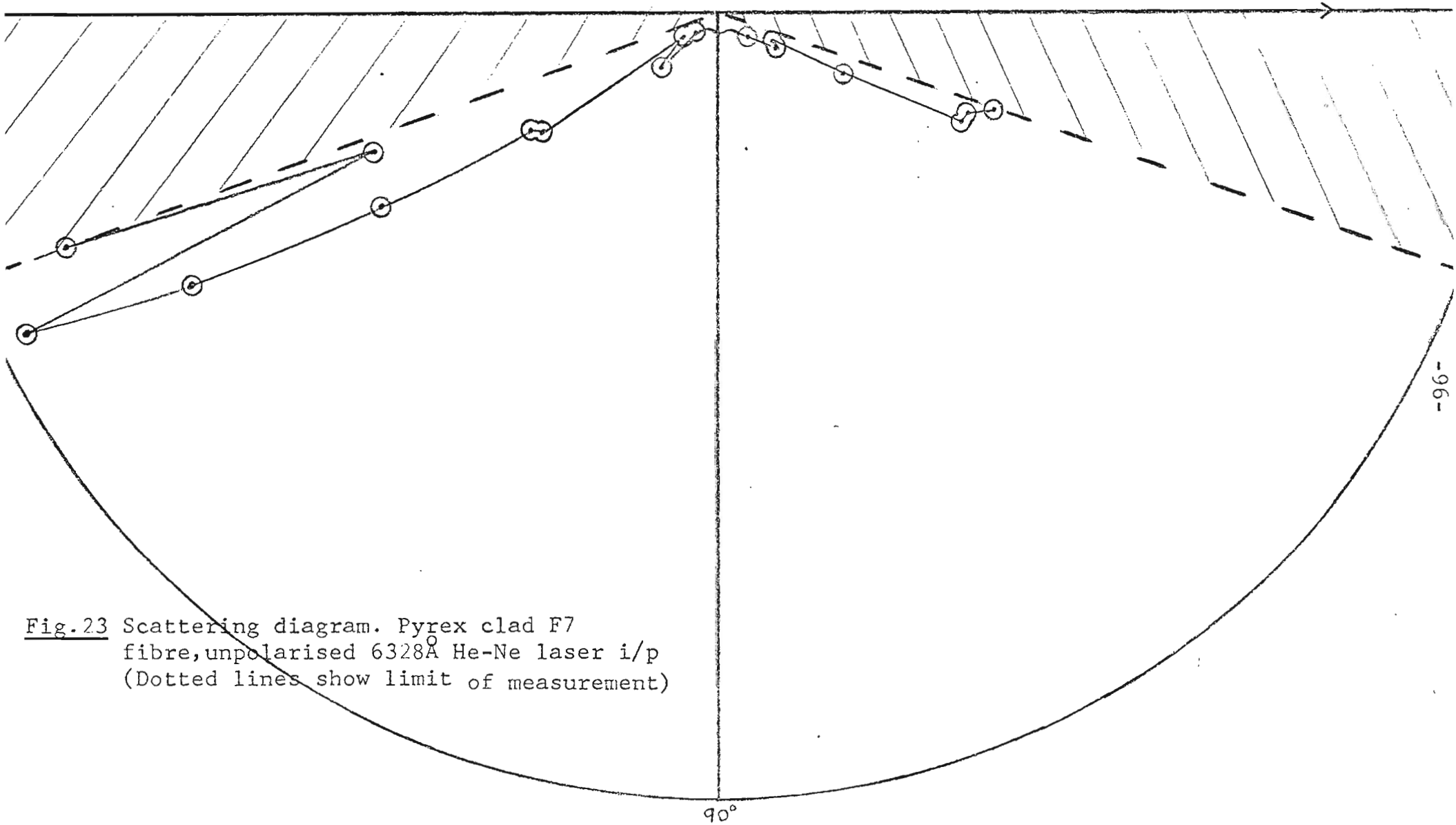

Fig.23 Scattering diagram. Pyrex clad F7 fibre, unpolarised 6328Å He-Ne laser i/p (Dotted lines show limit of measurement)

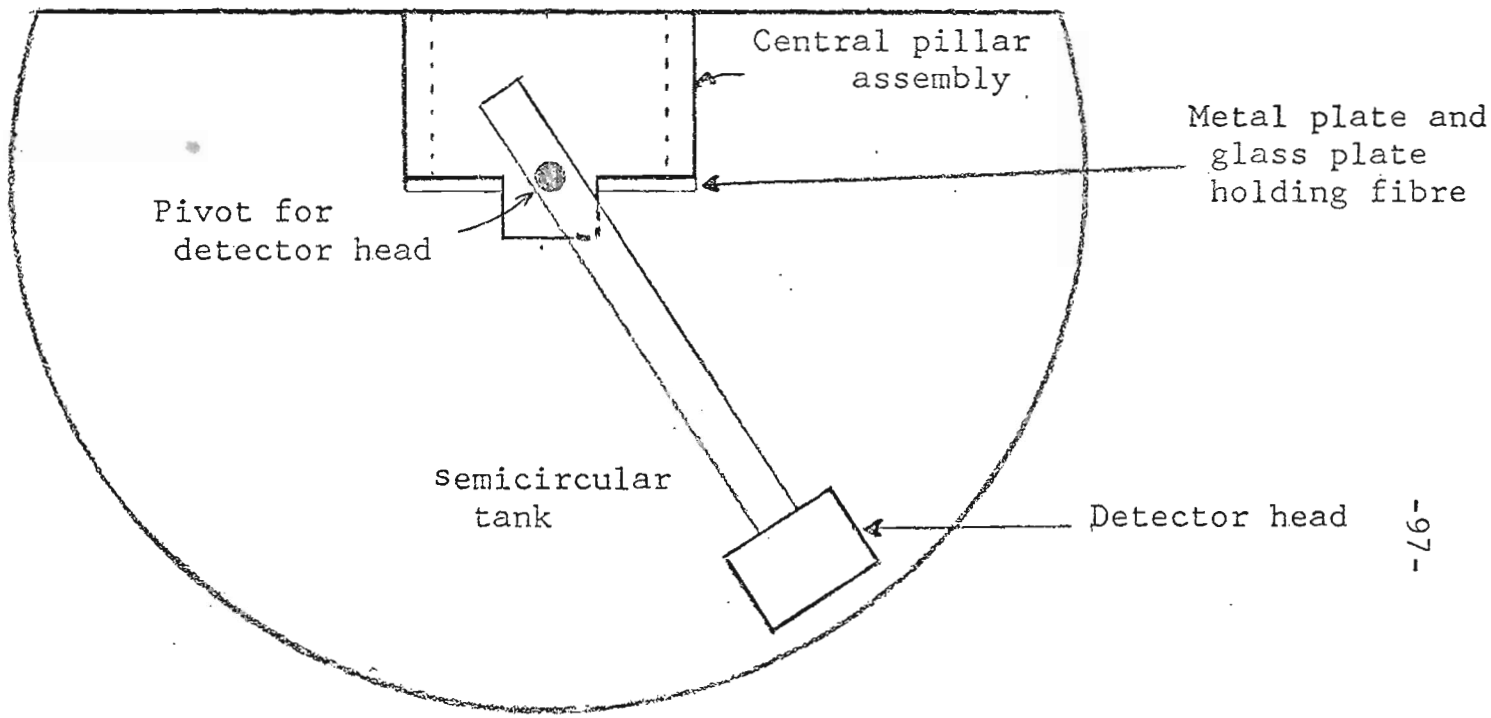

Fig 24 Plan view of modified fibre scattering apparatus
(Stepping motor omitted for simplicity)

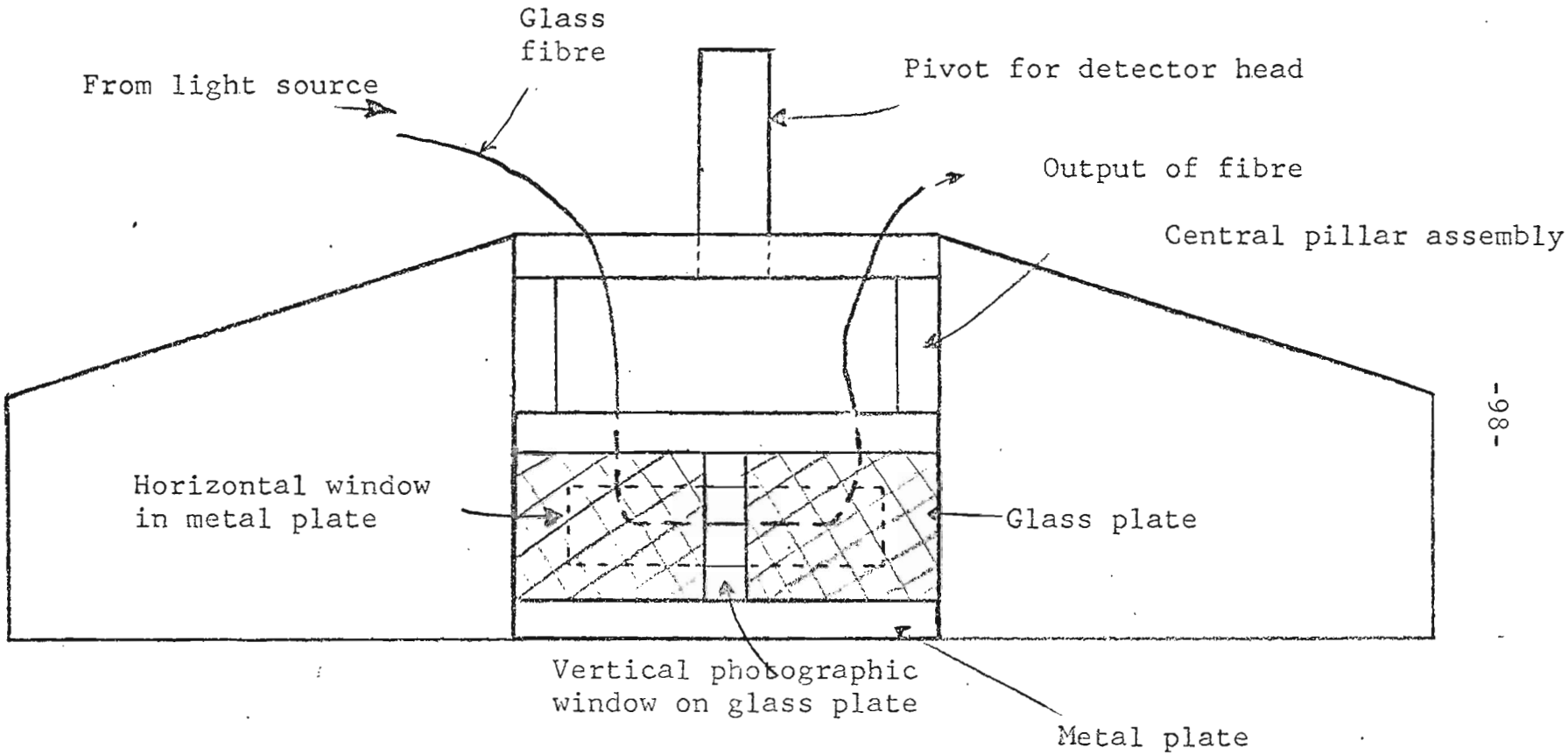

Fig. 25 View of back of tank and central pillar assembly showing mounting of fibre behind photographic window
(Stepping motor not shown for simplicity)

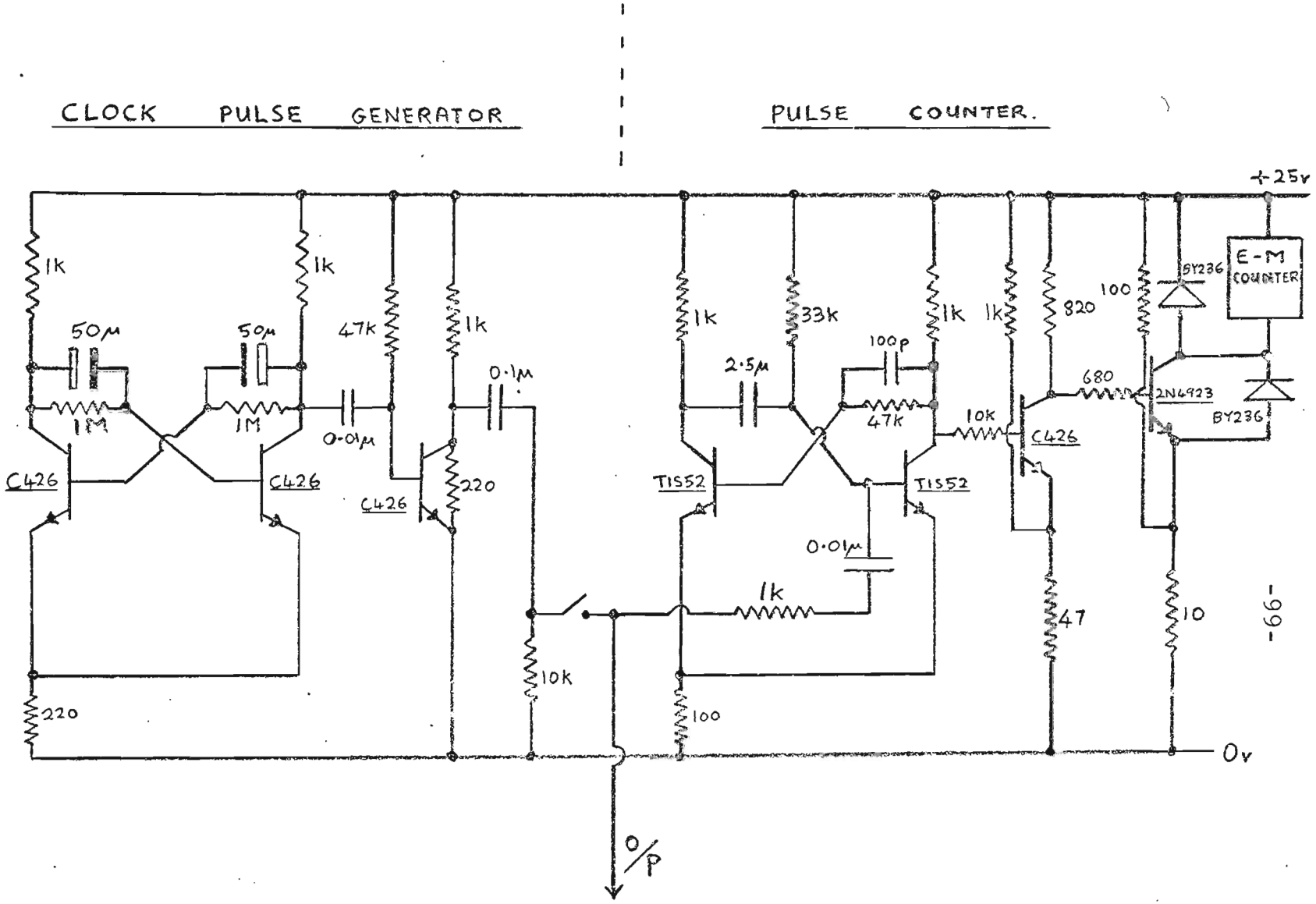

Fig.26 Clock pulse generator and step counter

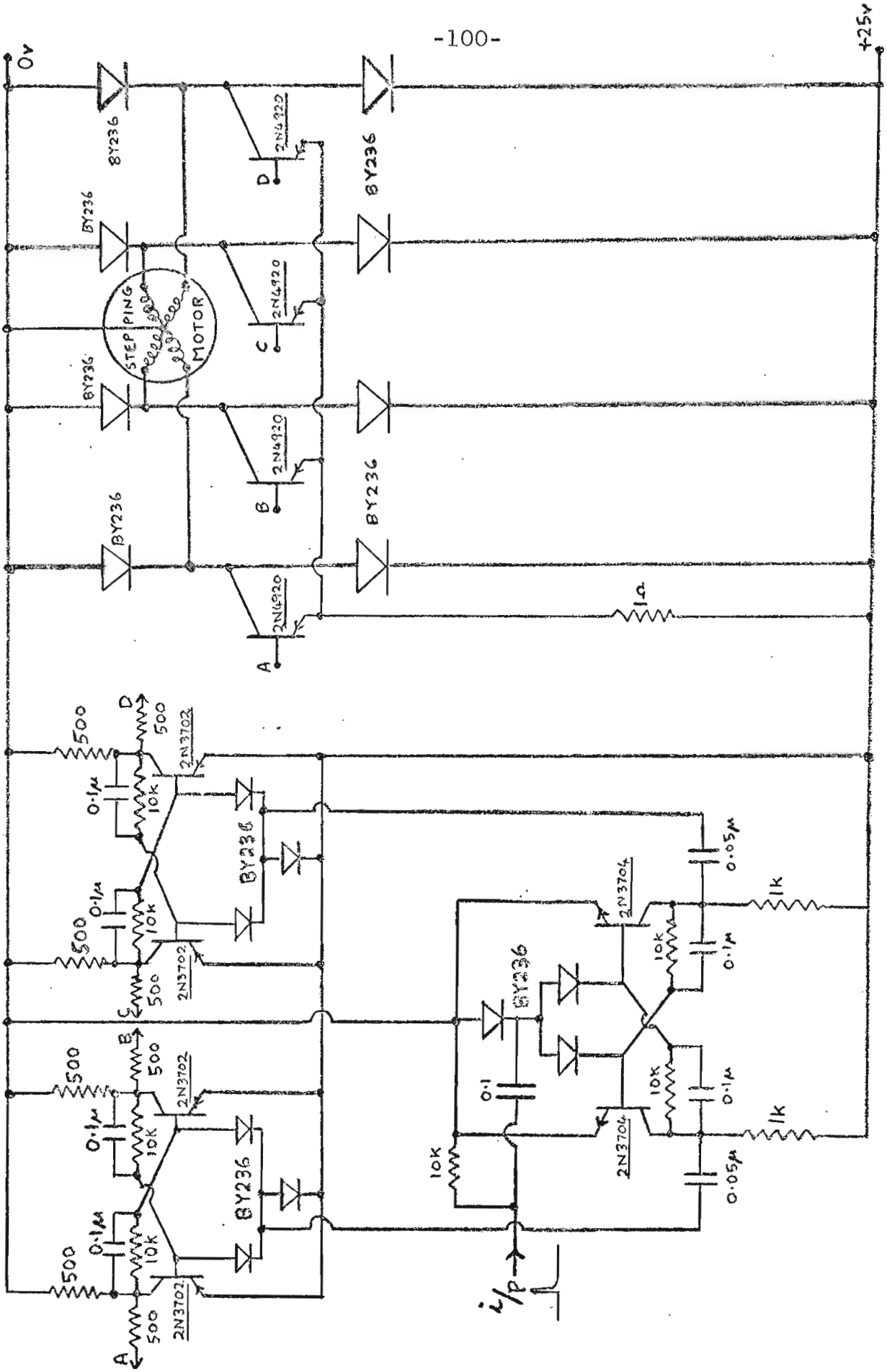

Fig 27 Stepping motor driving circuit (motor moves 1 step of 1 8^{o} for each

4. MANUFACTURE OF GLASS FIBRES

4.1. INTRODUCTION

Since the advent of cladded fibre optics, interest has been expressed in low loss large core fibres, both for optical communicati and for the more conventional light guiding applications, such as aircraft fire detection systems[1]. The interest in large core fibres as the guiding medium for use in optical communications arises from the fact that such a system may prove to be more easily realisable than one using single mode small core fibres, and will find application where the large bandwidth of the single mode fibre system is not required.

This report describes the initial evaluation of large core fibre production technology, an assessment of the problems involved in production of low loss fibres, and the construction of the fibre drawing machine. The work has advanced to the point where fibres of good commercial quality have been produced, and the drawing machine has been proved. Work will now progress to improving the process for the production of low loss fibres.

4.2. FIBRE SPECIFICATION

The initial specification for large core fibres is often a direct result of factors other than those resulting from the optical theory. The following specification is an indication of this.

4.2.1 Diameter

This was chosen to lie between 50μ and 100μ for ease of handling, flexibility and good mechanical strength.

4.2.2. Core-Cladding Ratio

In order that there should be minimum energy propagating in the cladding, which has a greater loss than the core, the core should occupy as much of the 50μ to 100μ overall diameter as possible, provided that the cladding thickness is sufficient to allow negligible electromagnetic field at the fibre-air interface. A core-cladding ratio of about 10:1 is satisfactory and can be realised using available glass tubing in the drawing process. The resulting core diameter of around 70μ and the relatively large refractive index difference between core and cladding permits multimode waveguide propagation of light, and is characteristic of large core fibre light guides.

4.2.3 Length

With present attenuation the maximum fibre length required is about 200 metres, so a length of 4 kilometres was specified to allow several samples to be taken from one fibre draw, and to allow for the expected improvement in attenuation.

4.2.4 Attenuation

An attenuation of about 20dB/km is ultimately required in an optical communications link. However, as a preliminary check on the drawing process, a 500dB/km attenuation was specified, as claimed for good commercial fibre.

4.2.5 Durability

A chemically stable fibre with good weathering properties and high mechanical strength is required.

4.3. MATERIALS SURVEY

Two highly transparent materials are required for an optical waveguide, the core material having a higher refractive index than the cladding material. The bulk loss of the cladding material is less critical than that of the core[2], as a high percentage of the energy propagates in the core. The following is a survey of possible materials.

4.3.1 Plastics

At the present time only two plastics have sufficiently high optical transmittance to be considered, these being polystyrene and methyl methacrylate. In common with other plastic materials they suffer from high optical scattering resulting from their long chain molecule constitution. Fibres fabricated from polystyrene cladded with methyl methacrylate have shown an attenuation of 2000dB/km[3], and exhibit an absorption band at 0.9μ, the suggested wavelength for an optical communication link.

4.3.2 Silica

At first sight silica appears to be an ideal material as it shows both low absorption and scattering loss. Total bulk attenuation as low as 11dB/km has been measured[4]. The low scattering may be attributed to the lack of large ions in the glass structure, and to the fact that silica is a single phase system, so that phase separation into microscopic domains of differing refractive indices cannot occur. The low absorption, however, may be largely attributed to the care taken during manufacture to eliminate impurities.

Silica has three disadvantages when considered as a material for use in optical waveguide fabrication.

a) The working point (10^4 poise) of silica is very high, about 2300°C, at which point considerable volatilization occurs[5]. The advanced technology required to obtain this high temperature is a disadvantage, and the choice of a thermally compatible cladding material is difficult.

b) The refractive index of silica is low, 1.4518 at 0.9μ, and a cladding material of lower refractive index cannot easily be found.

c) The expansion coefficient of silica, $5.5.x10^{-7}/°C$, is more than an order of magnitude lower than that of possible cladding materials. Fibre manufacture by high temperature drawing is difficult as the cladding material may fracture on cooling of the fibre, owing to the high tensile stress.

Silica fibres cladded by vacuum deposition of MgF_2, or by extrusion of plastic coatings, have been fabricated. Unfortunately the fibres show high attenuation (1000dB/km at 0.9μ [6]) possibly as a result of interface imperfections, to be discussed later.

4.3.3 Glasses

The majority of glasses are formed by the addition of metal oxide to silica, known as the classic glass former. The simplest silicate glass is pure fused silica, which on average is a random arrangement of silicon-oxygen tetrahedra connected to one another by oxygen ions

at the corners. The structure lacks the long range order of atoms periodically located on a regular lattice, as found in crystalline solids. On the addition of a metal oxide, the metal ion can be accommodated within holes in the structure. The excess oxygen require that the network be broken at several points corresponding to oxygen ions bonded to a single silicon-oxygen tetrahedron, known as non-bridging oxygen ions. The excess negative charge of the non-bridging oxygen ions is compensated by the presence of the metal cation[7,8].

The breaking of the oxygen-silicon bridging bonds by the addition of metal oxides, called network modifiers, has numerous effects on the physical properties of the glass, the most important in the present context being the following.

a) The viscosity of the glass at a given temperature is reduced to a considerable degree, in direct relation to the remaining fraction o oxygen atoms which bind the infinite network together by joining two silicon ions. Thus the addition of 20% Na_2O to silica reduces the viscosity at 1400°C from 10^{12} poise to 10^{2} poise.

b) The expansion coefficient of the glass is increased as a result of a less tightly bound structure.

c) The refractive index is increased owing to the addition of ions whose polarizability is high. In general the refractive index increases both with ion concentration and with the polarizability o the ion.

Commercially available optical glasses are complex mixtures of as many as twenty components, many of which are added for ease of

manufacture. Amongst these are As_2O_3 used as a fining agent to remove bubbles from the viscous melt, B_2O_3 and BaO used as melting fluxes, Al_2O_3 used to retard crystallization and improve weathering properties, ZnO used to improve acid resistance and the oxides of Ca, Na and Mg used to lower the viscosity or increase the durability. Other constituents are added to enhance a particular desired optical property, examples being PbO used to increase the refractive index, BaO and TiO_2 used both to increase refractive index and modify the dispersion, and B_2O_3.

As can be seen the production of optical glass is highly complex, and necessarily involves an element of trial and error. However by suitable choice of glasses the previously mentioned disadvantages of silica as an optical waveguide material may be overcome. A wide range of refractive indices, expansion coefficients and softening points are available. For this reason glass was chosen as the material to be used in the manufacture of optical fibres for communication.

4.4. GLASS SPECIFICATION

Optical glasses cannot at present meet the requirements for use in an optical waveguide core. The following is a discussion of these requirements.

4.4.1 Loss

The most important property in the present context is the bulk attenuation of the glass. The loss mechanism may be divided into two parts.

4.4.1.1 Absorption

Absorption is the dominant loss mechanism in available optical glasses, and is mainly the result of impurity ions present in the glas Absorption bands due to the resonance of the interatomic bonding in the glass structure are not apparent in the visible region of the spectrum, the difference in energy states corresponding to resonances at wavelengths greater than 5μ [9]. The nearest structural absorption band to the visible is the so-called 'water' band occuring at about 2.8μ, caused by the retention of water in the form of the OH radical [10] This absorption is particularly strong, but is is thought that the 'ta of the band would have a negligible effect in the visible region.

Absorption in the visible and near infra-red regions is caused by electronic transitions, broadened into bands of allowed states by the interaction of ions in close proximity [11]. The transition elements, characterized by an incomplete d shell and the rare earth elements characterized by an incomplete f shell, are the main causes of visible

absorption, and may be present as impurities in the glass. Ferrous iron is the main impurity present in the raw materials and consequentl is the most difficult to eliminate. It is responsible for the characteristic yellow-green colour in commercial window glass.

In addition to the ion concentration and its oxidation state, absorption phenomena are affected by the host material. It is hoped that with further advances in glass technology a high purity glass wil become available with a bulk absorption of less than 20dB/km, the design limit for a communication system.

4.4.1.2 Scatter

Scatter in a glass may be attributed to the atomic structure of the glass, in particular to the presence of large ions[12], and to macroscopic inhomogeneities in the glass. These inhomogeneities may be caused by phase separation into regions of differing refractive index[13,14], or on a larger scale, by the presence of air bubbles, stones, or the crystal phase.

In general optical glasses show very low scatter, as great care is taken during manufacture to eliminate any form of inhomogeneity. The figures obtained to date indicate that a scatter loss well below the design figure of 20dB/km may be expected[15].

4.4.2 Viscosity Range

A glass with a 'low viscosity' and a long viscosity range is required to simplify fibre fabrication. A 'low viscosity' glass is a glass with a low temperature softening point ($10^{7.6}$ poise), allowing

fibre drawing at more easily attainable temperatures. The viscosity at a given temperature is reduced in proportion to the ionic radius of the cation replacing silica on a cation for cation basis[16], so that low viscosity glasses may be expected to have high refractive indices, as refractive index is generally also dependant on the cation ionic radius[17].

A long viscosity range indicates a wide range of drawing temperatures, again simplifying fibre fabrication. A high liquidus viscosity is a further advantage, as fibre drawing above the liquidus is then possible, thereby reducing the risk of the glass devitrifying into the crystal phase. Fig. 1 shows the viscosity-temperature relationship for a typical glass, and indicates the commonly quoted viscosity points.

4.4.3 Glass Stability

Glasses tend to revert to the crystalline state when cooled below the liquidus, until a temperature is reached at which the viscosity is sufficiently high to hamper the rate of crystal growth. The rate of crystal growth reaches a maximum at a temperature about 100°C below the liquidus, and falls to a negligible value at about 200°C below the liquidus. Although spontaneous nucleation of a crystal may occur, the number of crystals found in a partially devitrified glass is a strong function of the number of nucleating centres, usually inhomogeneities present in the glass[19]. Glass surface abrasion or contamination acts

as a strong nucleating force, and devitrification is usually observed at surfaces.

There is a risk of devitrification in any process involving heating of a glass to temperatures at which forming can take place. However with careful glass manufacture the nucleating impurities may be removed, and by the judicious selection of glass composition a highly stable glass may be obtained. The size of any nucleated crystals may be reduced to negligible proportions by rapid cooling of the glass from above its liquidus temperature, where only the liquid phase may exist, to a temperature at which the crystal growth rate is small[20]. This is easily achieved in the fibre forming process, particularly if the viscosity of the glass is such that the drawing temperature is well above the liquidus. Rapid cooling through the critical temperature range then occurs, as the glass cools in the fibre form. However even under these rapid cooling conditions, of the order of 10^{-2} sec [21], some particularly unstable glasses devitrify, and selection to avoid these compositions is desirable.

The linear velocity of crystallization is inversely proportional to the ionic radius of the glass cation, and inversely proportional to the first or second power of the viscosity at a given temperature[19] Therefore a glass relatively free from devitrification may be expected to have a high refractive index as generally this is also a function of cation ionic radius. In particular the lead silicate glasses are very stable, and may be held for several hours in the critical temperature range.

In selecting a suitable glass for fibre drawing, a glass with high refractive index and a high liquidus viscosity is likely to have a slow rate of devitrification. Further advantages may be gained by the high liquidus viscosity in that rapid cooling through the critical temperature range is possible, and that any existing crystalline phases will be reduced once the temperature rises above tl liquidus temperature.

4.4.4. Chemical Durability

Selection of a chemically durable glass is desirable, particularl for the fibre cladding. Many glasses form weathered films on contact with trace gases present in the atmosphere, or are leached by water vapour leaving a skeleton of the less soluble constituents[22]. Most glasses contain additives to improve their durability, but there is a marked difference in their resistance to corrosion, particularly amongst optical glasses where durability may be sacrificed to obtain a particular optical property.

4.4.5 Availability of Cladding Glass

The selection of both core and cladding glasses is influenced by the following matching requirements.

4.4.5.1 Refractive Index

In order for guided waves to propagate the cladding material must be of lower refractive index than the core material. Although

in this respect air is a suitable cladding material, the core- claddi interface requires protection from mechanical abrasion and contaminat so that a glass cladding is essential.

As discussed in sections 4.2 and 4.3 a suitable core glass is likely to have a high refractive index, and this has the advantage that a wide range of glasses are available for use as a cladding glas The absorption and stability requirements for the cladding glass are not as critical as those of the core glass, and the cladding is generally selected as a match for a chosen core glass.

4.4.5.2. Expansion Coefficients

Ideally the expansion coefficients of the core and cladding glasses should be matched in order to produce no residual stress in the fibre. In practice, however, provided the expansion coefficient of the cladding is lower than that of the core so that the cladding cools to a compressive stress, the match is suitable. In common with most brittle materials, glass is weak when the surface is in tension, and a low strength fibre results.

Fortunately most glasses, and particularly high refractive index glasses, have expansion coefficients in the range 70-100 x 10^{-7} /^{o}C, the exceptions having a coefficient lower than this value. Selection of a matching cladding glass is relatively easy provided the exceptional glasses are avoided as candidate core materials.

4.5. PROPERTIES OF F7

On consideration of the requirements enumerated in section 4, it can be seen that a correlation exists between various properties, and that a glass selected to satisfy some of the requirements is likely to satisfy others. Unfortunately at present there are no available glasses designed specifically for low loss fibre optics, the loss of an optical glass being relatively unimportant. Of the available optical glasses the lead silicates are the most suitable, and of these Schott F7 is the best example. The following is a discussion of the properties of F7 glass.

4.5.1 Total Bulk Attenuation

The attenuation is quoted by the manufacturers in the form of a transmission of .999 in 25mm at 0.7μ, corresponding to a loss of 170dB/km. However losses less than 60dB/km have been measured between 0.7μ and 1μ [23]. F7 shows the lowest loss of all commonly available optical glasses, this being partly attributable to the oxidizing nature of the high lead host material. The glass shows no evidence of a divalent impurity ion absorption band at about 0.9μ as the divalent io is oxidized to the trivalent state, resulting in ultra-violet absorptio Thus the main impurity, ferrous iron, is oxidized to the ferric state.

The glass is thought to be phase separated into an emulsion of high PbO areas, of about 100Å average size, in a matrix of SiO_2. This inhomogeneity causes greater scattering loss than would be expected in a non-phase separated glass, but the loss is of an acceptably low value and has been measured at 4dB/km at 0.9μm [25].

4.5.2 Refractive Index

The refractive index of 1.612 at 0.85μ is sufficiently high to enable any commercially available glass tubing to be used as a cladding material.

4.5.3 Expansion Coefficient

The expansion coefficient of $96 \times 10^{-7}/^{\circ}C$ is high, and is higher than or equal to available glass tubing.

4.5.4 Viscosity

F7 has a softening point of 580°C, so that pulling temperatures ranging from about 700°C to 1200°C may be used. The glass has a high liquidus viscosity, and is very stable.

4.5.5 Durability

F7 has excellent humidity and acid resistance. A disadvantage is the poor mechanical strength and hardness; however this is not a serious disadvantage in the fibre form as the cladding material acts as a protective sheath.

4.6. FIBRE PRODUCTION

4.6.1 Methods Available

Cladded glass fibres for light transmission are made by a number of down-draw processes, each having particular advantages.

4.6.1.1 Rod and Tube Method

This is the softening of solid core and cladding material with simultaneous drawing into a fine fibre. A rod of core glass is fitted within a tube of cladding glass, and the composite assembly softened and drawn into a fibre. The ratio of the fibre core to cladding diameter is equal to that of the rod and tube.

The disadvantages of this process are that the cladding material is restricted to glasses available in tube form, and that available tubing wall thickness dictates the core-cladding diameter ratio. Possibly the major disadvantage, however, is the possibility of core-cladding interface imperfections, resulting either from contamination of the rod and tube surfaces, or by scratching of these surfaces. Research into the production of high strength silica fibres has shown that surface imperfections are not entirely smoothed by drawing from a rod [26].

4.6.1.2 Concentric Crucible Method

This method involves the simultaneous drawing of softened core material from a central container and cladding material from an annular container. The method overcomes the previously mentioned disadvantage of interface imperfections, as the surfaces are freshly

formed and are expected to be of good quality. Disadvantages are the difficulty of process control, volatilization of the glass constituents, entrapped air bubbles in the molten glass, the close viscosity match required at the drawing temperature, and the possibility of contamination by the crucible material[27].

4.6.1.3 Two Stage Processes

The core is first drawn by one of the above methods, and provided with a cladding in a subsequent process. This may either be by the addition of a cladding material, possibly during the initial drawing process in an annular furnace located below the main furnace, or by the modification of the surface of the core material to produce a lower refractive index. The surface treatment may involve ion diffusion[28] or chemical reaction.

4.6.2 The Fibre Drawing Machine

One of the most important factors in the design of an experimental fibre drawing machine is versatility. In order to investigate the fibre drawing technique and the effect of various parameters on the process the machine must be designed to allow a wide range of pulling speeds, feed rates and temperatures, and in addition must be able to accommodate the inevitable design changes associated with any experimental machine used in an unfamiliar field.

The rod and tube method of fibre production would appear to be the most versatile of the available techniques, and the relative simplicity of the process allows greater control variations to be made.

The process does not involve large scale glass remelting with associated gassing and contamination problems, and avoids the expense of high purity glass containers. However the core-cladding ratio of the fibre is to some extent dependant on the availability of suitable glass tubing, and also on the forms of supply of optical glass rod. For this reason a rod diameter of 10mm was chosen, allowing commercial glass tubing with a wall thickness of 1-2mm to be used as the cladding material. Using this diameter the convenient rod length of 400mm yields 6km of 100um diameter fibre. This fibre length is adequate for present requirements and permits several parameter variations during the fibre pull, whilst using a relatively small quantity of glass per draw. The rod length of 400mm allows several centimetres of wastage at the beginning and end of the draw, and the relatively small diameter of 1cm permits rapid heating of both the glass and the furnace to the pulling temperature.

The fibre drawing machine is shown in Fig. 2 and Plate 1, and consists of a framework of two vertically mounted 2" diameter, 10ft long, ground steel bars supported by angle girders and secured to the floor and ceiling of the laboratory. The rigid framework thus constructed allows all other equipment to be clamped to the steel bars whilst remaining both demountable and fully adjustable in height about a fixed fibre drop The height of the machine is limited by the laboratory ceiling, so that a relatively short fibre drop from furnace to winding drum (1.5 metres) is used. This limits the maximum pulling speed as at high speeds the fibre has insufficient time to cool

before being wound onto the drum.

The concentrically assembled rod and tube are clamped in a chuck and smoothly lowered into the furnace at a predetermined rate by a vertically mounted lead screw. The lead screw, of sufficient traverse to accommodate the rod length of 400nm, is clamped to one of the ground steel bars, and driven by a variable speed D.C. motor through a 100:1 worm reduction gearbox and a system of pulleys. The final fibre diameter is given by :

$$d_f = d_r\sqrt{\frac{v_f}{v_r}}$$

where d_f = fibre diameter

d_r = overall rod and tube diameter

v_f = fibre pulling rate

v_r = rod and tube feed rate

Thus if fibre diameters ranging from 30µm to 120µm are required, the feed rate must be variable over a 16:1 range, in addition to the normal motor speed control used to match the feed rate to the pulling rate. This 16:1 range is achieved by a system of pulleys providing 1/4, 1/2, 1, 2, 4 x motor speed to the worm reduction gearbox. The 8 T.P.I. lead screw drives a closely machined slider on one of the ground steel bars, giving a smooth accurately controlled feed rate variable from 0 - 3mm/sec. The driving motor is a 1500rpm, 1/4H.P. D.C. motor, thyristor controlled over a 30:1 range, with a 0.1% load/speed variation, and has an automatic stop facility to prevent inadvertent damage to the furnace by excessive slider travel.

Having obtained an accurately controllable feed to the furnace, and hence good diameter control, it remains to ensure that the rod and tube assembly is lowered concentrically through the close-fitting furnace. Commercial glass rods and tubes are significantly bent in long lengths so an articulating ball-joint mount is utilised for the glass clamping chuck, and the glass is guided into the furnace by an iris, spring loaded to close around the glass.

The glass softens within the furnace and attenuates into a fine composite glass filament. After consideration of the 1.5m fibre drop available, and the expected range of fibre diameters and pulling temperatures, it can be calculated[21] that the maximum pulling speed to allow sufficient fibre cooling will be of the order of 10 metres/sec. The fibre is wound in a mono-layer onto a cast aluminium drum, 50cm long by 50cm diameter, accurately machined to ensure an even pulling speed. The drum is designed to have a mono-layer capacity of 3km of fibre, and provides maximum mechanical stability with minimum inertia to enable high acceleration to the pulling speed. The drum is driven by a thyristor controlled 1500rpm ½H.P. D.C. motor via a 4:1 toothed belt reduction, giving a pulling speed variable from 0-10 metres/sec. Acceleration to the maximum speed of 375rpm occurs in approximately 1·5 seconds, and the speed control is accurate to .01%.

It is a considerable advantage in an experimental fibre drawing machine to have the fibre produced in a monolayer, as sections of fibre may then be easily removed for examination, and the effects of varying parameters investigated. Monolayer winding is achieved by

mounting the drum and drive motor on a slide table utilizing linear crossed-roller bearings, and traversing the table 150u for every revolution of the drum by means of a lead screw driven from the drum shaft . In this way the main fibre pulling axis is maintained, and all equipment is able to work on a common fibre line. A graphite guide with a gentle radius is used to lead the fibre onto the drum, thus avoiding breakage due to tight fibre radii. Graphite has proved to be particularly successful for this application, owing to its machinability, low friction, and heat resistance. Both the graphite guide and the drum may be moved to allow a clear drop for the hot end of the rod and tube on starting a draw.

The control circuits for the feed motor and drum motor may be locked together so that the speeds may be adjusted in synchronism. This facility is provided to allow adjustment of pulling speed to a particular furnace temperature whilst maintaining a substantially constant fibre diameter. In practice the diameter response to a change in pulling speed is considerably faster than to feed rate, so that time must be allowed for transient diameter changes to subside. Results to date suggest that the mechanical and control accuracy is sufficient to produce a fibre diameter variation of less than 1%.

The fibre diameter may be continuously monitored during a draw by an ultra-violet shadow method. The apparatus is located immediately above the drum , thereby allowing maximum fibre cooling time before passing through the graphite guides locating the fibre between the low pressure mercury ultra-violet lamp and the shadow-projecting objective.

An ultra-violet source is used to avoid errors due to edge diffraction effects, and, since the glass is opaque to ultra-violet, corrections due to fibre transmission and interference. The projected shadow is compared with an aperture and a photomultiplier tube used to detect the difference. The fibre positional accuracy requirement is $\pm 100\mu$ in a line transverse to the optical axis, and $\pm \frac{1}{2}$mm along the optical axis. The guiding system pushes the fibre 2mm from the fibre drop line in a 5cm radius, and is adjustable in the required optical plane, adjustment being for a minimum in transmitted light to the photomultiplier. Both light source and optical system may be swung out of the fibre drop line at the start of a draw.

The furnace is shown in fig.3. The furnace requirements are summarised as follows :

a) Fast thermal response to enable rapid temperature changes for fibre starting conditions, and to allow fast recovery from thermal disturbances.

b) Accurate temperature control to ensure close diameter control, and to allow pulling parameters to be accurately specified.

c) Variable hot zone length, adjustable thermocouple position, and variable thermal gradient through the furnace to permit optimization of the glass thermal cycle.

d) To ensure good heat transfer to the glass, and close glass temperature control over the thermal cycle the furnace should be close fitting about the rod and tube, and convection currents should be minimised.

e) Low external heat losses to reduce the watt loading on the small gauge resistance wire, and thus extend the life of the furnace.

f) Close dimensional tolerances and mechanical stability to ensure concentricity of the rod in the furnace, giving even glass heating.

g) Maximum design temperature of 1300°C. This temperature is above the working point of Pyrex, 1220°C , the most heat resistant of proposed cladding materials.

h) To prevent variable cooling conditions during the critical cooling zone directly below the furnace, the furnace should be fitted with a shroud in this area.

The furnace consists of a 1.8cm bore by 10cm long threaded alumina tube, externally wound with 1mm diameter Kanthal A1 wire. This is cemented within a larger alumina tube and a slot cut in each side of the assembly to allow passage of the terminal wires and the thermo-couple probe. The annular clearance between glass tube and furnace wall is 1-2mm depending on the glass tubing used. The furnace windings are tapped into 1cm sections allowing a minimum hot zone length of 1cm, and a maximum length of 6cm. In practice the lower three windings have been found most suitable for high speed, high temperature fibre pulling.

The alumina tube is accurately located within a machined stainless steel caseing clamped between two 'Sindanyo' end plates, and insulated with 'Fiberfrax' block. A finned stainless steel fitting provides heat isolation for the glass-rod-centralising entrance iris, and a finned brass fibre cooling chamber is provided below the

furnace. This chamber is fitted with an iris closing around the fibre to reduce convection effects. A Pt/Pt13%Rh thermocouple probe passes through a slot in the alumina tube, and into the hot zone of the furnace. The furnace hot zone is controlled to within 1°C by a three-term temperature controller driving a phase-controlled thyristor power circuit. The furnace insulation is such that a power of 200 watts is sufficient to reach the maximum design temperature of 1300°C, and the response time to a 100°C change in temperature is about 1 min, this being limited only by the risk of thermal shock breakage of the alumina tube. The furnace is mechanically centred about the fibre drop line by means of three adjustable clamps mounted on the furnace table.

The furnace as described has proved successful over several months running, but finally burnt out at one of the Kanthal leads. This had been anticipated as the maximum working temperature of Kanthal A1 wire of 1350°C, and is not entirely satisfactory in the smallest wire gauges. The furnace has since been redesigned to utilise 0.6mm platinum windings, with a design limit of 1500°C, the remainder of the furnace being unchanged except for the thermocouple entrance. The thermocouple now enters the furnace vertically from a slot in the brass cooling chamber to allow the platinum furnace winding to be totally embedded in cement.

To commence a fibre draw the glass rod and tube are cleaned and assembled concentrically, with the rod restrained from falling out of the tube by a metal clip. The assembly is then clamped in the chuck and

lowered through the spring loaded iris in the top of the furnace. The iris is released to centralise the glass in the furnace and the furnace temperature set to about 800°C. The rod and tube are then lowered through the furnace hot zone until they are seen to emerge from the open fibre exit iris. The furnace temperature is then increased to the point at which the glass softens and the weight of glass below the hot zone causes the glass to neck and descend down past the diameter measuring equipment and drum, drawing a filament of glass with it. This filament of glass is attached to the drum, the drum and diameter measuring guides moved back to the fibre centre line, and the drum and feed control motors started. The temperature of the furnace is then quickly raised to the required pulling temperature and the drum and feed controls increased together in a preset ratio to the desired pulling rate The pulling and feed rates, and the pulling temperature, are previously decided from a consideration of the working points of the core and cladding, the requirement of good interface fire polishing at high temperatures with the corresponding disadvantage of increased diffusion of impurities into the core from the cladding, and the drawing stability of the particular core-cladding combination.

After completion of a fibre draw the entrance iris is opened and the rod and tube withdrawn from the furnace, after which the entrance iris is used to exclude the high convection currents inherent in a vertically mounted tube furnace. The fibre is them removed from the drum, after selection of a particular section, by a rewinding process. An 11cm diameter, 15cm long section of plastic drainpiping

is used as a storage container for ½km lengths of fibre. This drum is driven by a low inertia printed circuit motor fed by a variable constant current source, so that the motor torque, and hence the fibre tension, is held substantially constant regardless of rewind speed. In this way the main aluminium drum sets the rewind speed, and the plastic rewind drum follows automatically in speed whilst maintaining a constant fibre tension set between 10 and 50gm. The fibre is wound in a monolayer to permit observation of scattering centres when propagating light, and to allow removal of known lengths by measurement of winding width.

In summary the design and construction of an experimental fibre drawing machine has been completed, and the machine proved in practice. The machine is sufficiently versatile to fabricate a wide range of fibre diameters under varying conditions of pulling speed, feed rate, and furnace temperature, and has the ability to accommodate widely varying glass specifications. The control accuracy of the pulling parameters has yet to be fully investigated, but on initial observation has proved to give excellent fibre stability.

4.6.3 Fibre Drawing Techniques

A certain skill is involved in fibre drawing, together with a feel for the correct conditions. The possible variations are complex and are not amenable to analysis. It has been found, however, that the process is extremely stable, and initial fibre drawing was conducted to determine the limits of this stability. Basically the viscosity of the glass, the surface tension and the drawing speed defi a region in which filamentisation may take place. If the temperature of the glass is too high and the viscosity too low, the drawing force is insufficient to balance the surface tension acting upwards at the attenuating zone, and the fibre 'burns off', that is to say the glass drips. However this upper temperature limit is further complicated by the hot zone length, as the rate of heating of the glass is dependent on the glass diameter, the temperature of the rod and tube being somewhat lower than the furnace temperature. If the hot zone extends below the point at which the diameter is substantially that of the final fibre diameter, there is a risk that the increased rate of heating will cause the fibre temperature to reach a point at which 'burn off' will occur. Since the attenuating zone length is dependent on the drawing temperature an optimum hot zone length exists, and may be achieved by selection of furnace taps.

The maximum pulling temperature for a particular glass is a complex function of surface tension and viscosity. The surface tension decreases approximately linearly with increasing temperature[29], while the viscosity reduces approximately as a square law (fig.1). The temperature at which the surface tension forces exceed the viscous forces corresponds in most glasses to a viscosity of about 10^2 poise, the viscosity of golden syrup.

The lower temperature limit for fibre drawing occurs when the viscosity rises to such a value that the drawing force is sufficient to break the fibre. This temperature limit is not well defined as the drawing speed may be reduced to decrease the pulling force, since for constant fibre tension the drawing speed is a function of furnace temperature.

The situation is further complicated by the fact that the bulk glass is a two glass composite, each glass having different characteristics. In general three empirical rules emerge for a successful fibre draw.

1) Filamentization may occur at temperatures corresponding to viscosities in the range 10^6 to 10^2 poise. A glass with a long viscosity range will have wide temperature limits.
2) The lower the viscosity the higher the pulling rate required to maintain stable attenuation.
3) The lower the drawing viscosity the shorter the furnace hot zone required.

The degree of perfection of the core-cladding interface is dependent to some extent on the initial state of the rod and tube surfaces. These surfaces undergo a smoothing by surface tension induced fluid flow during the drawing process, and therefore it is possible that the lower the drawing viscosity the better the interface quality. Work has been directed towards high temperature, low viscosity fibre drawing, using tubes of a high softening point relative to that of F7, the core glass. This has the effect of forming a stable attenuating cone containing a pool of low viscosity core glass, and the advantage that the core glass surface is completely lost within the pool It is hoped that the inside surface of the cladding tube will not cause interface imperfections as this surface remains untouched. Work is continuing on this aspect of fibre drawing in an attempt to determine the limits of stable pulling conditions.

Fibres pulled to date consist of F7 core cladded with either Pyrex glass or Chance Pilkington ME1 glass. Since a rigorous glass cleaning facility has not been completed, test runs have been directed towards establishing optimum pulling conditions, although some measurements of the optical properties have been undertaken.

4.7. FIBRE EVALUATION

4.7.1 F7 Core - ME1 Cladding

ME1 glass is a relatively pure glass tubing made for critical electrical applications, and has a bulk attenuation of 19,000dB/km at 0.633μ, as measured by S.R.D.E., Christchurch. This attenuation figure is excellent for a commercial glass tubing, compared with figures in excess of 10^5dB/km for an average soda glass.

The relevant properties of ME1 compared with those of F7 are as follows.

	ME1	F7
Softening point ($10^{7.6}$poise)	720°C	580°C
Working point (10^4 poise)	1040°C	850°C
Thermal expansion coefficient	50×10^{-7}/°C	97×10^{-7}/°C
Refractive index n_d	1.487	1.625

There is a large viscosity and expansion difference between these two glasses, but stable fibre drawing was achieved from 900°C to 1150°C at drawing speeds up to 5 metres/sec. Plate 2 shows a section of this fibre set in wax.

Several fibre draws were completed in order to evaluate the drawing machine and the process. The fibres proved to scatter badly when transmitting light as can be expected with no initial surface preparation.

4.7.2 F7 Core - Pyrex Cladding

The properties of Pyrex are as follows.

Softening point	820°C
Working point	1220°C
Expansion coefficient	$33 \times 10^{-7}/°C$
Refractive index n_d	1.475

Pyrex is a boro-silicate glass manufactured for its high service temperature and its low expansion coefficient, this giving good thermal shock resistance. It is of interest as it permits pulling at temperatures as high as 1350°C, at which the F7 core is very fluid, and should provide good interface wetting. The expansion mismatch results in a high strength fibre as the cladding is in strong compression. Available wall tubing thickness permits cladding thickness of 10-20μ in a 100μ fibre, using an F7 rod diameter of 1cm.

A more complete evaluation of this fibre has been undertaken as other workers in the Optical Communications Group had reached a stage at which a supply of fibres was required. Consequently more care was taken in cleaning of the rod and tube, although fibre drawing was still being conducted on a process evaluation basis. As a result of these measurements it was determined that the fibre had an attenuation of 620dB/km at 0.722μ, comparing well with commercially available fibres, in spite of the inadequate cleaning procedure. However, if fibre diameters exceeding 50μ were drawn, air bubbles were entrapped in the core-cladding interface. Since this was diameter dependent it is

reasonable to assume that air bubble trapping is a function of the rate of closure between core and cladding interfaces during the drawing process. Evacuation of the space between rod and tube is expected to overcome the problem, and may further improve the interface quality both by removing gases evolving from the softened glasses, and by excluding contaminants.

Plates 3 to 7 show various views of the Pyrex-clad F7 fibre.

4.8. CONCLUSIONS

It is thought that the high attenuation experienced in optical glass fibres can be mainly attributed to light scattering from the imperfect interface between core and cladding. Evidence for this is the high forward scatter seen from the fibre, and the diameter dependence of the fibre attenuation[30,31]. Experiments to determine the optimum fibre drawing conditions to improve the interface must now be conducted, using various cleaning techniques and a variety of cladding glasses.

Surface preparation of the two glasses is thought to be crucial, as glass surfaces are quickly contaminated by adsorption of water vapour and atmospheric impurities. It is proposed to etch the surfaces of the rod and tube to remove the layer of contaminated glass, followed by a sequence of high purity degreasing and rinsing baths. Rod and tube assembly will be carried out in clean conditions, and the air space evacuated.

The rod and tube method of fibre drawing cannot as yet be evaluated as the initial technology has just been completed. Results to date are encouraging, and the method is sufficiently versatile to enable many variations of the basic process, while remaining controllabl However, of the available processes it would appear that the rod and tube method is the most prone to interface contamination, and it remains to be seen whether this will dominate. The alternative process, the

concentric crucible method, is likely to give improved interface quality, but may result in increased absorption loss owing to glass contamination. However, if high purity low-loss core materials become available the process will become a necessity as low loss cladding materials are unlikely to be available in tube form.

4.9. REFERENCES

1. Phillips, B.G., 'High Transmittance Long Fiber Optics', Proc. of the Society of Photo-Optical Instrumentation Engineers, 14, p.69, April, 1968.

2. Roberts, R., to be published.

3. Hager, T.C., Brown, R.G. and Derick, B.N., '"Crofon" Plastic Fiber Optics', Society of Photo-Optical Engineers Annual Technica Conference, 13, p.338, 1967.

4. Jones, M.W. and Kao, K.C., 'Spectrographic Studies of Ultra-Low Loss Optical Glasses II: Double Beam Method', J. Sci. Instr., 2, 4, p.331, 1969.

5. Plascon, D., Bradford, D. and Otto, W.H., 'Silica Fiber Forming and Core-Sheath Composite Fiber Development', U.S. Navy Bureau of Weapons Research Report AD 620055, 15 June, 1965.

6. Li, P.C., Olson, O.H., Pontarelli, D.A., and Schwartz, M., 'Ultraviolet Fiber Optics', Proc. of the Society of Photo-Optical Instrumentation Engineers, 14, p.47, April 1968.

7. Holland, L., 'The Properties of Glass Surfaces', Chapman and Hall 1966.

8. Kingery, W.D., 'Introduction to Ceramics', Ch. 5, John Wiley and Sons, 1965.

9. Cleck, G.W., Villa, J.J., and Hahner, C.H., 'Refractive Indices and Transmittances of Several Glasses in the Infrared', J. Opt. Soc. America, 49, 11. p.1090, 1959.

10. Dietzel, A. 'Research on Quartz Glass', Translation from Excerpt from '60 Jahr Quarzglas - 25 Jahre Hochvakuumtechnik', issued by W.C. Heraeus GmbH, Hanau, 1961.

11. Bates, T., 'Modern Aspects of the Vitreous State', 2, ch. 5, Butterworths 1962.

12. Winter, A., 'Some Aspects of Rayleigh Scattering in Glass', J. Jap. Ceramic Soc.

13. Andreev, N.S. and Ershova, T.I., 'Interparticle Interference in Light Scattering by Glasses Containing Submicroscopic Inhomogeneities', Soviet Physics - Doklady, 12, 2, p.149, 1967.

14. Hammel, J.J. and Ohlberg, S.M., 'Light Scattering from Diffusion-Controlled Phase Separations in Glass ', J. Applied Physics, 36, 4, p.1442, 1965.

15. Daglish, H.N., 'Light Scattering in Selected Optical Glasses', Glass Technology, 11, 2, p.30, 1970.

16. Kingery, W.D., 'Introduction to Ceramics', p.575, John Wiley and Sons, 1965.

17. Kingery, W.D., 'Introduction to Ceramics', p.520, John Wiley and Sons , 1965.

18. Grauer, O.H. and Hamilton, E.H., 'An Improved Apparatus for the Determination of Liquidus Temperatures and Rates of Crystal Growt in Glass', J. of Research of the National Bureau of Standards, 44, p.495, May 1950.

19. Lambert, W.A., Aiken, D.B., and Girard, E.H., 'Continuous Filamen Ceramic Fibers', WADD Technical Report 60-244, June 1960.

20. Milne, A.J., 'The Measurement of the Devitrification Characteristics of Glass', J. Soc. Glass Technology, 36, p.275, 1952.

21. Glicksman, L.R., 'The Cooling of Glass Fibres', Glass Technology, 9, 5, p.131, 1968.

22. Holland, L., 'The Properties of Glass Surfaces', Ch. 3, Chapman and Hall, 1966.

23. Dakin, J.P. et al., 'Fibre Optical Communications 3', to be published.

24. Vogel, W., Silikattechnik, 10, p.241, 1959.

25. Laybourn, P.J.R., Dakin, J.P. and Gambling, W.A., 'A Photometer t Measure Light Scattering in Optical Glass', Opto-Electronics, 2, p.36, Feb. 1970.

26. Plascon, D., 'Silica Fiber/Core-Sheath Fiber', . S. Navy Report AD 62005, 1965.

27. Kapany, N.S., and Simms, R.J., 'Infrared Fiber Optics Investigations', Air Force Avionics Laboratory Report, AD 601572 1964.

28 Pearson, A.D., French, W.G. and Rawson, E.G., 'Preparation of a Light Focusing Glass Rod by Ion Exchange Techniques', Applied Physics Letters, 15, 2, p.76. 1969.

29. Shartsis, L., and Spinner, S., 'Surface Tension of Molten Alkali Silicates', J. of Research of the National Bureau of Standards, 46, 5, p.385, 1951.

30. Jones, A.L., 'Coupling of Optical Fibers and Scattering in Fiber J. Optical Soc. America, 55, 3, p.261, 1965.

31. Potter, R.J., 'Transmission Properties of Optical Fibers', J. Optical Soc. America, 51, 10, p.1079, 1961.

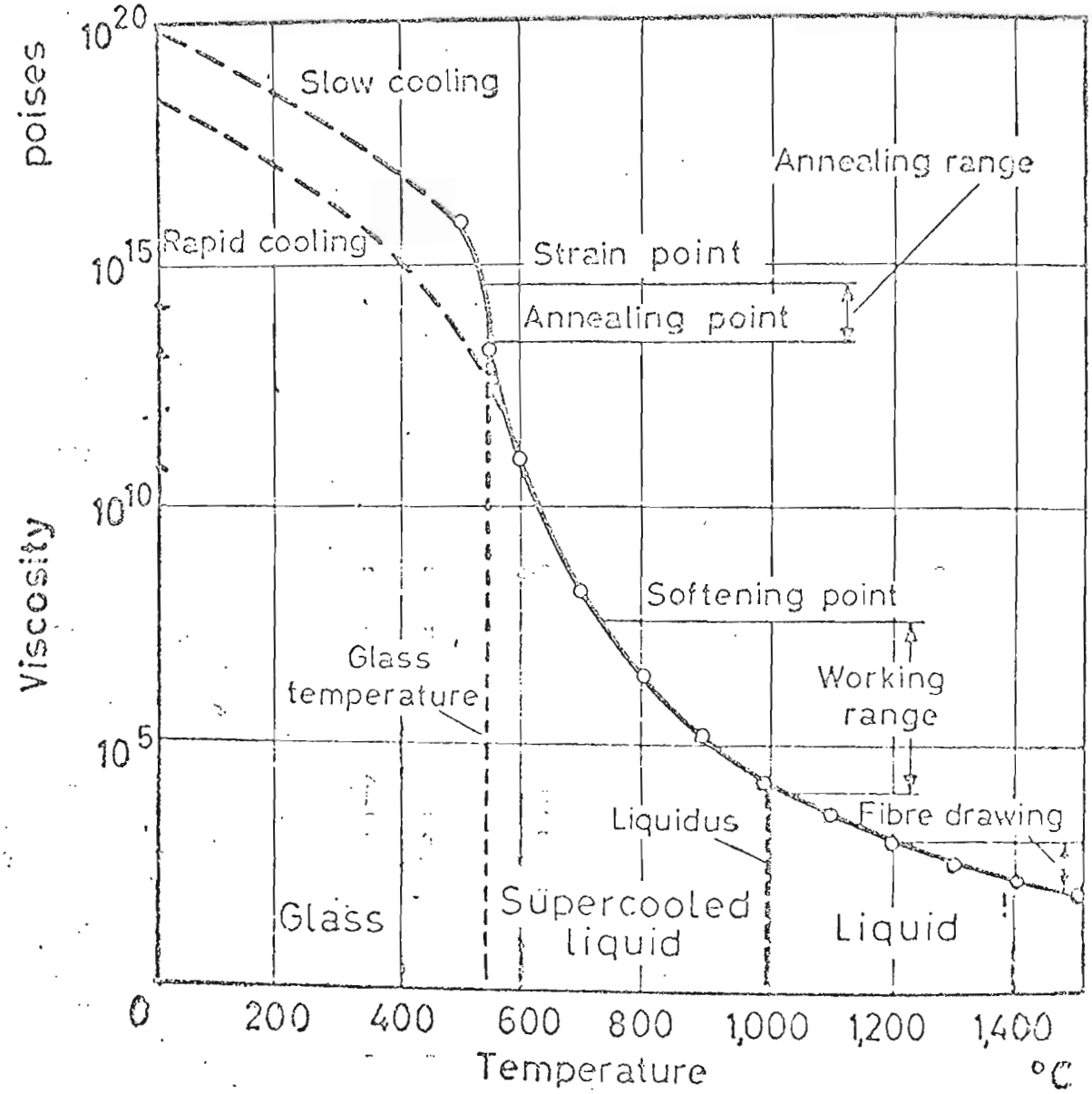

Figure 1: Viscosity vs. temperature, soda-lime glass.

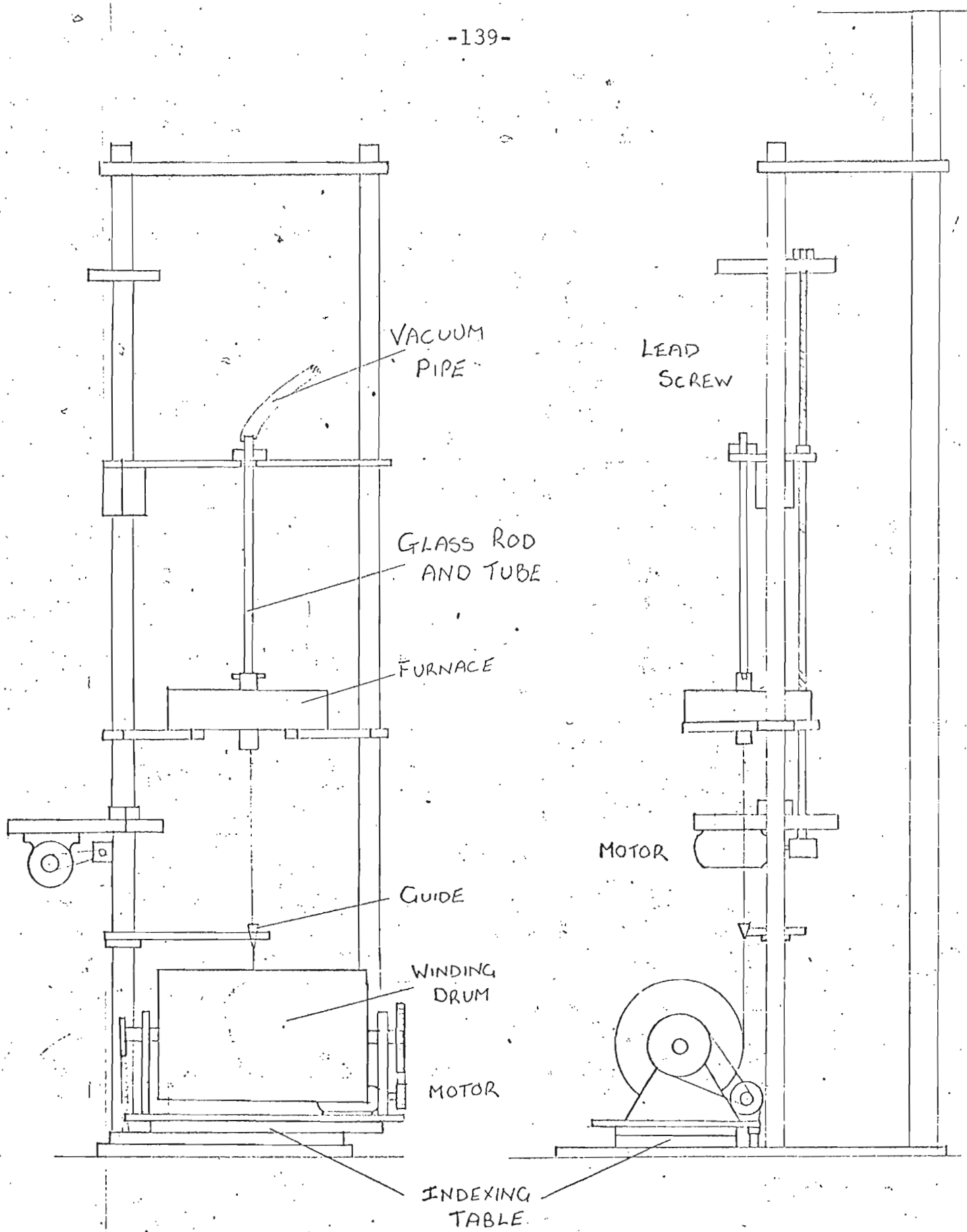

Fig. 2 Fibre pulling apparatus

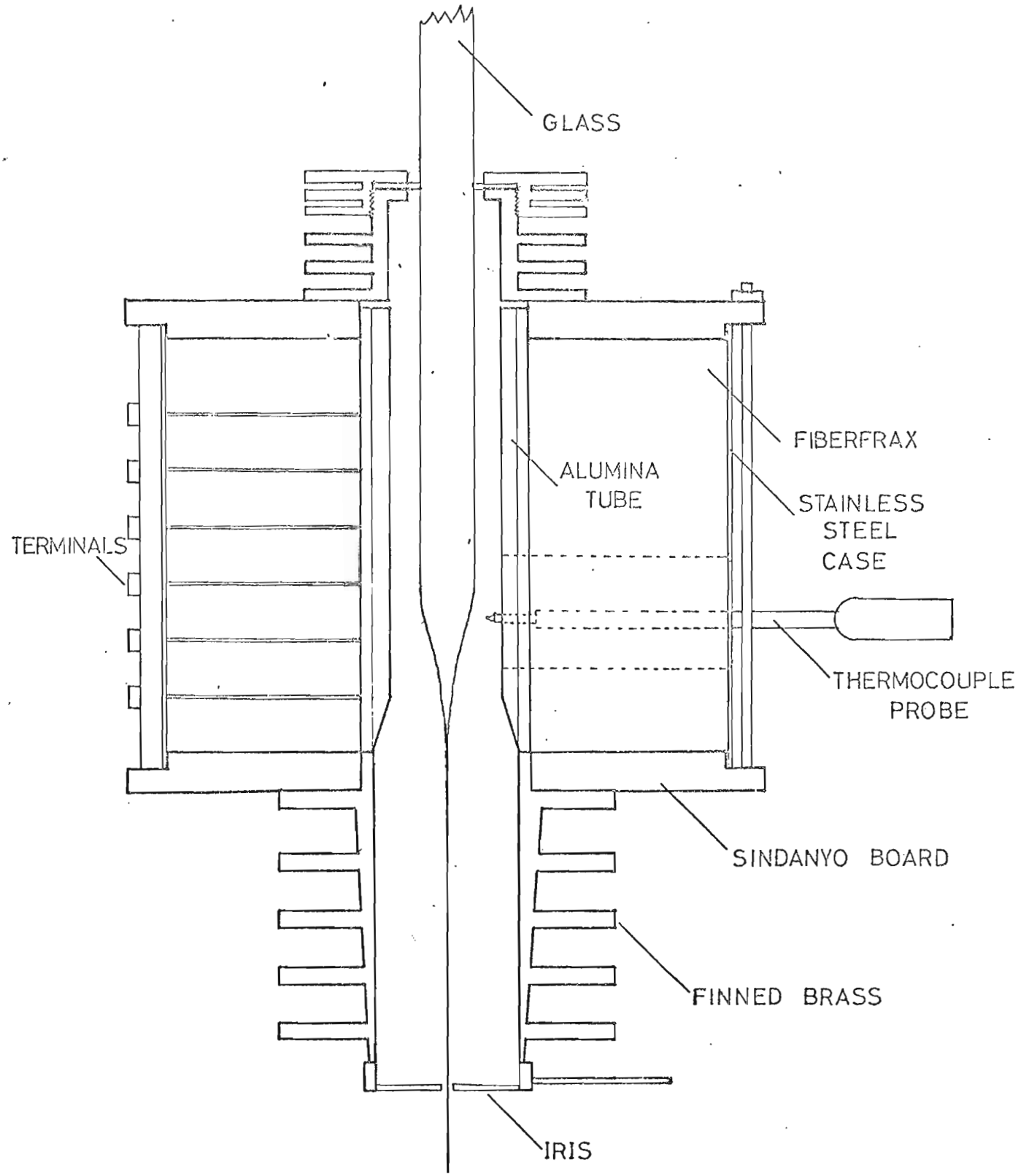

Fig.3. THE FURNACE

PLATE 1

Fibre drawing machine

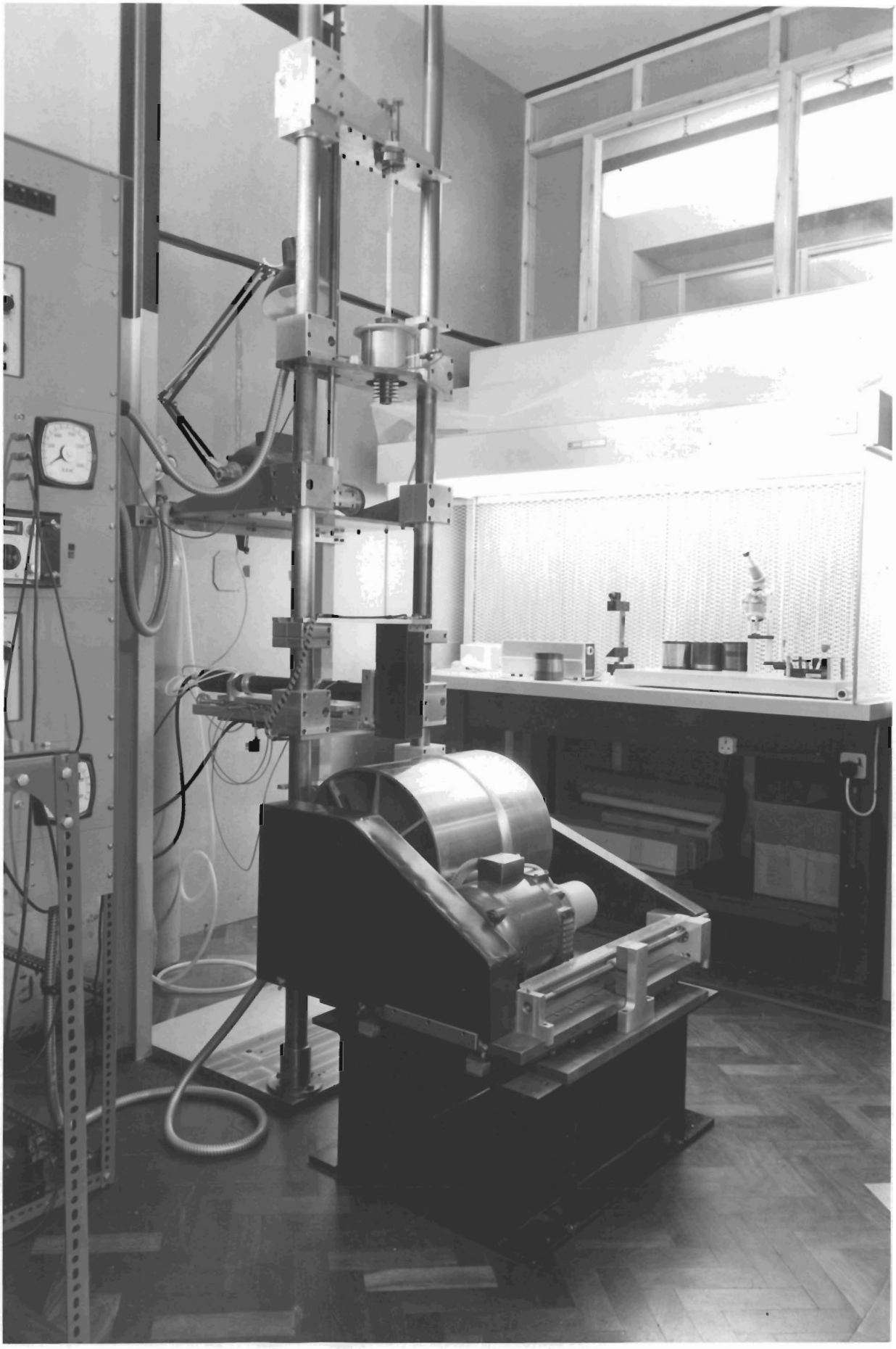

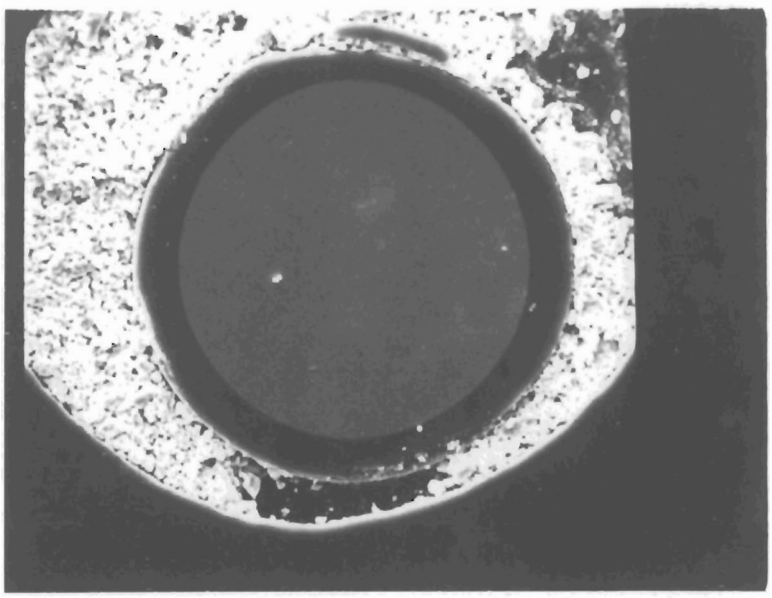

Plate 2. F7 - ME1 FIBRE. Polished end set in wax. Mag. x 425

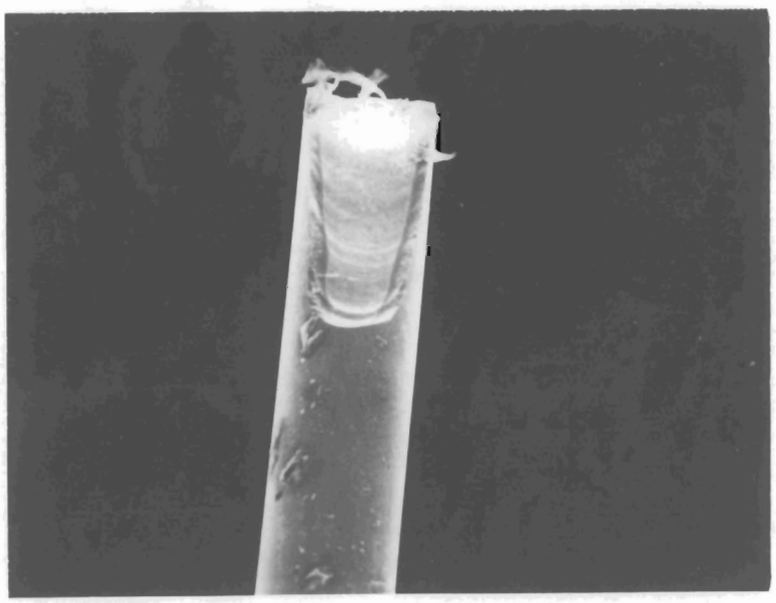

Plate 3. F7-PYREX FIBRE. BROKEN END x 400.

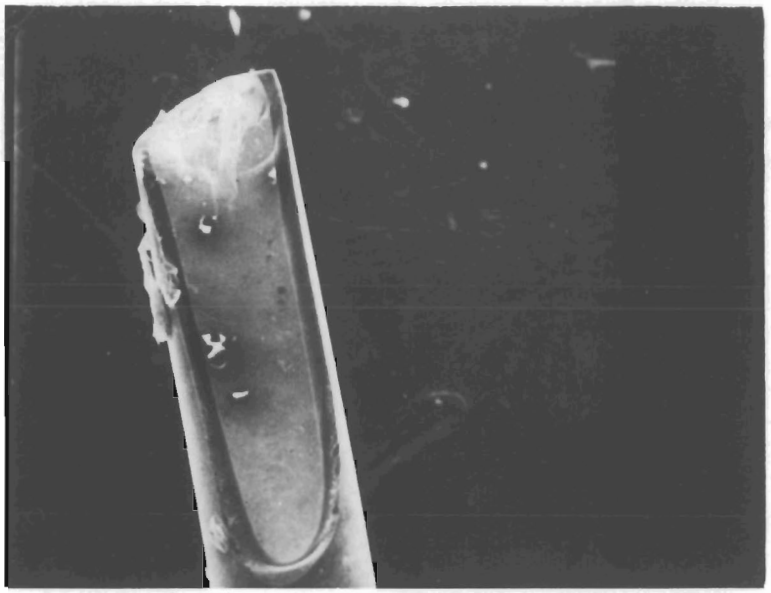

Plate 4. F7-PYREX FIBRE. BROKEN END x 475

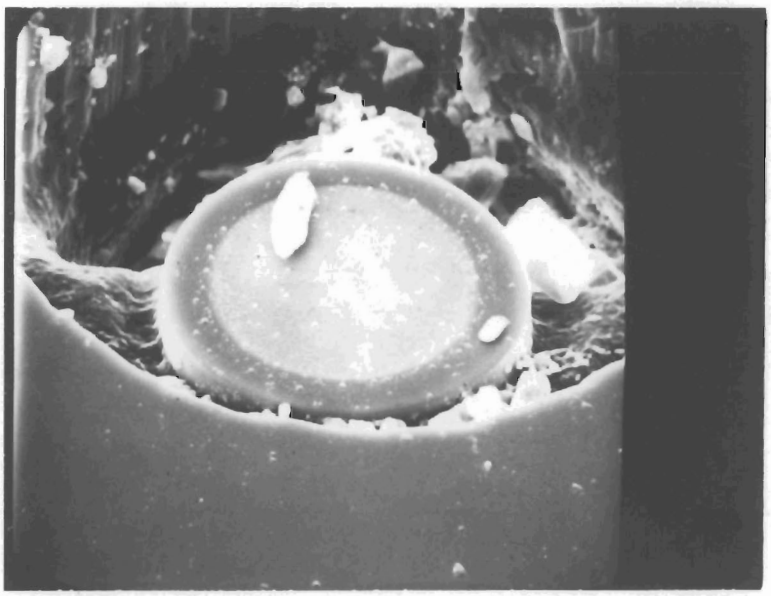

Plate 5. F7-PYREX FIBRE. POLISHED END SET IN WAX
MAG. x 1220

PLATE 6

PYREX - F7 Fibre with air bubble x 350

PLATE 7

PYREX - F7 Fibre x 350